Spring 2017

The synergistic effects of orthogonal biofilm mitigation strategies: thermal and antibiotic treatment

Erica Noyes Bader Ricker
University of Iowa

THE SYNERGISTIC EFFECTS OF ORTHOGONAL BIOFILM MITIGATION STRATEGIES: THERMAL AND ANTIBIOTIC TREATMENT

by

Erica Noyes Bader Ricker

A thesis submitted in partial fulfillment
of the requirements for the Doctor of Philosophy
degree in Chemical and Biochemical Engineering in the
Graduate College of
The University of Iowa

May 2017

Thesis Supervisor: Associate Professor Eric E. Nuxoll

Graduate College
The University of Iowa
Iowa City, Iowa

CERTIFICATE OF APPROVAL

_____

PH.D. THESIS

_____

This is to certify that the Ph.D. thesis of

Erica Noyes Bader Ricker

has been approved by the Examining Committee for
the thesis requirement for the Doctor of Philosophy degree
in Chemical and Biochemical Engineering at the May 2017 graduation.

Thesis Committee: _____
Eric E. Nuxoll, Thesis Supervisor

_____
C. Allan Guymon

_____
Aliasger K. Salem

_____
Jennifer Fiegel

_____
David A. Stoltz

ACKNOWLEDGEMENTS

I would like to thank many people for their help and support throughout my research and personal development. First, I would like to thank my advisor, Eric Nuxoll, for his help and patience for the last five years. He has helped me through the ups and downs of research and has taught me how to present my work in a more compelling manner, for which I am grateful. The faculty members on my committee have provided invaluable support and advice from my research questions to helping me navigate the academic world to improve my professional development. All the faculty and staff members who work in the Chemical and Biochemical Engineering Department and the Graduate College, both currently and previously, have been a great support throughout the day-to-day tasks and I truly value their guidance and knowledge. The other graduate students who have worked in my laboratory with me helped a great deal and helped form who I am today. The undergraduates who I mentored provided great research support and provided me with additional teaching and leadership experiences.

I have been fortunate to have received research support from grants from the National Science Foundation and the American Heart Association. I personally was fortunate to receive a fellowship from the Center for Biocatalysis and Bioprocessing National Institutes of Health T32 trainee program and to receive the Ballard and Seashore Dissertation Fellowship. Without this support I would not have been able to enjoy my research and expand the field as effectively.

Lastly, I would like to thank all my friends and family who have been here to support me through the good times and the bad. My parents helped foster my interest in

science and supported my intellectual curiosity while showing me how to maintain a balanced lifestyle. My husband has always shown a great deal of belief in me and my work while helping me to see the humor in life and knowing when to take a break. Without the support of these amazing friends, family members, and mentors I would not be the person I am today and I attribute my success to their help and support—thank you.

ABSTRACT

Upon forming a biofilm, bacteria undergo several changes that prevent them from being eradicated with antimicrobials alone. These biofilms manifest as persistent infections and biofouling in the medical and industrial world, respectively, constituting an ongoing medical crisis and creating a huge financial burden. Biofilms on implanted medical devices cause thousands of patients each year to undergo multiple surgeries to explant and replace the implant, driving billions of dollars in increased health care costs due to the lack of viable treatment options for *in situ* biofilm eradication. Heat has been used to reliably eliminate biofilms for many years, but the temperatures employed are infeasible for many applications, particularly *in vivo* medical treatment. Remotely activated localized heat can be applied through a superparamagnetic iron oxide nanoparticle polymer coating when paired with an alternating magnetic field. However, there is very little known about the temperatures required to kill the biofilms and the effects of the heat in conjunction with antibiotics. To better understand the required parameters to effectively kill off bacteria in biofilms a variety of heat treatments were investigated for a variety of *Pseudomonas aeruginosa* biofilms grown in different conditions. Additionally, these heat treatments were combined with antibiotics to better understand any combined effects of the two orthogonal treatment plans. It was found that heat is an effective method for killing the bacteria in biofilms. Temperatures ranging from body temperature, 37 °C, to 80 °C were used to heat shock the biofilms for 1 to 30 minutes. Higher temperatures for short exposure times yielded similar results to lower temperatures for longer exposure time. Biofilms grown in different conditions did vary in their susceptibility to the heat shocks; however, at the higher temperatures the differences became negligible. Therefore, the more effective

treatments were the higher temperature heat shocks with shorter exposure times to maximize bacterial cell death and minimize the potential heat transfer to the surrounding tissue. Regrowth studies indicate a critical post-shock bacterial loading (~10^3 CFU/cm^2) below which the biofilms were no longer viable, while films above that loading slowly regrew to their previous population density. Combined treatments with antibiotics had synergistic effects for all antibiotics across a window of heat shock conditions. Erythromycin in particular, which showed no effect on the biofilm alone, decreased biofilm population by six orders of magnitude at temperatures which had no effect in the absence of antibiotics. These studies will evolve the understanding of biofilms and how to efficiently eradicate them on implant surfaces. The introduction of such a novel coating in conjunction with antibiotics could obviate thousands of surgeries and save billions of dollars spent on explantation, recovery, and re-implantation.

PUBLIC ABSTRACT

Each year in the U.S. hundreds of thousands of people develop a biofilm infection on their medically implanted devices. These biofilms are a community of bacteria that attach to a surface and have a protective layer preventing antibiotics from being effective. When a patient gets a biofilm infection the implant needs to be removed via invasive surgery and the patient is left without an implant during a long recovery process. Once the infection has subsided the patient can receive a replacement implant; however, that second implant has twice the likelihood of infection as the first. This leads to poor patient quality of life and costs the U.S. billions of dollars annually. Alternatively, a coating can be placed on the surface of an implant and can be heated wirelessly to kill the bacteria without ever performing an invasive surgery. The required temperatures and exposure times to those temperatures were investigated and combined with antibiotics to determine any combined effect. Higher temperatures for shorter amounts of times were determined to be the most robust treatment and the temperature could be decreased when antibiotics were used at the same time to eradicate the infection. A coating that can be heated wirelessly could improve the lives of thousands of patients and improve quality of life by decreasing the needs for additional surgeries, reducing recovery time, and saving the U.S. millions of dollars in medical expenditures.

TABLE OF CONTENTS

LIST OF TABLES

LIST OF FIGURES

CHAPTER 1: INTRODUCTION

1.1. Motivation

Biofilms are ubiquitous, from covering the bottom of ship hulls to causing persistent infections in patients. They consist of a community of bacteria that attach to a surface and create a protective layer, called the extracellular polymeric substance (EPS), which makes them very difficult to eradicate. These communities of sessile bacteria can be found in many settings including the medical field, industrial plants, water lines and pipes.

About 45% of all nosocomial, or hospital acquired, infections are device related.[1] Each year 3.6 million medical devices are implanted in patients in the United States. Of the patients with these medical implants over 100,000 have nosocomial infections form on their devices each year,[2] with biofilms being the cause of about 80% of all implant related infections in the body.[3,4] Adding dental implants and catheters, these numbers increase by an order of magnitude.[5] The biofilms can lead to bloodstream infections causing the mortality of otherwise relatively healthy patients. Of the total episodes of bloodstream infections, 51.4% are nosocomial[6] and of these bloodstream infections acquired in U.S. hospitals *Pseudomonas aeruginosa* infections have a crude mortality of 38.7% of patients;[7] it is also the third most common bacterium to cause orthopedic implant infections.[8]

The most common method doctors use in the United States to treat these infected implants is dosing the patient with high levels of antibiotics and removing the implant until the infection subsides.[3,9] Once the patient is clear of infection a third surgery can be performed to place in a new implant.[1,10] Nosocomial prosthetic joint infections increase from 1.5-2.5% upon initial surgery to 3.2-5.6% of revision surgeries demonstrating that additional surgeries increases the risk of gaining infections.[11–13] The total cost in the United

States from the resulting hospitalization, surgeries, and replacement devices adds up to over five billion dollars a year,[2,14] in addition to a low quality of life for patients with infected implants. To prevent nosocomial infections greater care and effort is devoted to prevention via hand washing, sterilization, and prophylactic antibiotics regimens. However, infections still remain high and have remained steady over a twenty-year period.[14,15]

Sessile bacteria have been found to be much more robust and difficult to eradicate than their planktonic or free swimming counterparts.[16–19] Biofilms are a growing concern for the medical and industrial fields since they are hard to eradicate and provide resistant infections and biofouling.[20] Food and pharmaceutical industries have struggled with biofilm contaminations on the walls of their processing equipment for years as well.[21,22] The CDC estimates that about 48 million people fall ill to food borne diseases with about 128,000 hospitalizations and 3,000 deaths per year in the United States alone, with bacteria estimated to cause 64% of the hospitalizations and deaths.[23] This biofouling on the processing equipment not only increases the contamination potential of these goods, but also leads to more expensive processes since it decreases the heat transfer efficacy and requires thorough cleaning, requiring the plant to shut down for a few days.[24] Water processing plants have similar issues with biofilms contaminating the water systems.[25]

Biofilms are found in many environments and cause many problems for the medical and industrial fields. However, when these infections are found on an implant device surface the consequences are dire and require a more immediate response. These infections have a more limited treatment window since the patient cannot be exposed to anything harmful that may be used in an industrial setting to deal with a biofilm. A solution to this

more complicated problem could provide a broader solution and save lives of struggling patients.

1.2. Biofilms

Biofilms are formed when planktonic, or freely swimming, bacteria adsorb to a surface and begin to form an extracellular matrix called extracellular polymeric substance (EPS). One of the most well studied biofilm formers, *P. aeruginosa* attaches to a surface irreversibly and is mediated by its single polar flagella and its type IV pili.[26] Once the bacteria have attached to a surface the EPS is formed creating a protective layer for the community of bacteria. With time, the bacteria replicate and can disperse causing a systemic infection in the patient or colonization of another surface, see Figure 1.1.[27–35] Not all bacteria form biofilms, but the bacteria that do rely on quorum sensing.

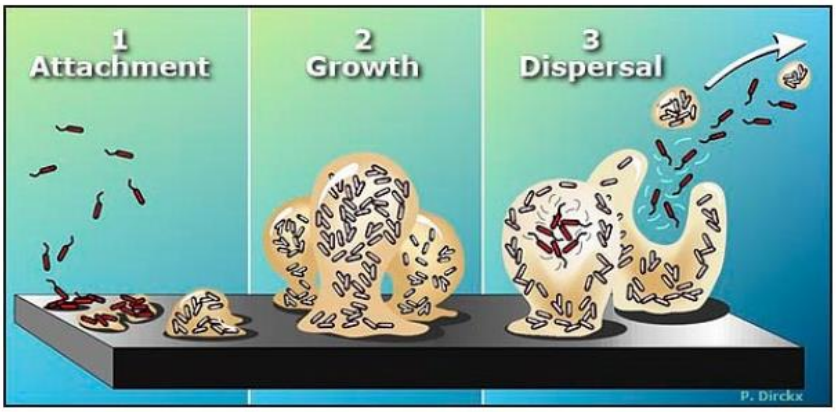

Figure 1.1: Schematic of a Biofilm Formation. *The basic formation of a biofilm on a surface from free swimming bacteria.*[27]

1.2.1. Quorum Sensing

Bacteria communicate with each other via quorum sensing (QS). QS is accomplished via autoinducers, small molecules that serve as signal molecules for bacteria.

Bacteria constantly produce autoinducers and once a high enough population density is reached, the binding frequency triggers signaling molecules that initiate virulence, specific gene expression, or the formation of a biofilm.[28,36–40] Some of the most common and well-studied quorum sensing molecules are the acyl-homoserine lactones, AHL.[41,42] The two major AHL signaling molecules for *P. aeruginosa* are butyryl-homoserine lactone, called C4 AHL, and 3-oxo-dodecanolyl-homoserine lactone, called 3-oxo-C12 AHL, see Figure 1.2.[42,43] It was found that these signaling molecules differ not only in their structures, but also in their delivery out of the cell. C4 AHL has been found to diffuse freely out of the cell into the environment while 3-oxo-C12 AHL is transported across the cell membrane through the MexAB-OprM efflux pump.[43] C4 AHL has been shown to affect virulence through regulation of the type II secretion system and biofilm formation.[43,44] 3-oxo-C12 AHL has been shown to regulate genes as well as inhibition of other species.[45,46] 3-oxo-C12 AHL has also been suggested to serve as a scaffolding, holding the biofilm together.[42,47] Quorum sensing holds an important role in the virulence, gene regulation, and biofilm formation which can contribute to the resistance of these bacteria to antibiotics, chemical treatment, and the immune system.

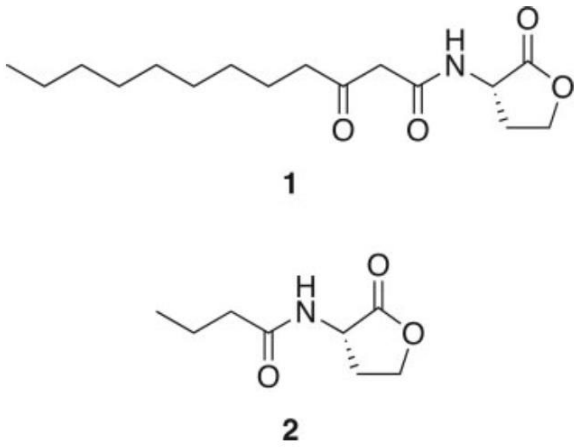

Figure 1.2: Chemical Structure of Two Common Quorum Sensing Molecules*. 1) 3-oxo-C12 AHL and 2) C4 AHL which are similar in structure with differing carbon tails.*

1.2.2. Increased Resistance

One reason for the increasing interest in biofilms is their heightened resistance to antibiotics. Both antibiotics and the host's immune system are not as effective against biofilms as they are against planktonic bacteria,[17,48–51] effectively negating the primary clinical approach of antibiotic administration for bacterial infection.[16–18,48] Bacterial viability after exposure to antibiotics has been studied for many antibiotic concentrations and planktonic bacteria typically show inhibition at concentrations significantly lower than an antibiotic concentration of 128 μg/mL.[52–55] Biofilms, on the other hand, have been shown to require up to 128 times higher antibiotic concentration to exhibit inhibition than their planktonic counterpart.[55,56] However, increasing the antibiotic concentration to eradicate a biofilm leads to host cell toxicity long before eradication of biofilm bacteria can occur.[57] There are many factors currently being researched to better understand the reasons for this increased resistance to antibiotics. Some of the reasons for the increase in

antibiotic resistance in biofilms are the protection from the EPS, persister cells, efflux pumps, and increased mutation rates.

1.2.3. Extracellular Polymeric Substance

EPS acts as a physical barrier and is the first line of defense for the bacteria from the host immune system and antimicrobial agents. EPS is composed of glycolipids, glycoproteins, polysaccharides, proteins, and DNA.[58,59] For *P. aeruginosa* the majority of the EPS is composed of Psl, Pel, alginate, and eDNA. Psl is a polymeric pentasaccharide that is neutrally charged, while little is known about Pel's positively charged polymeric structure.[59] Alginate helps initiate attachment and helps create a thick biofilm during the initial development of the biofilm.[58] The eDNA is of varying length and has no apparent pattern indicating that it might be from stochastic lysis of bacteria in the biofilm. The eDNA binds with the Pel to create a more structured architecture of the biofilm and provide more support.[60] This dense matrix creates a transport barrier for the cells involved in the immune system denying them access to the bacteria. The EPS also creates transport limitations of antibiotics, chemicals, nutrients, and oxygen.[16–18,31,61]

A host's immune system typically uses antibodies and phagocytes to mitigate infections. In the case of a biofilm, the antibodies and phagocytes cannot reach all the bacteria. The phagocytes actually do more harm to the host cells than to the biofilm due to the secretion of phagocyte enzymes, which end up harming the surrounding host cells while having a limited effect on the biofilm (Figure 1.3).[16,17,62] Additionally, the EPS limits antibiotic diffusion through the biofilm. This limited diffusion results in lower concentrations or no antibiotic present at the surface where the biofilm has formed, causing a population of bacteria to be present post treatment. The surviving bacteria have now been

exposed to a sub-minimal inhibition concentration of antibiotics which increases the adaptive resistance of the bacteria significantly.[63–66]

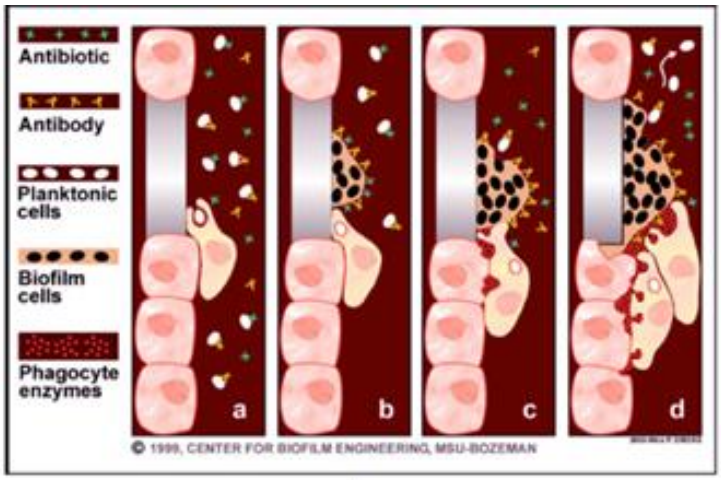

Figure 1.3: Schematic of Frustrated Phagocytosis. *Before a biofilm forms on a surface (a) the bacteria are planktonic and susceptible to antibiotics, antibodies, and phagocytes. As a biofilm starts to form (b), the bacteria inside the biofilm form the EPS which prevent the antibodies, antibiotics, and phagocytes from reaching the bacteria. The biofilm continues to grow and the host's phagocytes start to secrete phagocyte enzymes (c) to further the attack the bacteria. The phagocyte enzymes do not reach the bacteria in the biofilm, instead they begin to harm the healthy cells of the host (d).*[17]

Not only does the EPS decrease the diffusivity of antimicrobials, it also decreases the diffusion of nutrients and oxygen. It was found that the structure of the biofilm greatly changes the nutrient and oxygen diffusion.[42,63,67] For uniform carpet biofilms (*i.e.* biofilms with minimal structural changes across their surface) the decrease of oxygen is readily observed with an aerobic environment seen about 100 µm into the biofilm. However, in biofilms with more variation to their EPS and structure the oxygen limitations were smaller since there was less of a diffusion limitation.[67] Nutrient limitations have similarly been observed creating pockets of bacteria that are dormant in the biofilm and therefore less affected by antimicrobials.[68]

1.2.4. Persister Cells

Transport across the EPS is not the only problem biofilms pose for antibiotics; once in the EPS, antibiotics still have been found to be ineffective. This decrease in efficacy once in the EPS is speculated to be due to some bacteria niches in the biofilm decreasing their metabolism, rendering reproduction inhibition or metabolic targeting drugs useless.[31,68] This dormancy is most likely due to decreased nutrients and oxygen to the bacteria deeper in the biofilm, causing them to decrease their metabolism in order to survive.[63,67,68] This decreased metabolism has a direct effect on the efficacy of the antibiotics since the majority of the antibiotics require the bacteria to be metabolically active or to be actively dividing. For example, ciprofloxacin is a common antibiotic that targets the DNA gyrase and topoisomerase IV thereby hindering the cell's ability to replicate;[69] however, if the bacteria are not actively reproducing this mechanism of action is rendered ineffective. In addition to these persister cells the biofilm has means of actively pumping out the antibiotics from the biofilm via efflux pumps, decreasing the concentration of the antibiotics within the biofilm.

1.2.5. Efflux Pumps

Efflux pumps are a major contributor to *P. aeruginosa* virulence and its vast ability to survive in a variety of hosts. Efflux pumps regulate the movement of molecules through the cell membrane and are broken down into five families: the small multidrug resistance (SMR) family, the multidrug and toxic-compound extrusion (MATE) family, the ATP-binding cassette (ABC) superfamily, the major facilitator superfamily (MFS), and the resistance nodulation division (RND) family.[70] Efflux pumps can eject the antibiotics before the drugs have a significant effect on the bacterium. Common efflux pumps

identified thus far in *P. aeruginosa* are MexAB-OprM, MexCD-OprJ, MexEF-OprN, MexXY-OprM, and MexJK-OprM.[70] One of the most prevalent efflux pumps known for drug export in *P. aeruginosa* is the MexAB-OprM, belonging to the RND family, which expels antibiotics such as β-lactams, fluoroquinolones, chloramphenicol, tetracycline, and novobiocin, among others.[30] Efflux pumps have been found not only to regulate the expulsion of antibiotics, but also to export quorum sensing molecules, organic solvents, detergents, and invasive particles from the host.[30,32] The presence of efflux pumps, particularly MexAB-OprM, has been found to be upregulated in clinical strains rendering antibiotics less effective.[71–73] A sample of fluoroquinolone-resistant clinical isolates showed that about 75% had an overexpression of efflux pumps.[74]

Environmental factors and the stage of growth have been found to affect the expression of the *mexAB-oprM* gene. The major factors that have been discovered thus far are the phase of growth, oxidative stress, and disinfectants like pentachlorophenol. The production of MexAB-OprM is lowest during the lag phase and slowly increases during the exponential phase, hitting a maximum production at the late log phase.[75,76] The same result was seen both in planktonic and biofilms alike, but with a pronounced decrease in MexAB-OprM production for biofilms with extended growth time, speculated to be due to the decrease in metabolic activity in the cells. This is supported by the observed decrease in efflux pump production as the biofilm thickened. In addition, the bacteria on the substratum showed the highest rate of efflux pump expression compared to their neighboring bacterial cells further inside the biofilm.[76] This is explained via the oxidation of two cysteines in MexR which creates conformational changes making the repressor no longer able to bind to the DNA promoter and therefore *mexAB-oprM* is freely

expressed.[77,78] Since reactive oxygen species are produced in more abundance during growth this might be why there is a greater presence of MexAB-OprM during growth phase and not as much during the lag and stationary phase. Reactive oxygen species are often used as disinfectants and used by human immune systems in macrophages to get rid of pathogens. However, since this upregulates the MexAB-OprM efflux pump it could be a factor for why many hospital isolates of *P. aeruginosa* have overexpressed MexAB-OprM. One such disinfectant is pentachlorophenol which upregulates MexAB-OprM production.[77,79] This means that a hospital setting may increase the overexpression of MexAB-OprM in *P. aeruginosa*, rendering the bacteria more resistant to antibiotics.

1.2.6. Increased Mutations

The bacteria in biofilms have an increased mutation rate and differ in their regulations to increase their resistance. As mentioned before, some efflux pumps can pump out antibiotics and other antimicrobials and these can be upregulated in biofilms and are an intrinsic defense of *P. aeruginosa*. For example, the MexAB-OprM and the MexXY-OprM efflux pumps can pump out sulfonamides, tetracycline, novobiocin, macrolides, fluoroquinolones, chloramphenicol, β-lactams, and aminoglycosides.[62] The outer membrane can also change its permeability to antibiotics, and *P. aeruginosa* has been shown to be effective at this with a ten to one hundred-fold less permeable outer membrane than *Escherichia coli*.[26] Not only do biofilms have intrinsic defense mechanisms they also have adaptive defense mechanisms that increase their resistance. Through conjugation, transformation, or transduction bacteria can share resistant genes via DNA elements, such as plasmids, transposons, prophages, resistance islands, and integrons.[26] This information exchange can lead to all sorts of increased resistance, for example, a mobile genetic unit

containing genes for an aminoglycoside-modifying-enzyme decreases the binding efficacy of aminoglycosides, a family of antibiotics, to the 30S ribosomal subunit, rendering them less effective.[80] Natural mutations leading to resistance occur at a greater rate in the bacteria in a biofilm by over 100-fold more frequent than in their planktonic counterparts.[81] The many forms employed by bacteria in biofilms to increase their resistance to antimicrobials has created a growing problem that antibiotics on their own cannot solve.

1.3. Methods Currently Used to Deal with Biofilms

1.3.1. Prevention of Biofilm Formation

Techniques currently being investigated to decrease biofilm formation on implant surfaces include the inhibition of microbial adhesion, prevention of biofilm formation, and methods of mitigating the established biofilms. The means of inhibition of microbial adhesion are being studied using hydrophilic coatings and antimicrobial coatings.[28,30,82] The hydrophilic coatings have been shown to decrease the amount of bacteria that adhere to the device's surface.[28,82,83] However, these coatings also decrease the adsorption of mammalian cells, decreasing the ability of the device to be fully incorporated into the patient[82] and even low numbers of bacteria can still form a biofilm. Materials such as metals and polymers that prevent bacterial adhesion have shown some progress in preventing biofilm formation. The use of metals is a popular method for antifouling surfaces and has been shown to greatly decrease the attachment of bacteria to the surface.[1,84–86] However, these surfaces can be coated by proteins from the body creating a protective layer between the bacteria and the metal, rendering the initial antimicrobial surface ineffective.[11,30] A more promising antifouling approach utilizes a copolymer containing brushes that reversibly change the surface from antifouling activity to bactericidal. This copolymer was

found to decrease the bacterial adherence and clear the presence of the proteins, but it requires a cooling step to 4 °C which is very difficult to reach within a patient for an implanted device.[87] For most of these surface adherence mechanisms the tissue cells have also shown to adhere to the surface and spread at a slower rate increasing the recovery time due to slower tissue integration.[88]

Antimicrobial coatings are being studied by placing the antibiotics in a coating on the surface of the device with a release mechanism within the coating. The antibiotics released from the coating have shown a significant decrease in the targeted bacteria, but an increase in the non-targeted bacteria,[30] which can be equally harmful to the patient. Similarly, antibiotic polymer beads are currently being used in the clinical setting for implants requiring cement. The antibiotics elute out of the polymer beads and the bone cement to the biofilm; however, this technique has shown to elute antibiotics in sub-minimal concentrations increasing the prevalence of resistance to the antibiotic.[89–92] Techniques being researched on the prevention of biofilm formation, rather than bacteria adsorption or antibiotic elution, appear to be more promising.

As seen in Figure 1.4, a chemical that is similar in structure to the quorum sensing autoinducers will bind to the receptor sites of the bacteria instead of the autoinducers, creating a signal block that ultimately prevents the biofilm formation without triggering the signal themselves.[38,93,94] It has been found that the usage of norbgugaine in *P. aeruginosa* effectively blocks quorum sensing and decreases biofilm formation by 83%.[36] Although this is an effective tool, autoinducers are different for each bacterial species. Therefore, many different quorum sensing interfering molecules would have to be used to block any biofilm formation. Additionally, the potential for the emergence of multi-quorum

sensing inhibitor resistant bacteria is high indicating that the use of quorum sensing inhibitors may result in a similar problem as seen with multiple drug resistant bacteria.[95]

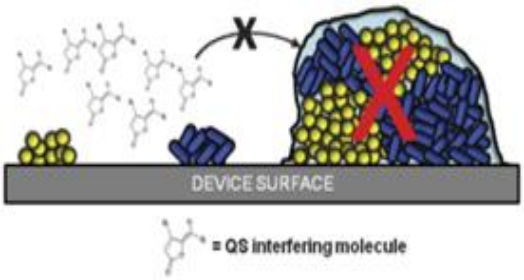

Figure 1.4: Schematic of Quorum Sensing Blocking. *Using quorum sensing interfering molecules as a means to deter biofilm formation on a device's surface. The X represents the blocking of quorum sensing and blocking the formation of the biofilm.*[30]

1.3.2. Treating Biofilm Infection Once Formed

Another means of fighting biofilm infections on implant surfaces is to address already fully-developed biofilms. One technique uses an enzyme that breaks down EPS and exposes the bacteria to the host's immune system and to antibiotics.[93] Disrupting biofilms through magnetic nanoparticles coated in antibiotics with enzymes that break down EPS provides another option. This method allows the nanoparticles to be magnetically directed to the biofilm and the antibiotics to be distributed more intensely around the biofilm as the enzymes break down the EPS.[30,96,97] This requires directing small drug systems through the body using a magnet which is very difficult to do, especially with large variation from one human body to the next. With the large increase in efflux pumps removing antimicrobials from the cells and biofilms many treatment plans will be ineffective anyway, therefore, methods addressing the efflux pumps by preventing them from pumping out the antibiotics is another valid treatment stragety.

Currently researchers are investigating novel ways of dealing with the increased resistance to antibiotics and cleaning agents that MexAB-OprM efflux pumps facilitate. The leading research on MexAB-OprM efflux pumps is exploring ways to administer a molecule that downregulates, blocks, or decreases the efflux pump's efficacy while administering a combined treatment with antibiotics. Phenylalanine arginyl β-naphthylamide has a competitive mechanism of inhibition of MexAB-OprM efflux pumps which blocks the pump from effectively pumping out other molecules, such as antibiotics.[98] Analogues of quinolones or pyridopyrimidine scaffolds have been effective since they interact with MexAB-OprM and just need different side chains to get the molecules to block efflux by binding to the MexB receptor site. The use of tetrazole as a side chain on these scaffolds is the most promising of the analogues when combined with the antibiotic treatment of levofloxacin or sitafloxacin.[99,100] The tetrazole ring interacts with the MexB residues Asp274, Arg620, and Lys151 blocking the binding of other molecules thereby preventing the movement of antibiotics out of the cell.[98] Azithromycin suppresses the expression of MexAB-OprM by about 70%.[101] This results in a two to four-fold increase in susceptibility to antibiotics, including novobiocin, chloramphenicol, tetracycline, carbenicillin, and aztreonam. The most promising combined treatment thus far is the synergistic effects of lanatoside C and levofloxacin which has a six-fold decrease in the minimum inhibitory concentration.[98] These molecules show promise for a means of dealing with the increased antibiotic resistance that *P. aeruginosa* efflux pumps, particularly MexAB-OprM, express.

Physical disruption of the biofilm has been investigated heavily with many innovative ideas. The use of near infrared lasers has been shown to be successful at killing

biofilms and has been employed for wound cleaning. It has also been suggested for use for a cranial biofilm infection for patients with a transparent implant in the scalp.[102] The biofilm was disrupted, however, the application of a near infrared laser requires a direct line of site to the biofilm for the laser since the laser can damage healthy tissue in its pathway. This makes it only applicable to biofilms that can be directly viewed with no healthy tissue in between the laser and the biofilm, limiting the use to a small subset of medical applications. Another form of physical disruption of the biofilm is the use of ultrasonic waves. Ultrasonic waves show great promise in conjunction with antibiotics for *E. coli*, decreasing its viability count to nearly indetectable levels. However, this method was found to not be as effective against all biofilm forming species. Other species showed to have little to no observable difference with the treatment potentially due to stronger cell walls and biofilm matrices.[103,104] This variation in efficacy depending on the species of bacteria makes the identification of the bacterial species in the biofilm an important step and it is possible that the method could be ineffective against most bacterial biofilms. DC-current has proven to be more effective for killing the bacteria in a biofilm bone pin implant infection.[105–107] In a goat bone pin model 88% of the goats showed no sign of infection post DC-current treatment.[105] The improvement of these infected bone pins was impressive, however, it requires either a large on-board power supply and telemetry or protruding external connections, both of which are undesirable for implanted devices.

The application of heat is another way to treat biofilms that have grown on an implant's surface. Most of the research using heat as a means to mitigate biofilms has been done within food industries. One example of these trials was done by Chmielewski and Frank. They studied the reduction of *Listeria monocytogenes* viability using heated water

flushed through food processing reactors as a way to disinfect the rubber gaskets where these biofilms have been found to grow. It was discovered that at higher temperatures the exposure time required to kill off the biofilms decreased linearly with temperature.[108]

Similar studies have been done using magnetic nanoparticles as the heat source. This heating can be achieved remotely via the use of an alternating magnetic field. The application of an alternating magnetic field to a magnetic nanoparticle causes the nanoparticle's atomic dipole to correspondingly change directions with the applied field. This change in field direction either rotates the particle with it or changes the atomic dipole without moving the particle itself, a process called Néel relaxation, depending on the surrounding matrix and applied frequency.[96,109] This change of the atomic dipole direction causes the nanoparticles to heat. Park *et al.* studied superparamagnetic iron oxide nanoparticles and their heating properties, and demonstrated this by applying them directly to a *P. aeruginosa* biofilm to show that remote heating of the nanoparticles would kill the bacteria in the biofilm via hyperthermia.[110]

These experiments show it is possible to mitigate biofilms with heat from nanoparticles. This can be taken a step further and would be even more effective with nanoparticles embedded and fixed to an implant's surface. Because the nanoparticles heat without movement, iron oxide nanoparticles can be stationary in a coating and still accomplish heating. In addition to the ability to heat while remaining stationary, the presence of iron oxide nanoparticles has been shown to increase the thermal stability of polyvinyl alcohol (PVA).[111] This stability is theorized to be from hydrogen bonds on the PVA connecting to the hydroxyl groups on the nanoparticles, thereby increasing the cross-linking within the polymer. This increased cross-linking has been proven to increase the

melting temperature of the PVA and increase its thermal stability,[111] which could also apply to other more biocompatible polymers. Thus far, the Nuxoll lab has shown that PVA cross-linked with glutaraldehyde is thermally stable and the amount of cross-linking can control whether or not the polymer remains or dissolves after heating. The fine control over the thermal stability or degradation with temperature allows for control over the coating to be a one-time use or a coating that remains for future heating applications. For the case when the polymer coating remains on the implant's surface, longevity tests of 16 months have been performed and have shown little sign of the polymer dissolving. Additionally, the normalized heating rate was measured after the longevity tests and there was a modest decrease, but this was attributed to the oxidation of the nanoparticles rather than loss of nanoparticles to the solution.[112] This fine control over the polymer's thermal stability or degradation with the application of heat an implant's surface coating can be changed for the desired effect.

The superparamagnetic iron oxide nanoparticles embedded in a polymer coating allow for wireless heating of an implant and the eradication of bacteria adhered to the surface. When the nanoparticles are exposed to an alternating magnetic field, the atomic dipoles in the nanoparticles change direction with the alternating magnetic field, causing the nanoparticles to heat. The ability to remotely heat just the implant's surface minimizes damage to the surrounding healthy tissue while providing an alternative sterilization technique. The synergistic effects of heating with antibiotics could allow for an increased efficacy of both the heating and antibiotics at lower intensities.[113] In addition, heat has been shown to increase the host's defenses via the production of heat-shock proteins by the bacteria, which are more readily recognized by the host's immune system.[114,115] This

heating could kill the biofilm and give the patient a chance to recover from a biofilm infection without having another major surgery to explant the implanted device and a third surgery for a new implant once the infection is gone.

1.4. *In Vitro* Methods to Investigate Biofilms

To develop a medical process or device several steps must be followed before implementation in a clinical setting can occur. Initially *in vitro* trials should be performed to better understand the science behind the effects of the process or device. Biofilms are typically studied *in vitro* before moving to a more complex model, such as a mouse model, to better understand the biofilm behaviors and to minimize unnecessary animal trials. Monoculture biofilms are studied initially to better understand the way a single bacterial species will react before increasing the complexity by adding a second bacterial species to the mixture. *P. aeruginosa* was used *in vitro* to better understand the necessary temperatures, exposure times, and antibiotics to effectively eradicate a biofilm.

An important aspect of this research was the use of different *in vitro* biofilm growth techniques. Three different reactor types were used, a drip flow reactor (DFR), a shaker table, and an MBEC^{TM} assay to better understand the biofilms and their thermal and antibiotic susceptibility. The DFR-grown biofilms produced large population biofilms which were used for quantifying the amount of decrease in bacterial population density for the full range of temperatures and exposure times. The large population was required for investigating the full parameter space since the highest temperature and longest exposure time resulted in a six order of magnitude reduction, requiring a large population density to accurately quantify the decrease in population. The shaker table-grown biofilms were more robust and had smaller population densities which may simulate biofilms found in the

human body better than the DFR-grown biofilms. These biofilms responded differently to the heat shocks, which improved the treatment plan parameters for future trials. To investigate the combined effect of heat and antibiotics a more high-throughput method was needed since the number of variables increased dramatically. The heat shock presented two variables, temperature and exposure time, while the antibiotics introduced two more variables, type of antibiotic and the concentration. For these trials the MBEC^{TM} assay was used for its high-throughput capabilities.

1.4.1. Pseudomonas aeruginosa

P. aeruginosa is a ubiquitous, rod shaped, Gram-negative bacteria that is an opportunistic pathogen that is attributed to infections worldwide.[71–73,116] *P. aeruginosa* is found in soil, plants, insects, animals, and people. Due to such a broad range of possible hosts, *P. aeruginosa* has various defensive mechanisms for surviving in each environment, which allows it to be robust and abundant. Within a hospital setting it accounts for many infections including patients in intensive care units on ventilators, patients with catheters, burn patients, infants and newborns, and patients with cystic fibrosis to name a few.[20,34,117] The spread of *P. aeruginosa* is varied because it can thrive in multiple environments and it can be spread via surgical equipment, hospital staff hands, surfaces such as door knobs, droplets, and aerosolization.[118] A survey of Mexican hospital intensive care units showed that, of the infected patients, 28% contracted *P. aeruginosa*; similarly in San Fernando, Trinidad, 35% of the 530 isolates were identified as *P. aeruginosa.*[119] A major reason for the prevalence and resistance of *P. aeruginosa* is its ability to readily form a biofilm.

1.4.2. Drip Flow Reactor

The DFR, obtained from Biosurface Technologies Corporation, Bozeman, MT, and seen in Figure 1.5, uses a fully frosted microscope slide as the substrate for growth in each well and has a steady drip of nutrients pumped from fresh media for the majority of the biofilms' growth. There are two distinct phases to the DFR operations, the batch mode and the continuous mode. The batch mode consists of placing media and inoculum into each well and allowing the bacteria to adhere to the microscope slides' surfaces for four hours by keeping the reactor flat. Once those four hours have passed the reactor goes into continuous mode by placing the reactor into a 10-degree slope and initiating a steady drip of fresh media onto the upper end of the nascent biofilm, from which it flows down across the biofilm to the waste portal at the lower end. The continuous phase is continued for the desired amount of growth time, 24 hours, and used for the experiments in Chapter 3 and 4. After the desired amount of growth time has passed the microscope slides are easily removed and placed into a heat shock well for thermal shock experiments. Visually, these biofilms are thick and have a clear growth on the surface which can be seen by the naked eye. Through microscopy and plating it was found that these biofilms grow to be about 100 to 150 μm thick covering all of the microscope slide's surface and have a high population density. The DFR produces highly populated biofilms which is quite advantageous; however, the growth procedure requires a large volume of broth and creates a lot of waste to dispose of, both of which are resource and time intensive.

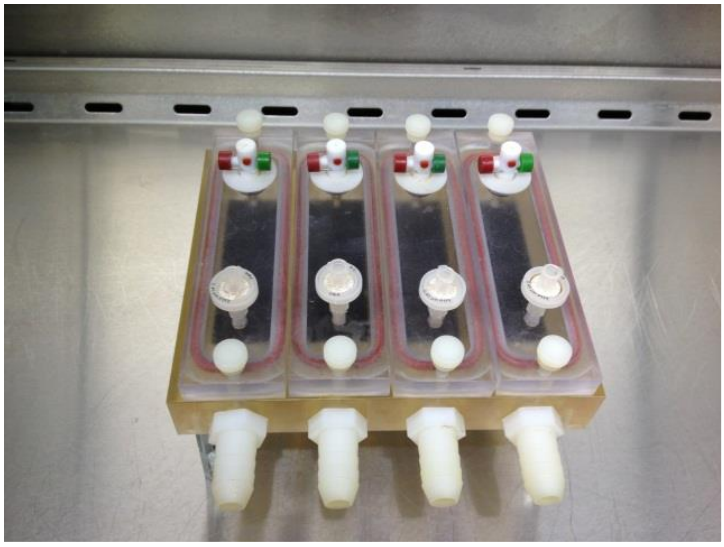

Figure 1.5: Picture of the Drip Flow Reactor (DFR). *The drip flow reactor has 4 channels, one for each microscope slide, to be placed with lids that have a port for a needle for the inlet broth drip and an outlet at the bottom of each well for waste collection.*

1.4.3. Shaker Table

The shaker table-grown biofilms were grown in a 4-well dish, see Figure 1.6, with fully frosted microscope slides as the growth surface, similar to the DFR-grown biofilms. The broth and inoculum are placed into each well, the same as the DFR, and the plate sealed via Parafilm®. The plate is then placed on an orbital shaker and the biofilms were allowed to grow in those conditions until the end of the desired growing period. This growth method produced much smaller amounts of bacteria in the biofilms with biofilm thicknesses reaching 50 µm. The growth of these biofilms was not always visible to the naked eye and did not cover the whole microscope surface. Shaker table-grown biofilms require less broth and less waste disposal making them easier to grow. It was also found that this technique of growing the biofilms made for hardier bacteria to kill thermally as discussed in Chapter 5.

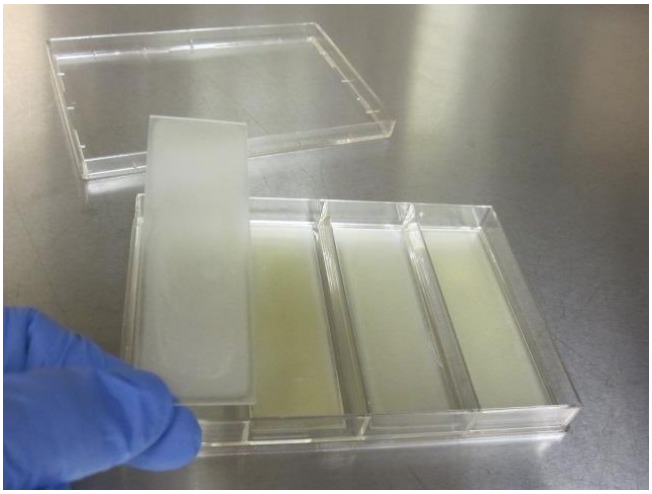

Figure 1.6: Picture of the Shaker Table Setup*. The 4-well dish has a microscope slide placed into each well along with broth and inoculum and placed on an orbital shaker table once sealed for the biofilm growth.*

1.4.4. MBEC™ Assay

The third biofilm growth technique used was the MBEC™ assay. This method was more similar to the shaker table method, but allowed for a higher throughput than either previous method. The MBEC™ assays were obtained from Innovotech, Edmonton, AB, Canada in individual sterile packaging. The assay consists of a 96-well plate with an array of pegs that fit into each well from the lid as shown in Figure 1.7. The starting broth and inoculum concentrations were the same as the other two methods and placed into each well. Similar to the shaker table method the assay was sealed with Parafilm® and placed on an orbital shaker. The biofilms on the lid pegs were allowed to grow in these conditions and were easily transferred to a challenge plate when the biofilms were needed for an experiment. The MBEC™ assays provided the highest throughput of the three methods and produced biofilms more similar in nature to the shaker table biofilms than the DFR biofilms. This technique was less labor intensive for the amount of data gained and was

used to gather the data when many factors were at play making the other methods too time consuming and difficult to run, as seen in Chapter 7.

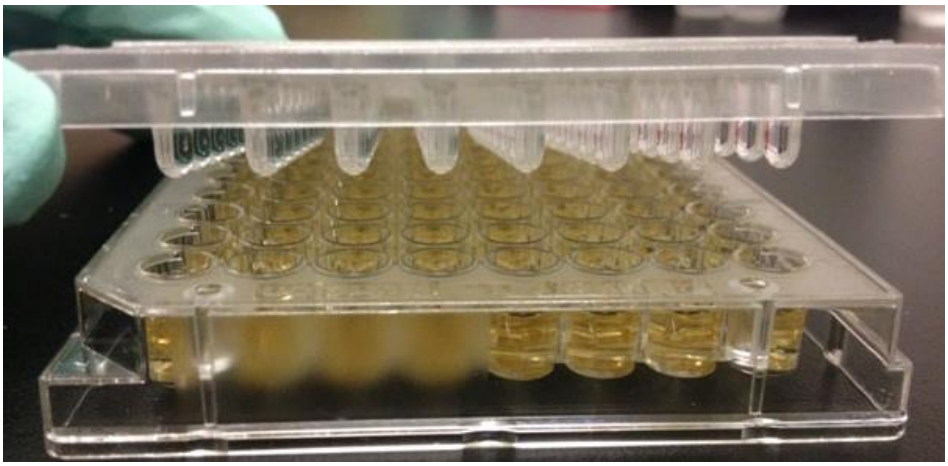

Figure 1.7: Picture of an MBEC™ Assay's Trough and Peg Lid Setup*. The MBEC™ assay consists of a 96-well microtiter plate and corresponding pegs attached to the lid for biofilms to grow on and to move the biofilms to challenge plates rapidly and easily for all 96 biofilms.*

The growth conditions studied via these three different methods provided valuable information about the different biofilm formations and how their growth conditions change the way the biofilms react to a treatment. Through the use of these growth methods and their thermal shock and antibiotic exposures, a better understanding of the requirements for an *in situ* wireless heating device via a superparamagnetic iron oxide nanoparticle, SPION, coating was determined. The development of such a novel coating could improve the lives of many patients and decrease the United State expenditure on infected implants by millions of dollars.

CHAPTER 2: OBJECTIVES

Biofilms cause many hospital setting infections which are difficult to eradicate due to several factors including their extracellular polymeric substance that protects the bacteria and prevents them from being effectively treated with antimicrobials alone. This persistence in infections and biofouling creates a huge financial burden in the medical and industrial world and constitutes an ongoing medical crisis. Patients who obtain biofilm infections on their implanted devices frequently must have their implant removed and undergo an aggressive course of antibiotics before a new implant can be implanted. This process requires many invasive surgeries resulting in poor patient quality of life and costs the United States billions of dollars annually. Means for dealing with these infections have been investigated for years, but few result in full eradication of the biofilm, resulting in a resurgent of the infection and increased resistance to the treatment. Heat has been used to reliably eliminate biofilms for hundreds of years, but the temperatures employed are infeasible for many applications, particularly *in vivo* medical treatment. The development of a superparamagnetic iron oxide nanoparticle, SPION, coating has been shown to effectively heat a surface wirelessly and can be applied to the surface of a medically implanted device to treat a biofilm infection. However, what temperatures are needed and how long those temperatures need to be held to kill off the biofilm need to be investigated to properly tune the parameters of the material.

In this work, I aimed to determine the required thermal shock temperature and exposure times of *Pseudomonas aeruginosa* biofilms based on their growth environment and regrowth potential, their thermal shock source, and the combined effect of the heat with antibiotics. This was investigated by the following goals:

1. Quantify and model the efficacy of thermal shock on biofilms across the full range of possible temperatures
2. Determine the most quantitative analysis technique for quantifying the large population decreases observed from treatments
3. Examine the thermal shock susceptibility of biofilms grown in different environments and their regrowth potential
4. Study the thermal effect from a SPION coating when compared to water bath heating
5. Identify the required temperatures and exposure times for effective biofilm mitigation when combined with antibiotics.

Chapter 3 addresses the first objective by investigating the full range of temperatures and exposure times with the use of drip flow reactor grown biofilms. The biofilms grown in a drip flow reactor typically form large, bacterially dense biofilms allowing for a large drop in viable bacteria populations to be observed, quantifying up to 7 orders of magnitude reduction. These biofilms were immature, grown for 24 hours, and were heat shocked at temperatures ranging from 50 °C to 80 °C, with controls at 37 °C, for exposure times ranging from 1 minute to 30 minutes. The results facilitated the development of a predictive model which could be used for future investigations and could determine needed temperatures and exposure times for a desired amount of bacterial reduction in a biofilm.

To address the most quantitative analysis technique, objective two, the drip flow reactor biofilms post heat shock were analyzed via a dilution and plating method and

microscopy to determine the best analysis technique (Chapter 4). The dilution and plating method is a reliable and common form of analysis among microbiologists for quantification of the bacteria. Microscopy is far more data-rich, providing information about both live and dead bacteria with spatial information on each, and with a faster feedback time, though typically with less quantification. The microscopy images could be quantified through thresholding and pixel counts when the bacteria are dyed one color when dead and another when alive. These two analysis techniques were investigated to determine the best form of quantification for future investigations. Quantification was best facilitated via the dilution and plating method since the bacterial population density decreased on a logarithmic scale, which is more easily quantified via dilution and plating rather than microscopy image analysis. However, the microscopy image analysis provided valuable information about morphology that the other technique could not provide, therefore, the two techniques were found to be complementary in nature.

The third objective, addressed in Chapter 5, compares the thermal susceptibility of biofilms grown in different conditions and investigates the regrowth potential of biofilms after the heat shock. More mature biofilms were grown in harsher conditions in varied media and compared to one another and compared to the biofilms grown in the drip flow reactor. The maturity of the biofilms and the harsher conditions had a larger impact on the thermal susceptibility of the bacteria than the growth medium did. A predictive model developed from the drip flow reactor grown biofilms, discussed in Chapter 3, was compared to the shaker table grown biofilms to determine if it was robust enough to predict the bacterial reduction of biofilms grown in different conditions and was found to be a good predictor of the number of viable bacteria after heat shocks at the higher temperatures,

however the lower temperature heat shock responses were not as consistent. This indicated that the higher temperatures were a more consistent treatment and more robust for a variety of biofilms. The biofilm regrowth post heat shock was investigated to determine the bacteria's ability to regrow as a biofilm and the growth rate changes post heat shock. These trials indicated a population density threshold, above which the bacteria will thrive in a biofilm again, below the threshold the bacteria failed to grow in a biofilm post heat shock. With this information, a treatment could bring the bacterial population density below that threshold to be considered a successful treatment.

Chapter 6 addresses objective four by demonstrating the use of the SPION coating to thermally shock the biofilms and comparing those results to the thermal shocks preformed in a water bath. Since all of the earlier heat shocks were done in a thermostatted water bath, the use of the SPION coating to wirelessly heat the biofilm was demonstrated and compared to the previous heat shocks. Temperatures ranging from 50 °C to 80 °C, with controls at 37 °C, and exposure times of 1 to 30 minutes were investigated. This comparison was done to determine the effect of the heat shock on the biofilm when the heat was coming from the substrate surface versus the surrounding area, as seen in a water bath. The SPION coating did have similar results to the water bath indicating that the water bath trials still hold pertinent information for the real-world application of heat shocking the biofilms *in situ* via a SPION coating.

Finally, objective five, the use of heat in conjunction with antibiotics was investigated to determine the combined effect of each treatment (Chapter 7). Most patients are treated with antibiotics at the first sign of infection and continue a course of antibiotics throughout other treatments. Due to the presence of antibiotics in the body during the

treatment of an infected implant the combined effect of heat and antibiotics on the biofilm is of particular interest. High throughput biofilm reactors were used to investigate the effect of thermal shock at a temperature range of 37 °C to 80 °C for 1 to 30 minutes, while exposed to antibiotics. Ciprofloxacin, tobramycin, and erythromycin were all identified as having stable chemical confirmations at the temperature range covered in these experiments and effective against *P. aeruginosa* planktonic bacteria while each had a different mechanism of action to better understand the effect of the combined treatment. The synergism of these orthogonal treatment strategies was studied and can be used for combined treatments for patients.

These experiments provide a better understanding of biofilms and what temperatures and exposure times are required for mitigating biofilms on an implant device. With this information, a better design of the SPION coating can be developed for wireless *in situ* heating of implanted devices. This technology can also be applied to industrial applications components that struggle with biofilm growth but are hard to reach for disinfecting, or for polymers with a low glass transition that cannot be autoclaved. Furthermore, this research helps to broaden the understanding of biofilms, the effect of heat on the biofilm and the combined therapy of heat and antibiotics to treat biofilms. The knowledge gained from these objectives will improve the development of the SPION coating and the technology would obviate thousands of surgeries a year in the United States alone and save patients from undergoing the long recovery process they currently endure.

CHAPTER 3: DRIP FLOW REACTOR GROWN *PSEUDOMONAS AERUGINOSA* BIOFILMS THERMAL MITIGATION*

3.1. Introduction

In order to design an efficient superparamagnetic iron oxide nanoparticle coating that will effectively mitigate biofilm infections *in situ* for patients with implant infections a better understanding of the required temperature and exposure time to kill the bacteria needed to be established. Pasteurization protocols have been used at a variety of temperatures for over a century, and thermal sterilization of biofilms at temperatures above 120 °C on medical and food processing equipment is also standard. Surprisingly little is known, however, about the cell viability of bacterial biofilms at more accessible temperatures (< 90 °C). One group has developed a predictive model for heat inactivation of *Listeria monocytogenes* biofilms on food processing equipment at 70 – 80 °C,[108] and another briefly studied heating effects on *Pseudomonas aeruginosa* biofilms when dosing them with superparamagnetic nanoparticles.[110] However, the nanoparticles may have induced their own negative effect on the bacteria and may not have applied the heat throughout the entire biofilm evenly. If the heat shock is too mild, then the biofilm will not be eradicated and may come back more resistant to the heat than before. If the heat shock is too aggressive then the surrounding tissue may be damaged unnecessarily. Additionally, the exposure time to the temperature will change the susceptibility of the biofilms adding another variable that needs to be investigated. Both the exposure time and the temperature

*Adapted by permission of Taylor & Francis LLC from O'Toole, A., Ricker, E. B. & Nuxoll, E. Thermal mitigation of Pseudomonas aeruginosa biofilms. *Biofouling* **31,** 665–675 (2015)[120]

have their own effect and may result in different positive or negative effects when used clinically so a model is necessary to determine the range of viable treatments.

The drip flow reactor has been shown to be a good model for growing large, bacterial dense, biofilms.[120] This was in comparison to other growth means, such as the shaker plate biofilm, explored more in Chapter 5, which had lower density biofilms than the drip flow reactor-grown biofilms. It was discovered early on that in order to quantify the amount of bacterial death observed a very high number of bacteria was required to accurately report the reduction. The drip flow reactor biofilms were large in population and could easily be quantified even in the face of large population reduction. The large, thick biofilms were also visible to the naked eye allowing for visual confirmation, in addition to quantification, of consistent growth from one trial to the next. For this chapter, the amount of bacterial cell death at temperatures ranging from 50 to 80 °C for exposure times ranging from 1 to 30 minutes was systematically quantified across the entire parameter space and correlated mathematically to each parameter. In conjunction with the development of a composite coating which can generate these temperatures precisely at the implant surface using an alternating magnetic field, this work aims to develop a new approach to mitigating biofilm infections on medical implants.

3.2. Materials and Methods

3.2.1. Organism and Inoculum

Pseudomonas aeruginosa biofilms have been heavily investigated and is commonly associated with nosocomial infections (Drenkard and Ausubel 2002, Gellatly and Hancock 2013). *P. aeruginosa* reference strain PAO1 (16952, American Type Culture Collection, Manassas, VA) was used for the current study. This strain is representative of

typical *P. aeruginosa* found in a nosocomial setting. For each trial, the bacteria were isolated from a frozen glycerol stock culture and streaked on an agar-filled plate (Difco Nutrient Agar, Sparks, MD). Using a sterile inoculum loop (VWR, Randor, PA) bacteria was scraped off of the stock agar slant in a biosafety cabinet and then gently streaked onto an agar plate. The first streak took up about a third of the agar plate starting from the wall and working in. Using a new sterile inoculum loop the next streak was made by dragging the loop across the previous streak next to the wall of the plate and brought in to take up about another third of the plate. The final streak was performed with a new sterile inoculum loop by dragging across the second streak's end, next to the plate wall, and brought in to the remaining unused surface of the agar plate, as seen in Figure 3.1. This technique is used to dilute the sample enough so that once the bacteria grow, individual colony forming units (CFUs) can be isolated. The streaked plate was incubated for 24 hours at 37°C, and then two colonies were used to inoculate 5 mL of tryptic soy broth (TSB) using a sterile inoculum loop. Prior to inoculation, TSB was autoclaved at 121 °C and cooled to room temperature. The inoculum was incubated at 37 °C in a sealed glass culture tube. Initially, 1 mL samples were removed periodically over the course of 36 hours and quantified via direct enumeration as described below in order to characterize the inoculum's growth curve. Inoculum for the heat shock trials was incubated at 37 °C for 24 hours.

Figure 3.1: Schematic of a Streak Plate Procedure*. To streak a plate a sterile inoculum loop is used to gently streak each section starting with the first section and then streaking the next two sections to get three different dilutions of growth on the plate.*

3.2.2. Media

Tryptic soy broth (TSB, BD Bacto, Sparks, MD) was obtained as a dry powder and dissolved in a ratio of 30 g / 1 L deionized water by heating in a 700 W microwave for 10 minutes. It was autoclaved at 121 °C and cooled to room temperature prior to use. Components for glucose-enhanced media were obtained from Fisher Scientific (Waltham, MA), consisting of 5.232 g MOPS free acid, 4.3 g potassium monophosphate, 2.7 g potassium phosphate dibasic, 24 mg magnesium sulfate and 1.44 mg ferrous sulfate heptahydrate in 500 mL of deionized water. Once mixed well this media was vacuum filtered to ensure sterility. The vacuum filtration was done with a nylon, 0.2 µm filter size filtration system (VWR, Radnor, PA) and attached to a vacuum water facet and the water run to pull the vacuum until all the solution was pulled through.

3.2.3. Drip Flow Reactor Biofilm Culturing

Biofilms were cultured in a 4-channel drip flow reactor (DFR, Biosurface Technologies Corporation, Bozeman, MT) according to ASTM standard E2647-08. Briefly, a single-side, fully-frosted glass microscope slide was placed in each channel along

with 15 mL of TSB and 1 mL of *P. aeruginosa* inoculum. The reactor was incubated at 37 °C for 4 hours, followed by tilting the channels by 10° in the longitudinal direction so that the media would drain from the channel. Fresh media was constantly dripped on the raised end of the slide at a rate of 1.25 L / day per channel, administered by a four-channel peristaltic pump (MasterFlex L/S, Cole-Parmer, Vernon Hills, IL). Dripping continued for 24 hours, producing thick, uniform biofilms with an average bacterial density of 1.65×10^9 CFU/cm^2.

3.2.4. Thermal Shock

To expose the biofilms to a uniform, precise temperature for a defined time period, thermal shock was performed by immersion in pre-heated water. A polystyrene 4-well rectangular plate (Thermo Scientific Nunc, Rochester, NY) was filled with 5 mL de-ionized water per well, covered, sealed in parafilm, and submerged in a thermostatted water bath (Isotemp 3013P, Fisher Scientific, Pittsburgh, PA) to preheat the water and plate.

Each well contained two type T thermocouples by which the well temperatures were recorded throughout the trial. Slides from the biofilm reactor were quickly transferred into the plate, one per well, and the plate was resealed and submerged for the prescribed thermal exposure time. The microscope slides with the biofilms were then transferred out of the thermal shock plate into a polystyrene 4-well plate with 5 mL / well of fresh media at room temperature and immediately quantified. The DFR biofilms were thermally shocked at temperatures of 50, 60, 70, and 80 °C in addition to 37 °C controls, with exposure times of 1, 2, 5, 10, 15, 20, and 30 minutes at each temperature. A minimum of three multi-biofilm trials were performed on each time/temperature combination, with replicates occurring on separate days in random order.

3.2.5. Confocal Laser Scanning Microscopy

The architectural characteristics and thickness of the biofilms were evaluated using confocal laser scanning microscopy (CLSM). In this technique, light from a single focal plane is collected; by stepping through multiple focal planes, a three-dimensional image of the sample is generated. Fluorescent dyes from a LIVE/DEAD BacLight Bacterial Viability Kit (Invitrogen, Eugene, OR) were used for imaging. The dyes are based on membrane integrity, with SYTO 9 entering all cells and fluorescing green when complexed with DNA. Propidium iodide enters only cells with disrupted membranes, quenching SYTO 9 and fluorescing red when complexed with DNA. Dyed biofilms were analyzed using an upright Bio-Rad 1024 confocal microscope with Kr/Ar lasers emitting at 488 and 568 nm to excite SYTO 9 and propidium iodide, respectively. Images were collected by scanning the entire sample area with one laser and collecting the resulting fluorescent light, followed by a scan using the other laser to minimize the effect of excitation/emission overlap. Each recorded image is the average of four sets of scans, recording a 512 x 512 pixel array with 256 intensity levels. Samples were imaged through a 40x water-immersion lens in 1 µm vertical increments. Subsequent image analysis was performed using ImageJ.

3.2.6. Quantification Via Direct Enumeration

While microscopy allows rapid analysis and determination of the spatial distribution of bacteria within the biofilm, its quantification limits for biofilm bacterial load are modest. To quantify the reduction in colony forming unit (CFU) concentration over multiple orders of magnitude direct enumeration was used. The polystyrene 4-well plate containing thermally shocked biofilms, each in 5 mL of fresh, room-temperature media was sealed and placed in a 45 kHz sonication bath (VWR 9.5L, Radnor, PA) for 10 minutes

to disrupt the polysaccharide matrix and homogenize the bacteria into the media. After sonication, a 100 µL sample was taken from each well and serially diluted by factors of 10 across several culture tubes. Samples of 100 µL from each culture tube were spread across agar-filled petri dishes using glass beads, then incubated at 37 °C for 24 hours. Duplicate dilutions and plating were performed for every biofilm. Following incubation, the number of colonies on each agar plate were counted. The logarithm of the CFU concentration in the biofilm was then calculated using Equation 3.1:

$$\log\left(\frac{CFU}{cm^2}\right) = \log\left[(plate\ count) * 10^{Dilution\ Factor} * \left(\frac{5\ mL}{0.1\ mL}\right)/18.75\ \frac{cm^2}{slide}\right] \textbf{(Equation 3.1)}$$

where plate count is the number of colonies on a particular plate and dilution factor is the factor by which the original 100 µL sample was diluted before being spread across the agar plate. Only plate counts between 5 and 150 were used; in instances where more than one plate in a dilution series met this criterion, the one with the lower dilution factor was used.

3.2.7. Statistical Analysis

Statistical analysis was performed using JMP 11.2 statistical software. Means comparisons were performed using a one-way ANOVA Tukey-Kramer method with $\alpha = 0.05$. Average log(CFU/cm^2) values are arithmetic averages of all log(CFU/cm^2) values for all samples from a given time/temperature thermal shock combination, with the corresponding standard deviation.

3.2.8. Safety and Sterilization

All equipment that could be autoclaved was autoclaved at 121 °C and at pressures above 1 bar before each experiment to ensure a sterile environment. Autoclave indicator tape was used as a check to make sure that the equipment did reach the appropriate

temperature, if the tape's indicator marks turned black then the equipment should be sterile. Before autoclaving any equipment, the equipment was thoroughly cleaned and sealed. Liquids were autoclaved in autoclave safe bottles with the lids loose, to prevent expansion and potential pressure explosions, and immediately sealed after the cycle was done. Equipment such as the 4-well plates and the inoculum loops could not be autoclaved. The inoculum loops came in sterile packaging and were used only once, while the 4-well plates were bleached and cleaned with ethanol before and after each use. Any waste liquid was autoclaved in a loose topped bottle before cleaning and dumping the waste. All the autoclavable equipment was autoclaved after they were used and then cleaned to remove any leftover contaminants before autoclaving the equipment again for future sterile use. Non-liquid waste products were disposed of in a biohazard waste receptacle and all glass waste was disposed of in a biohazard glass bin. To ensure a more sterile environment for the experiments they were performed in a biosafety cabinet which was wiped down with ethanol before and after every experiment. In addition, the biosafety cabinet's ultra violet light was turned on for 5 minutes at the end of each day to kill off any remaining bacteria.

3.3. Results

3.3.1. Growth Study

Incubated at 37 °C, the lag phase for *P. aeruginosa* was less than two hours, followed by an exponential growth phase plateauing approximately 24 hours after inoculation. Bacterial concentration from 24 to 36 hours post-inoculation was constant at 1.6 (± 0.2) x 10^9 CFU/mL (n = 7).

3.3.2. Drip Flow Reactor Biofilms

Biofilms cultured in drip flow reactors were thicker (50-150 μm) and more carpetlike, as shown in Figure 3.2, than biofilms grown in shaker plates.[121] Moreover, their bacterial concentrations were much higher, permitting quantification of the large CFU reductions observed after thermal shock of the shaker plate biofilms. Ninety-six control biofilms were thermally 'shocked' at 37 °C (*i.e.* no actual temperature change) for exposure times of 1, 2, 5, 10, 15, 20, or 30 minutes. Their average log(CFU/cm^2) following this treatment was 8.56 (0.66 SD), 2.3 orders of magnitude larger than the previously grown shaker-plate biofilms,[121] again with no apparent dependence on exposure time (Figure 3.3).

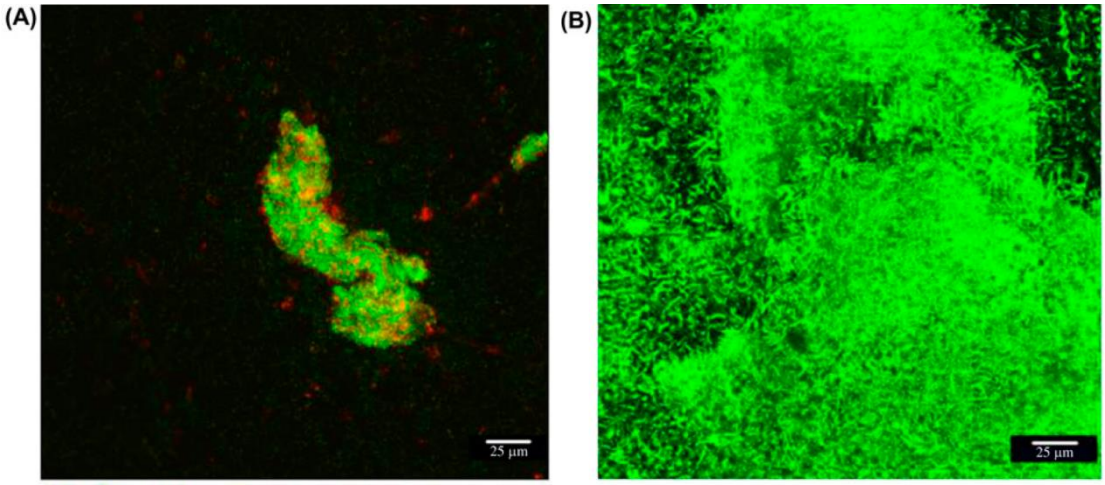

Figure 3.2: Confocal Images of a Shaker Plate Biofilm and a Drip Flow Reactor Biofilm. *CLSM images show the differences in the two biofilm controls with green indicating the live bacteria and red indicating the dead bacteria. The shaker plate biofilms (A) were smaller with thicknesses from 25 to 45 μm while the DFR biofilms (B) had thicknesses of 50 to 150 μm and carpeted the surface.*

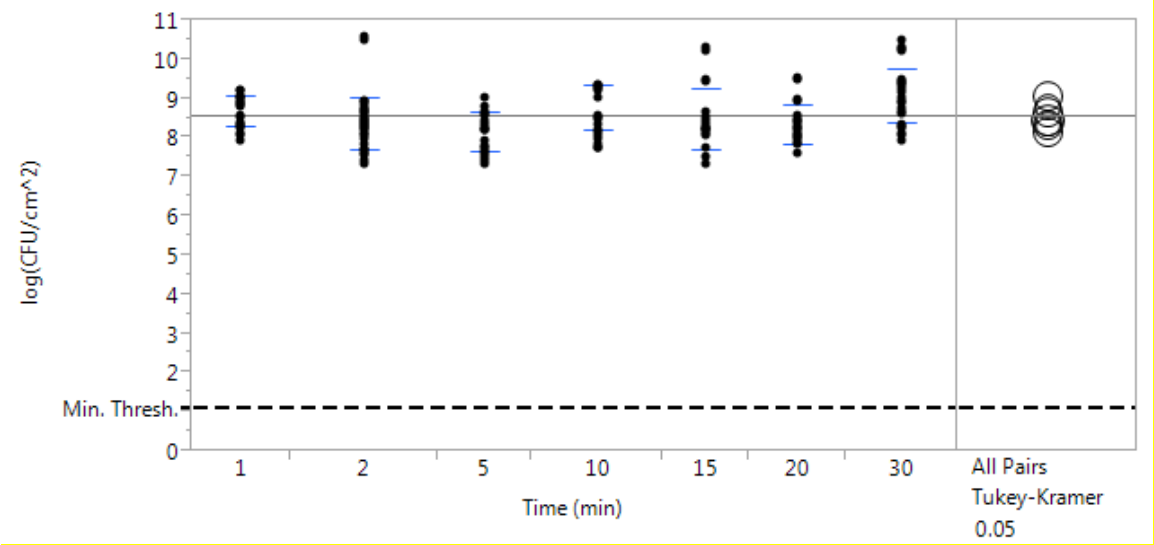

***Figure 3.3: Effect of Exposure Time on the Control Trials (37 °C)**. The "thermal shocks" were done at 37 °C for 1, 2, 5, 10, 15, 20, and 30 minutes. The data was analyzed via a one-way ANOVA Tukey-Kramer statistical analysis (α=0.05) and the means were found to be not statistically different from one another resulting in an overall average of 8.56 log(CFU/cm^2). The blue bars represent the standard deviation and the minimum quantification threshold is 1.12.*

Table 3.1 lists the average log(CFU/cm^2) at each temperature/exposure time combination, with a minimum of 9 biofilms per combination and an average n = 13.6 biofilms. CFU reductions of up to six orders of magnitude are observed, with CFU/cm^2 concentrations still well above the quantification limit, as indicated in Figure 3.4.

Table 3.1: Heat Shock Results from Biofilms Grown in a DFR. *The average log(CFU/cm^2) is reported in this table with the standard deviation (n≥9) represented via the ±.*

Average log(CFU/cm^2) ± Standard Deviation							
Thermal Shock Temp. (°C)	**Exposure Time (min)**						
	1	**2**	**5**	**10**	**15**	**20**	**30**
37	8.68 ± 0.38	8.37 ± 0.68	8.15 ± 0.51	8.79 ± 0.58	8.46 ± 0.78	8.34 ± 0.48	9.08 ± 0.70
50	8.21 ± 0.29	8.07 ± 0.50	7.65 ± 0.62	7.41 ± 0.27	7.66 ± 0.55	6.92 ± 0.61	6.88 ± 0.64
60	7.38 ± 0.59	7.47 ± 0.79	5.59 ± 0.78	5.32 ± 1.38	5.03 ± 0.87	4.14 ± 0.50	4.69 ± 0.76
70	6.13 ± 0.65	4.92 ± 0.65	4.51 ± 0.93	3.99 ± 0.59	3.63 ± 0.55	4.38 ± 0.77	3.69 ± 0.72
80	4.66 ± 0.69	4.36 ± 1.09	3.64 ± 0.76	3.23 ± 0.22	4.21 ± 0.60	3.21 ± 0.62	2.58 ± 0.61

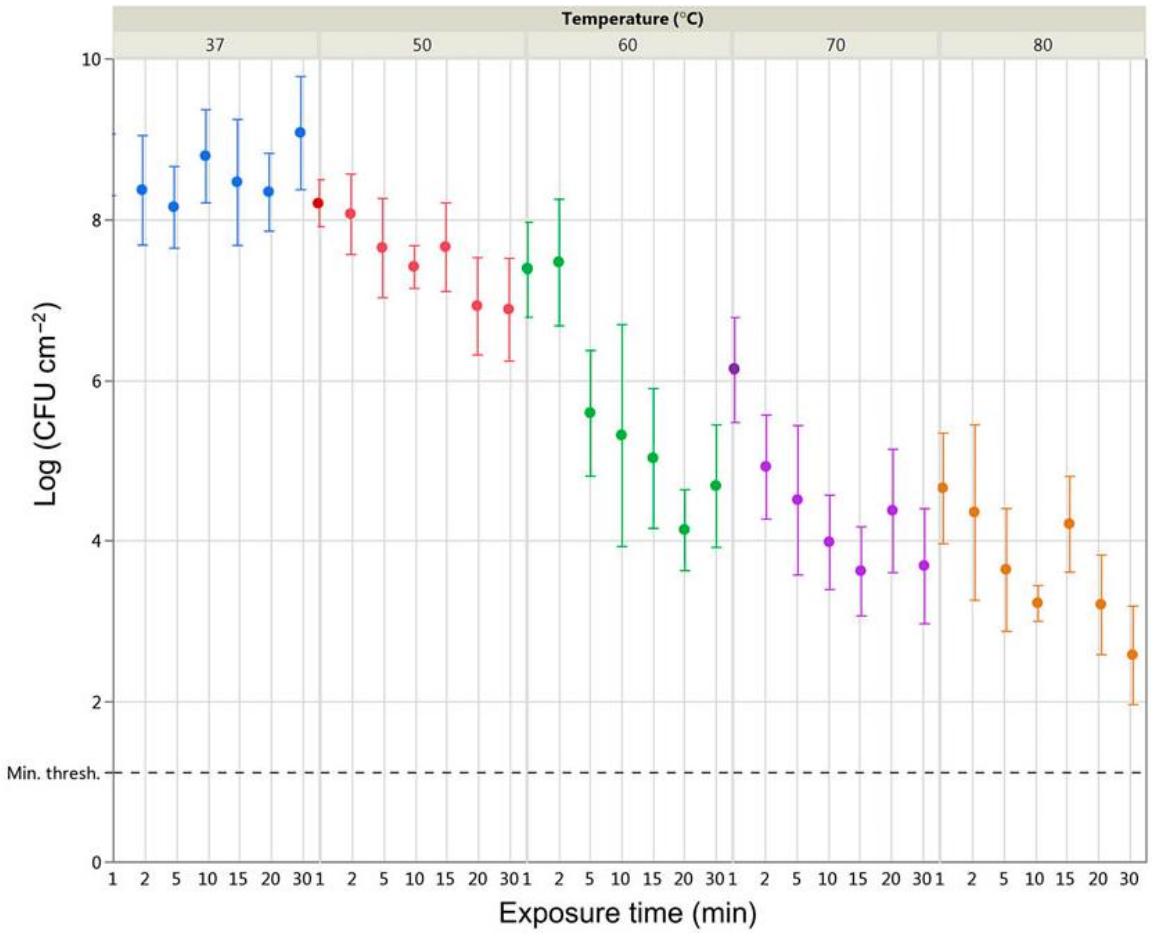

Figure 3.4: Average log(CFU/cm^2) For Each Temperature and Exposure Time*. The minimum quantification threshold indicated by the dashed line is 1.12 and the error bars represent the standard deviation (n≥9) of the log(CFU/cm^2) mean.*

3.4. Discussion

A wide variety of approaches to biofilm mitigation have been investigated, with most reporting CFU decreases of 1-2 orders of magnitude and it is unclear how these would be implemented *in situ*. Thermal biofilm mitigation, however, demonstrated CFU reductions of up to six orders of magnitude, necessitating the use of biofilms with much higher initial bacterial loads in order to fully quantify the reduction. The quantification limit was set to keep a single CFU from altering the calculated bacteria concentration by

more than 20%. Hence the plate count in Equation 3.1 must be at least five. Homogenizing an entire 18.75 cm^2 biofilm into 5 mL of media and plating 100 µL of the suspension on an agar plate, at least 13.3 CFU/cm^2 (log(CFU/cm^2) = 1.12) must be present to produce five colonies on average. With this quantification limit, the previously grown shaker plate films could demonstrate at best (6.24 – 1.12 =) 5.12 orders of magnitude reduction in bacterial load.[121] In practice, the observable range is smaller as any variability would otherwise push some results below the quantification limit. To fully quantify the reduction in log(CFU/cm^2), drip flow reactor biofilms (with initial log(CFU/cm^2) of 8.56) were required, though this load may be much higher than in a typical clinical infection.

Regarding *in situ* implementation, there are a variety of means for delivering heat at the precise location of the biofilm infection. One approach is to coat the implant with a magnetically susceptible composite. Any biofilm colonizing the implant would be in direct contact with the coating, which could apply the necessary temperature wirelessly on demand from an external alternating magnetic field. A magnetic nanoparticle and polymer composite coatings capable of achieving 80 °C in 15 s under static tissue have recently been reported.[122] As with pasteurization of planktonic bacteria, a continuum of temperature and exposure time combinations can be used to achieve a target CFU reduction. To interpolate the combination that will achieve the CFU reduction while minimizing damage to adjacent tissue, clear understanding of each parameter's role is needed. This research aims to assist in that understanding.

Table 3.1 indicates that increasing either exposure time or temperature decreased log(CFU/cm^2), however, increasing temperature had a much larger impact than increasing time over the range investigated. The effect of exposure time on the resulting

log(CFU/cm^2) was not statistically different or significant using a one-way ANOVA Tukey-Kramer method, see Figure 3.5A. However, with the same statistical test temperature versus log(CFU/cm^2) did show a statistical difference, see Figure 3.5B.

3.4.1. Correlation to Temperature Increase

Correlating the results with an analytical expression yields a similar conclusion. Linear regressions of log(CFU/cm^2) versus temperature increase at each exposure time yield tight correlations with R^2 values above 0.92 for all but two exposure times. Moreover, the deviations from linearity do not follow a clear trend suggesting any mathematical modification to the linear relationship, as shown in Figure 3.6. The intercepts of these regressions, however, should equal the log(CFU/cm^2) of the control experiments, where the temperature increase is zero. Pinning the intercepts of these regressions to the overall average control log(CFU/cm^2) of 8.553, the regressions maintain an average R^2 value of 0.85 as shown in Figure 3.7.

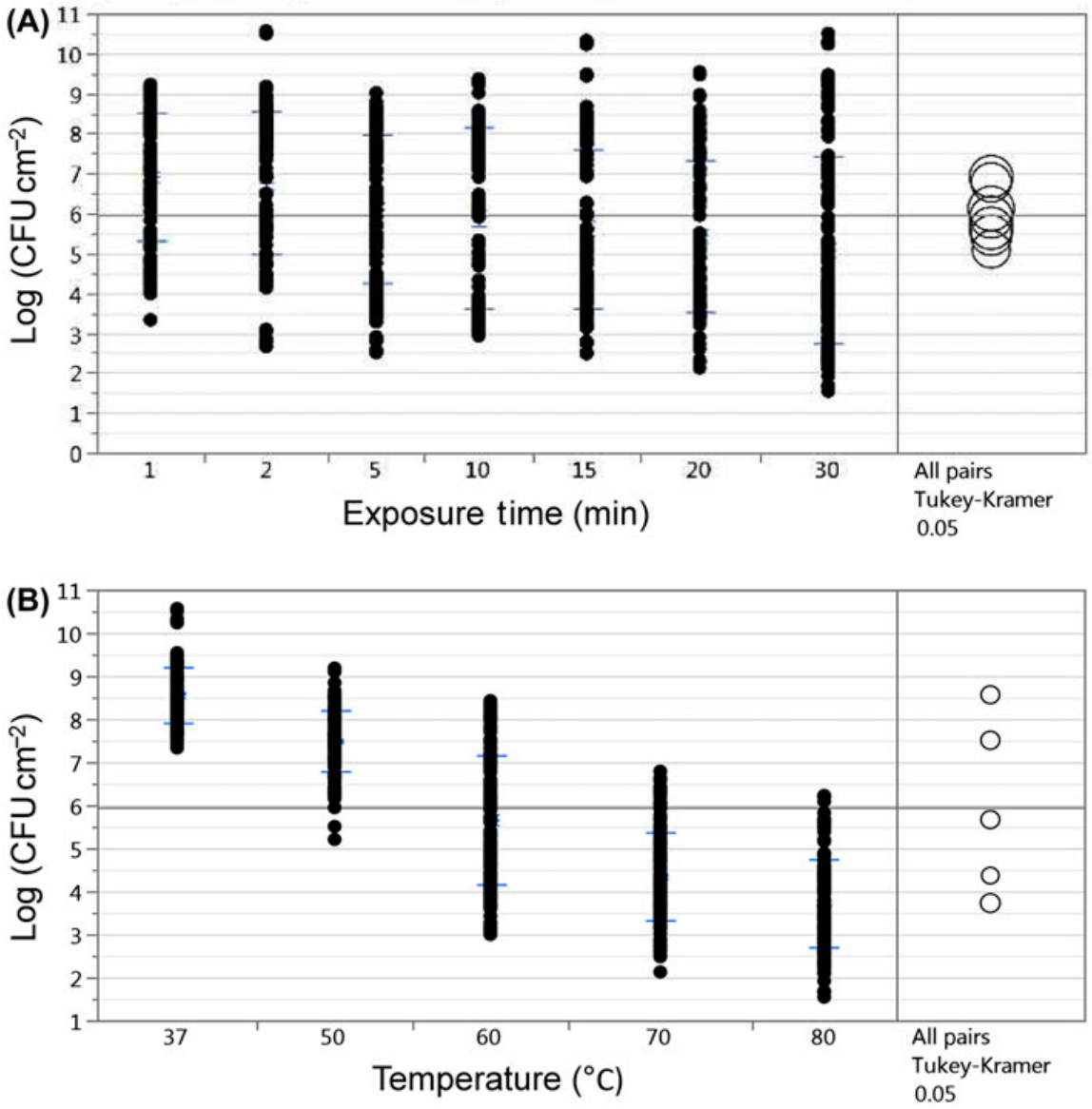

Figure 3.5: Analysis on (A) Exposure Time and (B) Temperature. *The log(CFU/cm^2) was affected by both the exposure time and the temperature, however, using a one-way ANOVA Tukey-Kramer analysis (α=0.05) the temperature had a greater effect overall.*

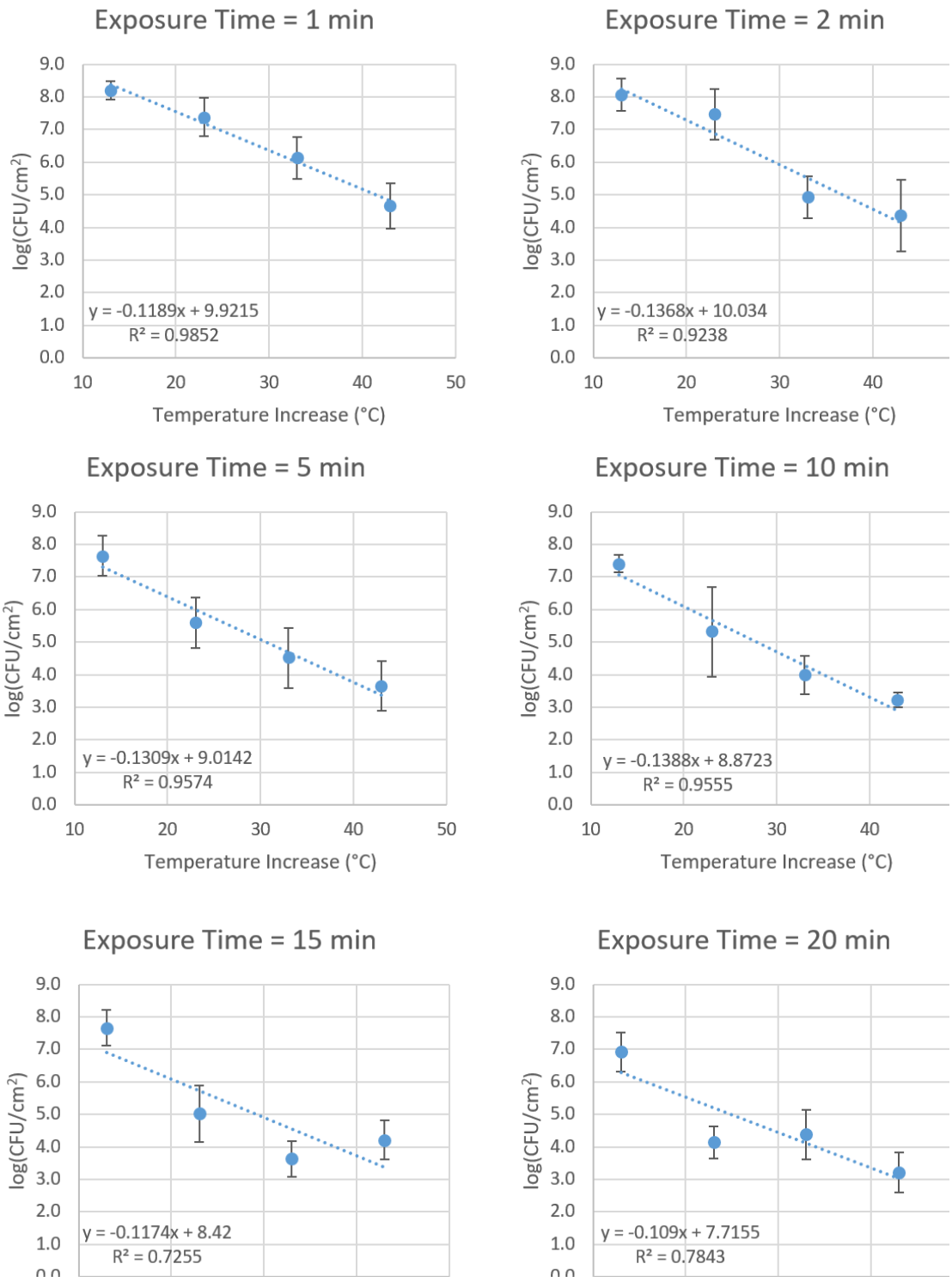

Figure 3.6: Average log(CFU/cm^2) versus Temperature. *Each exposure time had a unique dependence on the temperature. Error bars indicate the standard deviations.*

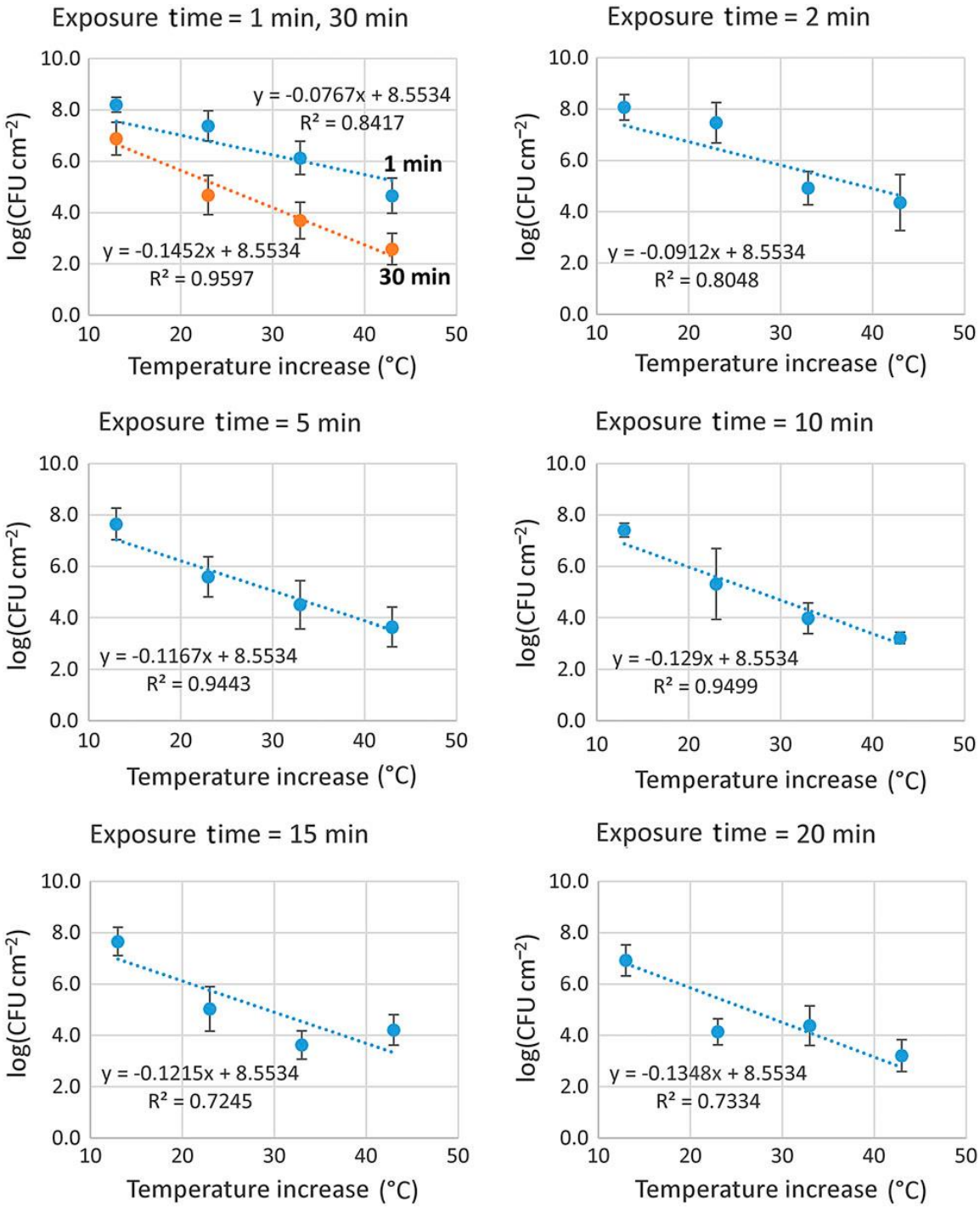

Figure 3.7: Correlation of log(CFU/cm^2) with Temperature Increase. *Each average log(CFU/cm^2) showed good correlation to the temperature increase even with the intercept pinned at 8.56 log(CFU/cm^2), the average of the control trials. Error bars represent the standard deviation.*

3.4.2. Correlation to Exposure Time

The relationship between log(CFU/cm^2) and exposure time does not appear to be best represented by a linear expression, however. Figure 3.8 compares linear correlations (left-hand-side) with logarithmic correlations (right-hand-side) indicating that log(CFU/cm^2) more closely correlate with log(exposure time) than with exposure time directly. One datum (80 °C, 15 min) is over a standard deviation away from both the linear and logarithmic trendlines, and therefore excluded from the analysis to provide a clear comparison. When included, the logarithmic correlation is still closer than the linear one.

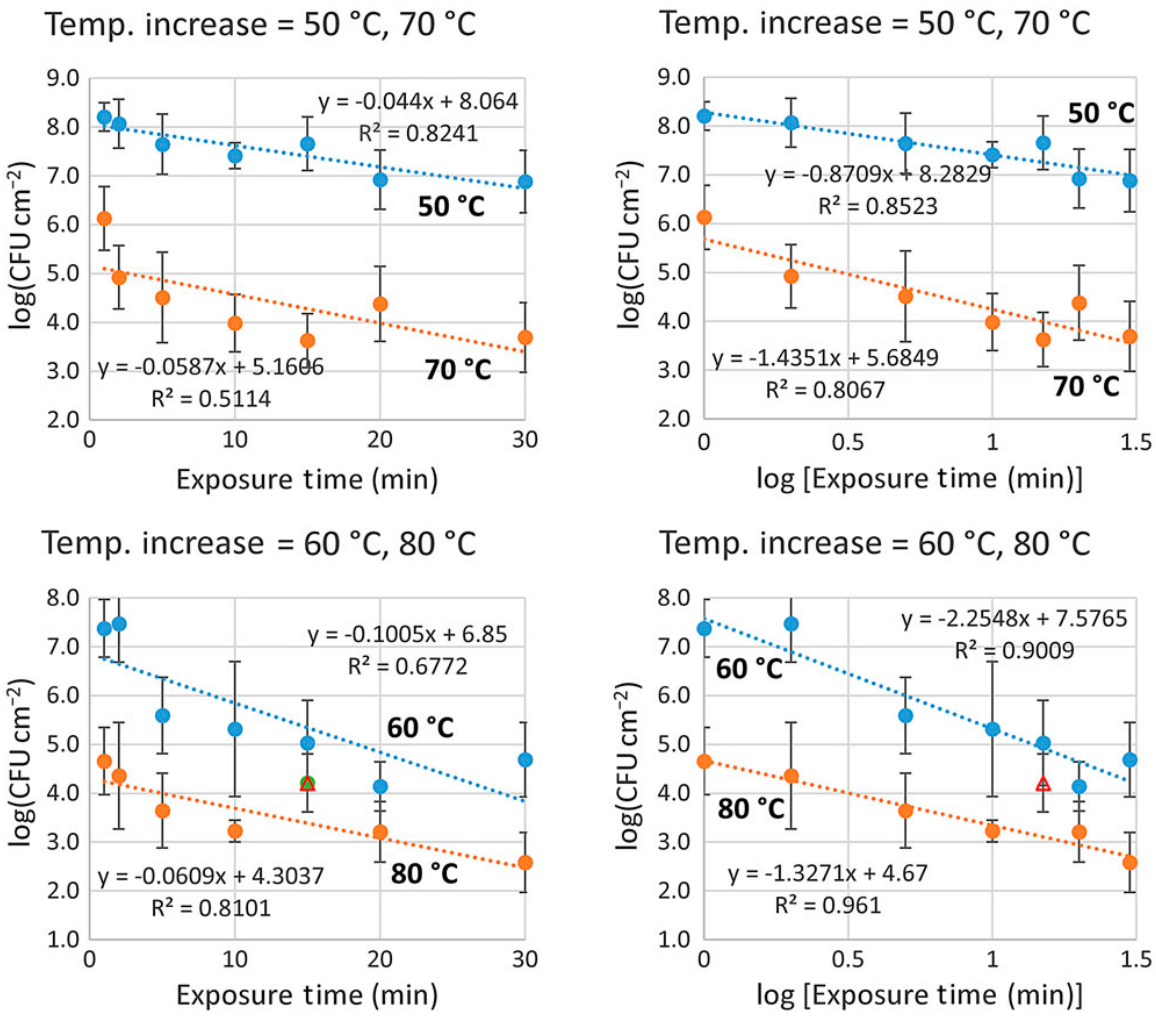

Figure 3.8: Correlation of log(CFU/cm²) with the Exposure Time. *The remaining bacterial density count corresponds more to the log(exposure time), seen on the right, than the linear exposure time, seen on the left. The triangle at 80 °C for 15 minutes was excluded for clarity with R^2 values of 0.6572 for the linear regression and 0.6741 for the logarithmic regression when included.*

3.4.3. Combined Correlation to Temperature Increase and Exposure Time

Figure 3.7 correlates log(CFU/cm^2) to temperature increase in the form

$$\log(CFU/cm^2) = \log(CFU/cm^2)_0 + slope * (T - 37°C) \qquad \textbf{(Equation 3.2)}$$

where $log(CFU/cm^2)_0$ is the overall average control value at 37 °C of 8.553 and T is the thermal shock temperature in °C. The slopes from these regressions at each exposure time

are compiled in Table 3.2. Plotting these slopes versus log(exposure time), we see a clear linear relationship (Figure 3.9) with an R^2 of 0.95.

Table 3.2: Slope of log(CFU/cm^2) Versus Temperature Increase. *Slopes obtained from Figure 3.7 when compiled reveals a correlation with exposure time.*

Exposure time (min)	Slope	R^2
1	-0.0767	0.9852
2	-0.0912	0.9238
5	-0.1167	0.9574
10	-0.1290	0.9555
15	-0.1215	0.7255
20	-0.1348	0.7843
30	-0.1452	0.9620

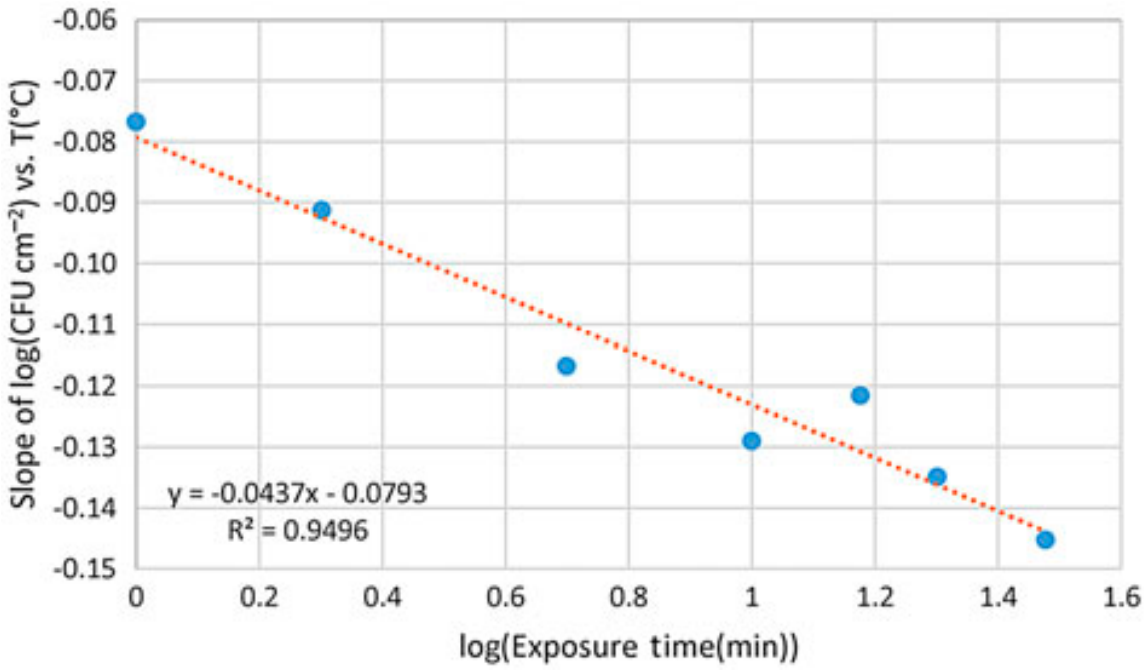

Figure 3.9: Correlation of Cell Death Temperature Dependence to log(Exposure Time).

Equation 3.3 was made as a function of thermal shock temperature and exposure time from the slope and intercept from Figure 3.9:

$$\log(CFU/cm^2) = \log(CFU/cm^2)_0 - [0.079 + 0.044\log(t)](T - 37) \quad \textbf{(Equation 3.3)}$$

where T is the thermal shock temperature in °C and t is the exposure time. Equation 3.3 may also be expressed:

$$(CFU/cm^2) = (CFU/cm^2)_0 * 10^{-0.079(T-37)} * t^{-0.044(T-37)} \quad \textbf{(Equation 3.4)}$$

which more clearly shows a modified Arrhenius dependence on temperature. However, not only is there no discernable lag time in cell death, the relationship to exposure time follows a Weibull-style relationship, while planktonic bacterial death is traditionally modeled with a linear relationship between log(CFU/cm^2) and time.[123] Moreover, the thermal shock temperature affects even this relationship, with higher temperatures prompting a stronger time dependence not just as a coefficient but also as an exponent. Figure 3.8 demonstrates that log(CFU/cm^2) is much more linearly related to log(t) than to t.

Comparing each experimental result from Table 3.1 with the corresponding calculation from Equation 3.3, we see that Equation 3.3 predicts the experimental log(CFU/cm^2) with an accuracy exceeding the precision of the experimental measurements. In all but nine instances, the calculation from Equation 3.3, seen in Table 3.3, is within one standard deviation of the experimental mean. The difference between the calculated and experimental log(CFU/cm^2) values are shown in Table 3.4.

Table 3.3: Log(CFU/cm^2) Calculated by Equation 3.3.

Thermal Shock Temp. (°C)	Exposure Time (min)						
	1	**2**	**5**	**10**	**15**	**20**	**30**
37	8.55	8.55	8.55	8.55	8.55	8.55	8.55
50	7.52	7.35	7.13	6.95	6.85	6.78	6.68
60	6.73	6.43	6.03	5.72	5.55	5.42	5.24
70	5.94	5.50	4.93	4.49	4.24	4.06	3.81
80	5.14	4.58	3.83	3.26	2.93	2.70	2.37

Subtracting these values from the experimental results in Table 3.1:

***Table 3.4*: Deviation Between Experimental and Calculated Log(CFU/cm^2).** *Highlighted cells indicate conditions where the deviation between experimental and calculated log(CFU/cm^2) exceeds one standard deviation of the experimental result.*

Thermal Shock Temp. (°C)	Exposure Time (min)						
	1	**2**	**5**	**10**	**15**	**20**	**30**
37	0.13	-0.19	-0.40	0.24	-0.09	-0.21	0.52
50	0.68	0.72	0.52	0.46	0.80	0.14	0.20
60	0.65	1.04	-0.43	-0.41	-0.52	-1.28	-0.56
70	0.19	-0.58	-0.42	-0.51	-0.61	0.32	-0.12
80	-0.49	-0.22	-0.19	-0.04	1.28	0.51	0.21

The average of the absolute value of the deviation is 0.45, indicating that on average, Equation 3.3 correctly calculates the post-thermal-shock bacterial load to within a factor of 3 (*i.e.*, less than half an order of magnitude), across the entire relevant parameter space. To place this in context, average of the experimental standard deviations is 0.65. In all but 9 of the 35 entries, Equation 3.3 calculates the resulting log(CFU/cm^2) within one standard deviation of the experimental average. There is no apparent pattern to either the experimental standard deviations in Table 3.1 or the deviation between experimental and calculated averages in Table 3.4, though the incidences of the latter exceeding the former do appear more often at lower temperatures, as indicated by the highlighted cells in Table 3.4.

3.4.4. Implications

For thermal mitigation of medical implant infections, the thermal shock can be applied directly by the substrate on which the biofilm is growing. While the maximum temperature will be experienced by the biofilm itself, heat will likely conduct into the surrounding tissue and damage it. This damage should be viewed in the context, however, of the current treatment, which is explantation surgery and removal of the surrounding tissue, followed by reimplantation surgery with a higher degree of infection. Besides all the other disadvantages to this treatment (extended hospitalization, time without a needed medical device, loss of alignment markers for joint implants, etc.) the tissue damage from the current treatment is significant. Importantly, the presence of a coating which can supply a thermal shock does not commit the patient to using thermal mitigation if an infection is diagnosed; it would only be applied if it were deemed better than the alternatives. There is the potential for damage to the surrounding tissue from the heated device, however, the

overall damage in comparison to the explantation method is minor. Additionally, the temperature drops off quickly as it travels away from the device surface minimizing its total potential damage.[112]

To determine an appropriate exposure protocol and make that decision, the effects of both temperature and exposure time must be understood. Standard conduction of heat into the surrounding tissue depends linearly on the applied temperature, and decreases with the square root of time as the penetration distance increases. As the cell death relationship expressed in Equation 3.3 has a larger dependence on temperature and a smaller dependence on time, these results indicate that to minimize damage to the surrounding tissue while achieving a set degree of bacterial death, higher temperatures at lower exposure times may be preferred. Investigations on whether antibiotics decrease the thermal shock required to achieve a set degree of bacterial death can be viewed in Chapter 7.

There are also many instances beyond the field of medicine where biofilm mitigation is necessary but conventional *ex situ* treatments such as autoclaving are not viable. Plastics with glass transition temperatures below 120 °C cannot be autoclaved, and may have surfaces inaccessible to UV light or antimicrobial chemicals. The current work provides a framework for thermally mitigating these biofilms at more accessible temperatures.

3.5. Conclusions

Infection of newly implanted medical devices by bacterial biofilms is a severe problem with no immediate solution. The increased chemical resistance of bacteria in biofilms, along with the continued evolutionary resistance of bacteria in general, make

chemical approaches problematic. Similarly, the diverse chemical environment of the body has confounded material-based approaches to non-fouling surfaces. Thermal shock of bacterial biofilms, however, can reduce their populations by six orders of magnitude at temperatures not exceeding 80 °C. The decrease in cell viability in *P. aeruginosa* bacterial biofilms has been experimentally determined for temperatures ranging from 50 to 80 °C and exposure times ranging from 1 to 30 min. These results have been correlated with an analytical expression which on average calculates the resulting bacterial loading to within a factor of three across the entire parameter space. The results indicate temperature has a larger effect than exposure time on biofilm cell death. With the development of implant coatings which can provide on-demand heating directly at the infection site, thermal mitigation should be a viable treatment strategy for medical implant infections.

CHAPTER 4: MICROSCOPY OF THE DRIP FLOW REACTOR BIOFILMS

4.1. Introduction

Once a biofilm grown in a drip flow reactor has been treated the biofilm is normally analyzed via sonication to disperse the bacteria into a homogenous mixture, serially diluted and each dilution plated. This, however, takes a lot of time (an hour per variable investigated), resources (2 agar dishes, 16 pipet tips, 8 dilution tubes, and 15 mL TSB per variable investigated), and the results cannot be read until the following day once the bacteria have grown enough to have visual colony forming units to count. An alternative analysis is the use of dyes in a confocal laser scanning microscopy (CLSM) and an objective thresholding system which allows for rapid analysis and minimal resources. CLSM is an optical microscopy technique that fluoresces the desired dye with a laser and then collects the information through a pinhole. The pinhole decreases the range of depth to a given layer eliminating the layers above and below the layer of focus.[124,125] Multiple dyes that are excited and fluoresce at different wave lengths can be used simultaneously to identify different aspects of the biofilm, such as a dye used to visualize the dead cells and a dye to visualize the live cells.[124,126] Using this technique biofilms can be scanned layer by layer to form a more detailed schematic and visual of the biofilm's live cells and dead cells.[127–132] Once the images are captured they can be analyzed via thresholding and the pixels counted.[126,133,134]

Ideally the pixels could be counted directly without any thresholding. If each bacterium were to be the size of one pixel and each bacterium obtained the same amount

of dye and therefore fluoresced with the same intensity, then pixel counts would be quite straightforward and easy. However, in reality the bacteria vary in size and may be located halfway or partially in different pixels. Additionally, the dyes do not always fluoresce evenly nor dye the bacteria consistently. There is also the problem of stray light coming from above or below the plane of interest which is dimmer, but still present. These complications create a range of pixel brightness from no light to very bright light and determining which should be counted as a bacterium can be difficult. Due to these challenges the bacteria in the biofilm become much more difficult to count from microscopy images and applying a rubric to determine which pixels to count becomes necessary, this is called thresholding.

Thresholding is a very important image technique to create images that are readily analyzed. Thresholding is a means of segmenting a gray scale image into a binary image with all the pixels brighter than a set constant becoming white and all the darker pixels than the threshold becoming black. This segmentation allows for a pixel counter to quantify the number of black or white pixels of each dye allowing for a percentage of live to dead bacteria to be counted.[126,133] The highest quality thresholds occur when the histogram of pixel brightness intensity yields two distinct peaks with a wide valley since this provides a clear separation point, seen in Figure 4.1. However, this is not as common as one would desire. Many images have more overlap or no distinction between the peaks (Figure 4.2) making thresholding a challenging feat. Since this is more common many people have explored thresholding through extensive mathematical image analysis.

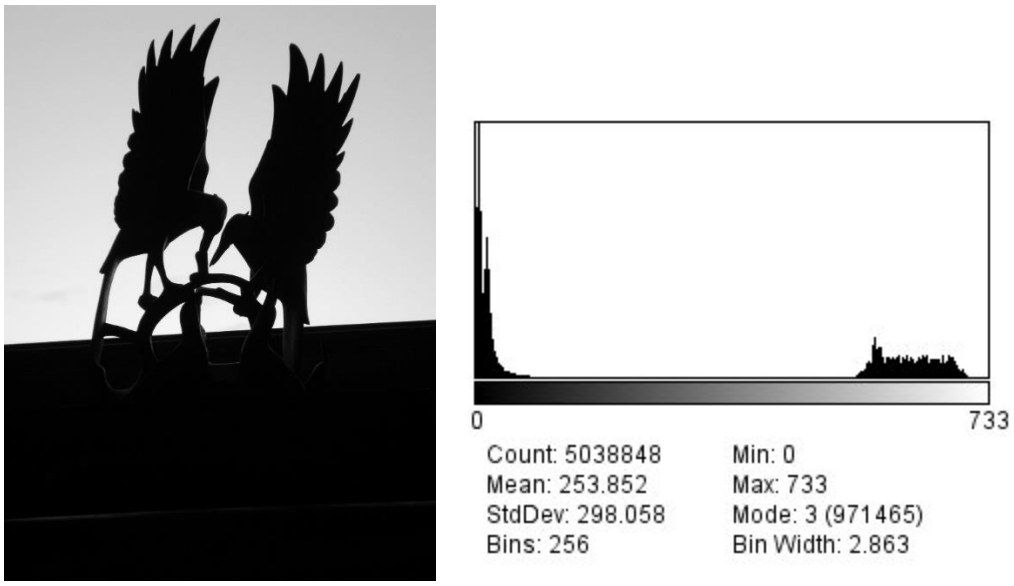

Figure 4.1: Silhouette Image and the Gray Scale Histogram of the Image*. The silhouette of a statue against a bright sky provides an ideal histogram with a distinct peak for the lighter and darker pixels with a large value in between the peaks. Due to the ease of separation between the pixel groups this image is simple to threshold.*

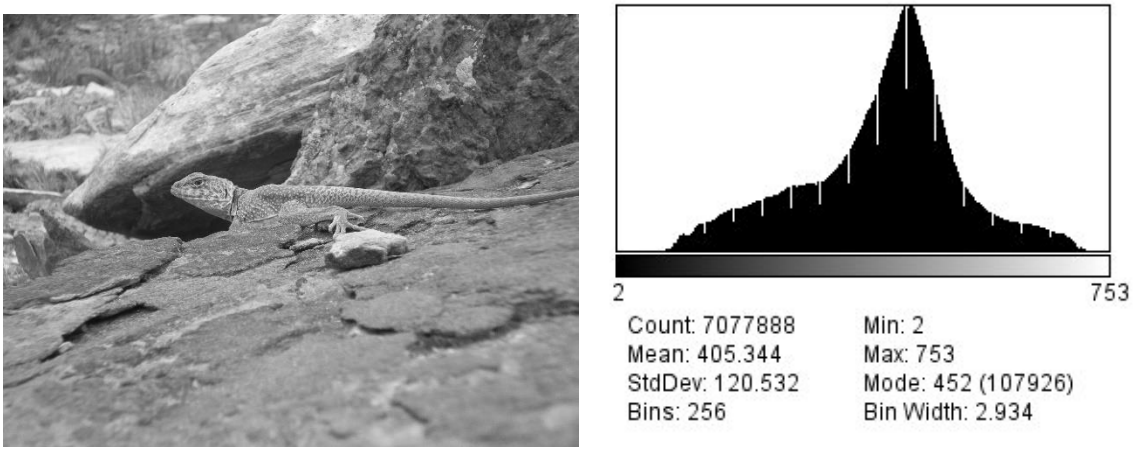

Figure 4.2: More Complex Image and the Gray Scale Histogram of the Image. *The picture of the lizard on the rock taken in Southern Colorado has little distinctions in the light and dark pixels creating a histogram with no clear separation point, making the threshold value very difficult to determine.*

There are many different approaches to objective thresholding that have been explored; however, most of them take long computing time which may be infeasible for

when each biofilm must be characterized by multiple stacks of high-resolution images. One method that is commonly used is the Otsu method, a probability calculation to determine maximum separation of the two histogram peaks. However, this method does not always work well when the histogram is too continuous and then has a small peak at an extreme, such as seen in Figure 4.3. It can be observed that the snow on the front of the main mountain top is not sorted as a white pixel, but rather a black pixel, demonstrating the limits of the Otsu method. However, in cases with more separation, such as Figure 4.4, the Otsu method sorts the pixels quite well.

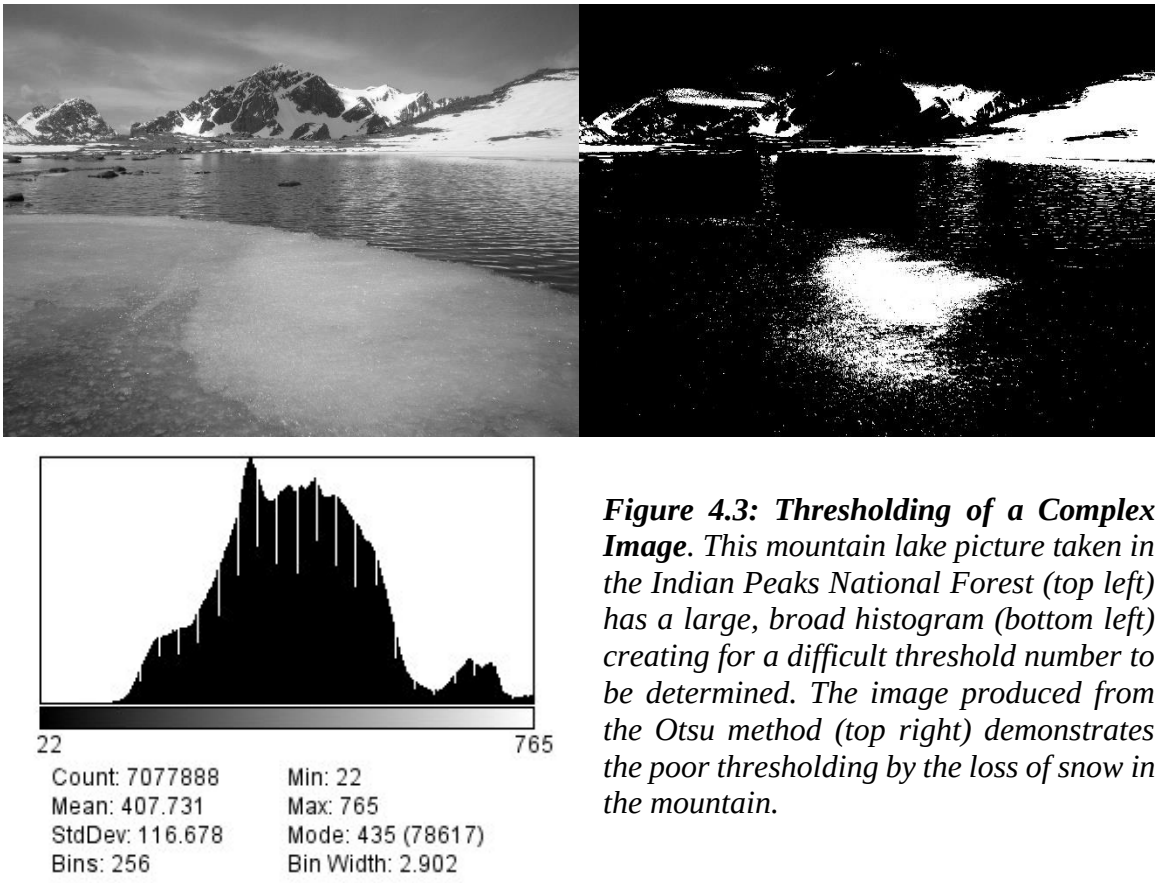

***Figure 4.3: Thresholding of a Complex Image**. This mountain lake picture taken in the Indian Peaks National Forest (top left) has a large, broad histogram (bottom left) creating for a difficult threshold number to be determined. The image produced from the Otsu method (top right) demonstrates the poor thresholding by the loss of snow in the mountain.*

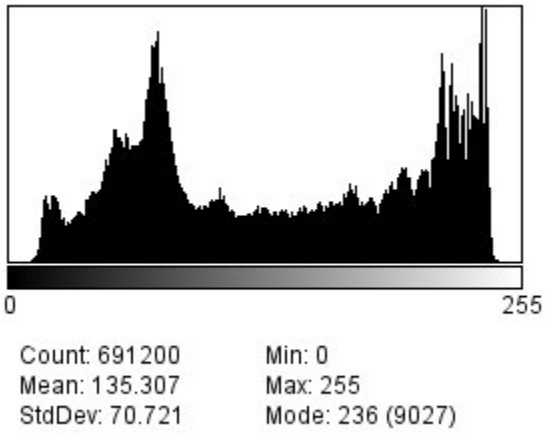

Figure 4.4: Thresholding of a Less Complex Image*. The image taken from my grandparent's wedding (top left) provides a good example of an image that contains plenty of contrast between the lighter and darker pixels to provide two main peaks seen in the histogram (bottom left). This more bimodal histogram made for easier thresholding analysis to produce a cleaner image using the Otsu method (top right).*

With the limits of the Otsu method many researchers have been exploring other means of objectively thresholding their images.[126,133,135] One method that is faster and more efficient than the Otsu method is to iteratively find the midpoint between the average bright and dark intensities.[126] After guessing an initial threshold intensity to categorize each pixel into either the bright or dark group, the average intensity of each group is calculated and

the midpoint between these group average intensities becomes the new threshold intensity for repeating the calculation, until the threshold intensity converges on a final value.

This chapter investigates the efficacy of the Otsu method and the iterative method by comparing the results to the plated values obtained from parallel biofilm cultures and thermal shocks. Additionally, a key advantage to microscopy is the data-rich information it yields from live-dead quantification to morphology and architecture. Microscopy shows the size and shape as well as the population distribution across the biofilm. The biofilms in this chapter prove to be mature biofilms with unique architectural and morphological elements.

4.2. Materials and Methods

4.2.1. Biofilm Growth

An agar plate was streaked with *Pseudomonas aeruginosa* PAO1 bacteria and grown at 37 ºC for 24 hours in an incubator. An inoculum was made by taking two colonies from the plate and placing them into a tube containing 5 mL of growth medium, tryptic soy broth, and allowed to grow for 24 hours at 37 ºC. A drip flow reactor with 4 wells (Biosurface Technologies, Bozeman, MT, USA) was used for the biofilm growth and each well contained a microscope slide inoculated with 1 mL of the inoculum. The bacteria were allowed to grow and start to form a biofilm in batch mode at 37 ºC for 4 hours. Once the batch mode was complete tryptic soy broth was pumped into the drip flow reactor over one day at a rate of 5 L/day using a rotary pump.

4.2.2. Heat Shocking the Biofilms

To obtain the time and temperature profile, the biofilms underwent heat shocks in 10 mL wells of water placed in a water bath. This set up ensured uniform heating of the biofilms. A temperature range of 37 ºC to 80 ºC and a time range of 1 minute to 30 minutes were explored. The time trials were broken down into runs of 1, 2, 5, 10, 15, 20, and 30 minutes and the temperatures broken down into runs of 45 ºC, 50 ºC, 60 ºC, 70 ºC, and 80 ºC. A control was run at 37 ºC, body temperature. A 4-well plate with 5 mL of water in each well was held at the heat shock temperature in the water bath and was removed momentarily to install the biofilm slides and temperature probes. Two thermocouples were placed in each well and closely monitored to ensure uniform heating of each well. Once the desired time had been reached the biofilms were then swiftly transferred to another 4 well plate containing 5 mL of room temperature water to abruptly end the heating. For more information on this technique see Chapter 3.

4.2.3. Enumeration

For direct enumeration, the 4 well plate containing the biofilms was sonicated for 10 minutes to ensure that the biofilm was effectively redistributed into suspension for uniform dilutions. Up to 8 dilutions in 5 mL tubes containing tryptic soy broth were plated onto agar gel plates and incubated for 24 hours at 37 ºC. The colony forming units (CFU) on each plate were counted and recorded at each dilution to determine the order of magnitude of the population reduction, or the log reductions. Dilutions of the biofilms determined how many CFU were present and determined that the biofilms were grown uniformly from one experiment to the next. For more information on this see Chapter 3.

4.2.4. Microscopy Methods

The biofilms were imaged using a confocal laser scanning microscope to be used for same day analysis. Using a LIVE/DEAD BacLight Bacterial Viability Kit (Invitrogen, Eugene, OR, USA) containing SYTO 9 and propidium iodide fluorescent dyes with the Bio-Rad Radiance 2100 confocal microscope (Bio-Rad laboratories, Hercules, CA, USA) allowed a fluorescent distinction between cells that were dead and cells that were still viable. The SYTO 9 enters all the bacterial cells and binds to the DNA, while propidium iodide enters cells with disrupted membranes and quenches the SYTO 9 and binds to the DNA of those cells. Bacterial cells that fluoresced red from the propidium iodide dye were dead and cells that fluoresced green, from the SYTO 9, were live cells. Four-well dishes with 5 mL of water per well with 5 µL of each dye per well were prepared during the heat shock (see Chapter 3 for heat shock specifications) and kept out of direct light. After the heat shock the biofilms were transferred to the prepared wells and quickly covered to minimize the light exposure. The samples were imaged on a top-down Bio-Rad Radiance 2100 confocal microscope 15 minutes after the biofilms were exposed to the dyes. The biofilms were imaged using a 40x water-immersion lens with Kr/Ar lasers emitting at 488 and 568 nm to excite the SYTO 9 and propidium iodide dyes, respectively. Images were collected starting from the substrate and then moving up to the top of the biofilm in one micron increments, scanning each slice with one laser at a time to minimize the effect of excitation/emission overlap with a pinhole (iris) setting of 2.0 µm for each laser. A total of 3 scans for each horizontal slice section were averaged using the Kalman filtering to improve the image quality. The images were recorded in a 1024 x 1024 pixel array with 256 intensity levels. The pictures obtained from the microscope were then objectively

thresholded using the Otsu method in ImageJ and using an iterative method created in MATLAB to calculate a percent of viable cells. Confocal microscopy techniques not only allowed for a means of quantifying the percent of the bacteria alive, but also allowed for a visual understanding of the biofilm through planar cross sections of the biofilm from the substrate surface to the top of the biofilm. The compiled z-series were used to determine if the biofilms grown were mature biofilms based off of their growth shapes.

4.2.5. Otsu Method Formulation

The Otsu method was established by Nobuyuki Otsu in 1979 using a probability calculation paired with the variance calculation. Pixels are divided into two classes, a bright class (C_1) and a dark class (C_0), which are above and below the postulated threshold intensity T, respectively. This method works by separating dark and light pixels where the pixels that are considered the background (darker pixels), C_0, and pixels that are considered the foreground (lighter pixels), C_1, (or *vice versa*) are separated into $[1, \dots \dots T]$ and $[T + 1, \dots \dots L - 1]$, respectively, where T is the threshold. The average pixel intensity within each class ($\mu_0$and μ_1) is calculated and then an overall mean is calculated by

$$\mu = P_0(T)\mu_0(T) + P_1(T)\mu_1(T) \qquad \textbf{(Equation 4.1)}$$

where $P_0(T)$ and $\mu_0(T)$ are the fraction of total pixels and gray mean respectively of C_0 and $P_1(T)$ and $\mu_1(T)$ are the fraction of total pixels and gray mean respectively of C_1. The intensity variance within each class (σ_0^2 and σ_1^2) is then calculated and multiplied by the fraction of total pixels that are in that class and the sum of those two products gets the weighted intra-class variance, σ_ω^2,

$$\sigma_\omega^2(T) = P_0(T)\sigma_0^2(T) + P_1(T)\sigma_1^2(T) \qquad \textbf{(Equation 4.2)}$$

where $P_0(T)$ is the fraction of pixels in C_0, $P_1(T)$ is the fraction of pixels in C_1, and $\sigma_0^2(T)$ and $\sigma_1^2(T)$ are the variance of C_0 and C_1 respectively. The calculations are repeated with different values of T until a minimum value for $\sigma_\omega^2(T)$ is reached, the value of T at that minimum is the threshold intensity.

Alternatively, one could calculate the inter-class variance, σ_b^2,

$$\sigma_b^2(T) = P_0(T)(\mu_0(T) - \mu)^2 + P_1(T)(\mu_1(T) - \mu)^2 \qquad \textbf{(Equation 4.3)}$$

where μ is the overall average pixel intensity calculated in Equation 4.1. Repeating the calculations with different threshold values, T, until the inter-class variance is maximized will yield the same final threshold intensity. All of these calculations were performed on the open access ImageJ Otsu analysis.

4.2.6. Iterative Selection Method Formulation

In the Otsu method the histograms are not cleanly described by an analytical equation making the search protocol for finding the minimum and maximum difficult requiring a repeat of all the calculations of the threshold parameter space. The iterative method, by contrast, has a built-in search protocol to quickly converge on the threshold number and does not require variance calculations making the calculations faster and has been shown to most closely mimic human expert thresholding.[126] For this method, an iterative approach is used to determine the threshold number by the midpoint between the average intensities of the pixels above the threshold and below the threshold value. Using T as the threshold the average foreground intensity (μ_1), or pixels that fall in the gray scale above the threshold, is calculated along with the average background intensity (μ_0), the darker pixels that fall below the threshold. The average of these two class averages

becomes the new threshold value, T', where

$$T' = \frac{\mu_1 + \mu_0}{2} \quad \textbf{(Equation 4.4)}$$

and the calculations are repeated until the threshold value converges to the final threshold intensity. This method is much more computationally simple allowing for faster computation time. The MATLAB code for the thresholding sequence can be found in the appendix.

4.2.7. Safety Precautions

The same safety precautions were taken, as was stated in Chapter 3, for the bacteria and sterilization techniques. Additionally, the use of the propidium iodide and SYTO 9 dyes use DMSO, a potentially hazardous chemical that permeates nitrile gloves as well as skin. Great care was taken during the dyeing process of the biofilms, and in the case of any drops getting on a glove the gloves were swiftly removed and hands washed before donning a new set of gloves. During the microscopy procedure, the eye protecting sash was used to avoid eye damage from the lasers and eyes were kept on a different plane from the lasers.

4.3. Results and Discussion

4.3.1. Image Analysis Method Comparison to the Enumeration Analysis

As discussed in Chapter 3, the amount of viable bacteria post heat shock, colony forming units (CFU) per square centimeter, showed a clear decrease with the increase of the heat shock temperature. A similar trend was seen with an increase in the exposure time; overall, the longer the biofilms were exposed to the heat the more bacterial death was observed in the biofilms. Since the data used to determine this relationship were collected via enumeration which is a very time consuming process and does not allow for analysis

until the bacteria have grown into visible colony forming units (CFUs) the next day, microscopy was explored to get results that same day. The biofilms were dyed using SYTO 9 which permeates all of the bacterial cells and binds to the DNA fluorescing green, along with propidium iodide which only permeates the cells with poor membrane integrity and outcompetes the SYTO 9 for binding with the DNA, fluorescing red. The dyed biofilms were then imaged using a confocal laser scanning microscope (CLSM) which captured the live and dead cell images for each horizontal plane with one micron separations between each plane. Analysis of the images was performed with the Otsu method in ImageJ and the iterative method in MATLAB, see the appendix for the code. As seen in Figure 4.5 the control temperature, 37 °C, has relatively similar results between the two image analysis techniques with a plausible percent viable cells based on visual observations. However, as the temperature increases, the reliability of both image analysis techniques decreases greatly as most evident in Figure 4.6. This is especially pronounced since the enumeration is decreasing on a logarithmic scale while the microscopy image analyses are changing on a linear scale and do not always have a decrease when expected. Overall, the Otsu follows the enumeration trend more closely than the iterative method; however, with the scale differences this improvement is negligible.

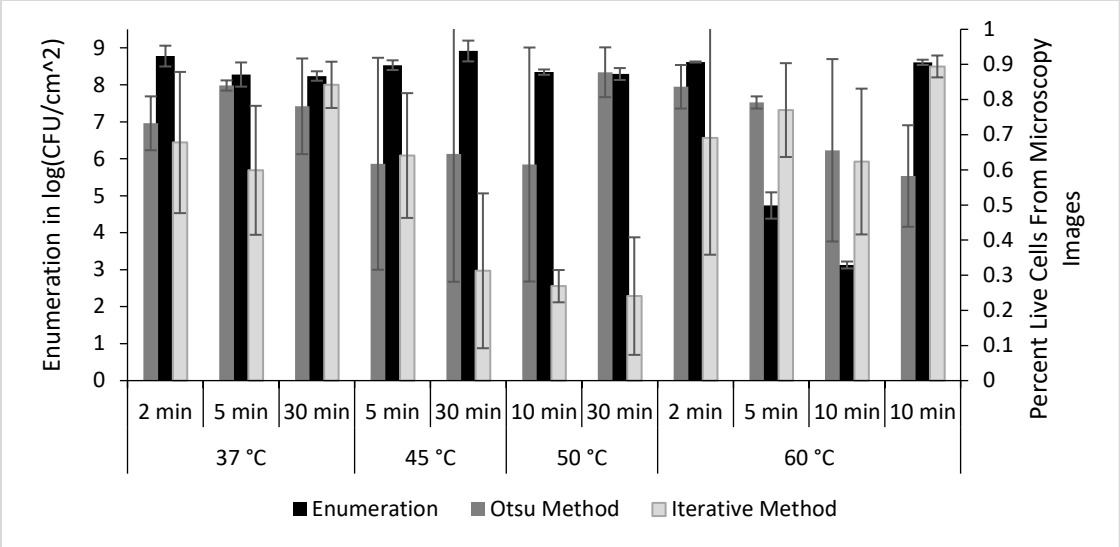

Figure 4.5: Comparison of the Enumeration and Image Thresholding Methods at Temperatures Ranging from 37 °C to 60 °C. *The enumeration method scaled logarithmically and via absolute population counts, left axis, while both microscopy image analysis techniques, the Otsu method and the iterative method, scaled linearly, via the percentage relative to the total, right axis.*

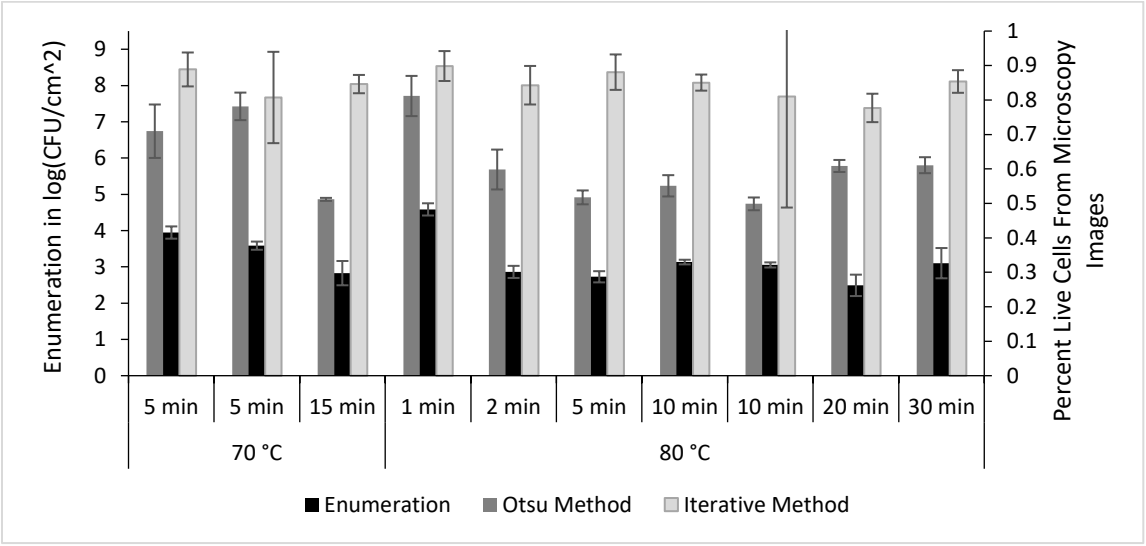

Figure 4.6: Comparison of the Enumeration and Image Thresholding Methods at Temperatures of 70 °C and 80 °C. *The higher temperatures indicated a clear discrepancy between the enumeration method and the two microscopy analysis methods. The Otsu method did follow the decreasing trend of the enumeration method better than the iterative method; however, this trend is negligible when put into context that the enumeration analysis scales logarithmically, left axis, while the microscopy analyses scale linearly, right axis.*

4.3.2. Biofilm Morphology and Image Observations

The stacks of confocal images were always taken from the center of the microscope slides and each end of the microscope slides. Even with the consistent location technique there is still more error observed using the microscopy analyses compared to direct enumeration. This is most likely due to the fact that despite all consistencies the bacterial biofilms do not grow equally throughout the whole microscope slide's surface and the dyes are not fully quenching, introducing greater error into the analysis. This discrepancy could also be due to the microscopy images analysis techniques scaling linearly which would be more accurate for a one or two order of magnitude decrease, but for larger decreases a logarithmic scale would be more appropriate as used in enumeration. However, microscopy is quite good at showing morphological differences and visualizing the amount of cell death. Some pictures of the controls can be seen in Figures 4.7 through 4.10 which demonstrate the different amount of dead cells in a control and the morphology differences. Figure 4.8 shows how different locations in a biofilm can have variability in the morphology and size of the biofilm. Figure 4.8A clearly shows a thinner section of a biofilm with a few sections of bacteria growing further away from the surface when compared to Figure 4.8B which is a biofilm section that has more depth and one large formation rather than small sporadic formations. This observed difference could be from morphology differences at each location site or from where, in the drip flow reactor, that section of biofilm was grown.

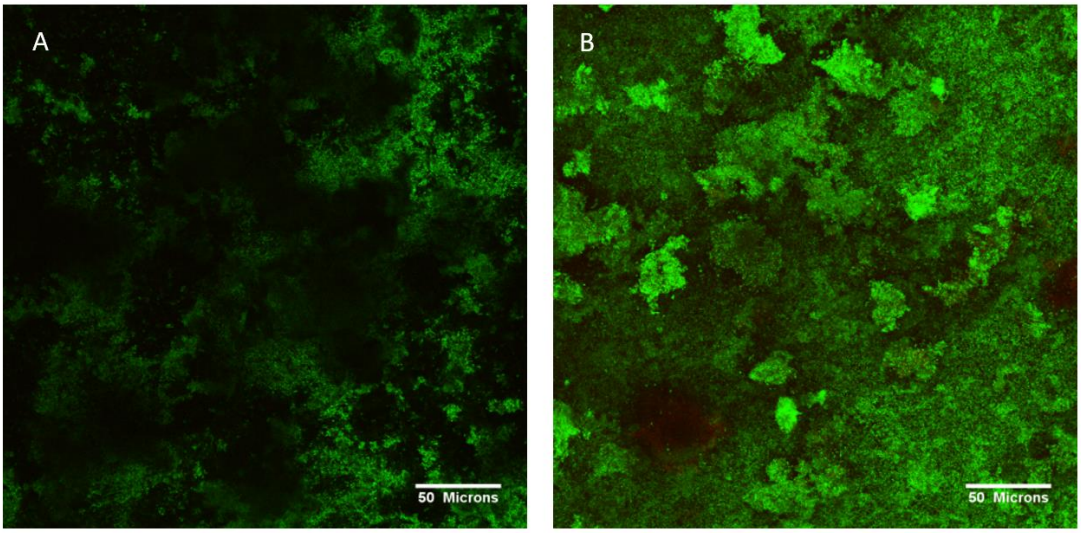

Figure 4.7: Confocal Microscopy Image of a Control Biofilm at 37 ºC*. Green represents alive bacteria and red represents the dead bacteria. (A) The brightest horizontal plane from the biofilm image slices. (B) The total horizontal plane slices compiled on one another into one picture.*

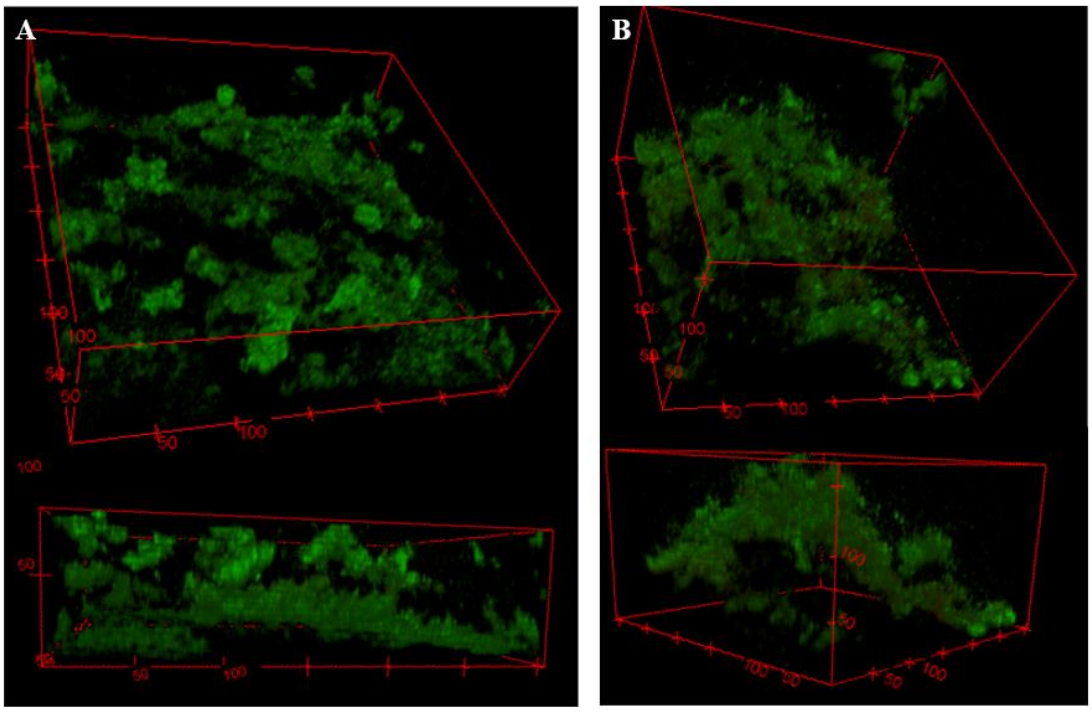

Figure 4.8: Confocal Microscopy Images of a Control Biofilm at 37 ºC Taken from Different Locations*. Green represents alive bacteria and red represents the dead bacteria. (A) The biofilm shows more sporadic formations with less depth in the biofilm. While in another location in the biofilm (B) there is more shape and height in the overall biofilm and the bacterial growth is more consistent throughout the biofilm. Scale bars are reported in microns.*

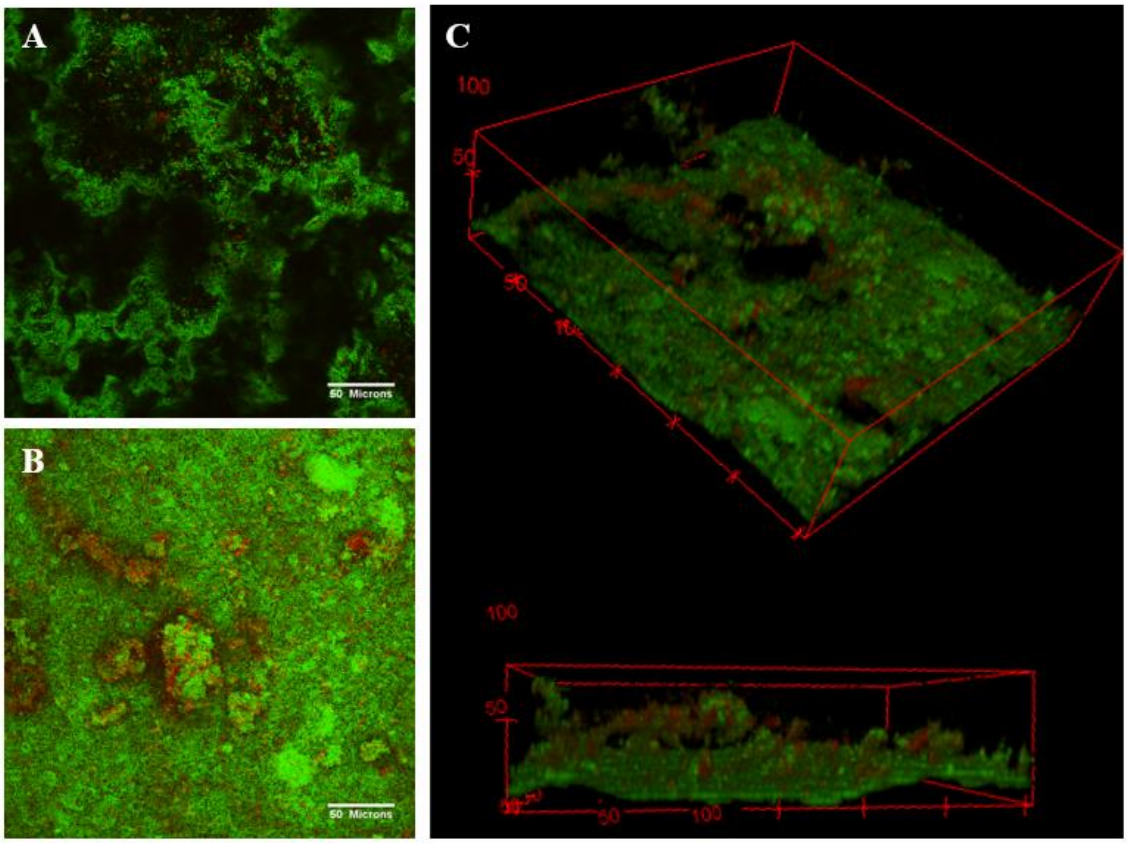

Figure 4.9: Confocal Microscopy Images of a Control Biofilm at 37 ºC with Ridges and Mushroom Shapes. *Green represents alive bacteria and red represents the dead bacteria. (A) The brightest horizontal plane from the biofilm slices. (B) The total horizontal plane slices compiled on one another into one picture. (C) The three-dimensional view of the biofilm better demonstrates the structures that coordinate with the locations where more dead bacteria are found with the axes measured in microns. This shows that where there are larger formations of the biofilms there are a larger amount of dead cells due to a decrease of nutrient diffusion.*

The morphology can decrease the diffusion of oxygen and nutrients where the biofilm is thicker, the nutrient gradient throughout the biofilm has an effect on the bacterial viability and this can be further observed in Figure 4.9. There are more dead cells in these pictures due to the presence of ridges and the mushroom-shaped formations the biofilms create. It can be seen that the dead cells congregate in and around the larger structures due to the decrease in nutrients diffusion in the biofilm. This observation can be further seen in

Figure 4.10, which is a biofilm composed primarily of a uniformly flat biofilm, called a carpeted biofilm, with only a couple columns extending away from the microscope surface. The morphology and amount of live bacteria can change based on where in the drip flow reactor the section was grown. If the section of the biofilm imaged was closer to the inlet of the nutrients it will be exposed to fresh nutrients more frequently, while a section of the biofilm located near the outlet of the drip flow reactor will have less fresh nutrients and potentially more waste products flow by.

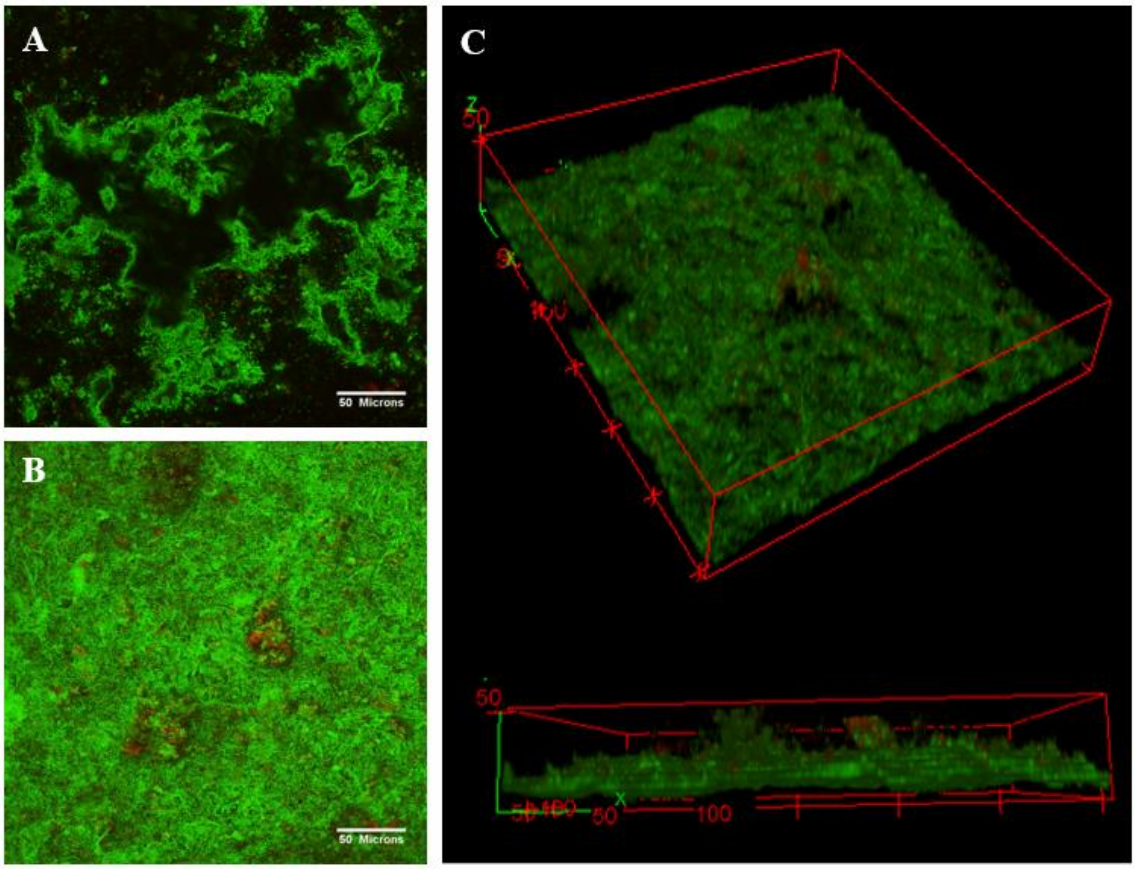

Figure 4.10: Confocal Microscopy Image of a Control Biofilm at 37 ºC with Small Morphological Changes. *Green represents alive bacteria and red represents the dead bacteria. (A) The brightest horizontal plane from the biofilm slices. (B) The total biofilm horizontal plane slices compiled on one another into one picture. (C) A three-dimensional representation of the biofilm which demonstrates the morphology of the biofilm, the scales are reported in microns. This further shows that where there are larger formations of the biofilms there are a larger amount of dead cells due to a decrease of nutrient diffusion.*

Heat shocks done at 60 ºC showed some cell death. Figure 4.11 shows that there is still quite a large percent of the biofilm's bacteria alive, but some increased cell death. Figure 4.11 also demonstrates that there is changing morphology of the biofilms and that they are not simply carpeted or columnar in shape. Figure 4.11A is a top down summation of all the horizontal plane slices to show the overall amount of cell death, while Figure 4.11B demonstrates the large and unique formation of this section of biofilm. The compiled images demonstrate the amount of cell death more clearly while the three-dimensional image demonstrates the morphology more clearly. Additional differences in overall morphology was observed for biofilms grown in different conditions, such as the shaker table-grown biofilms, as discussed in Chapter 5.

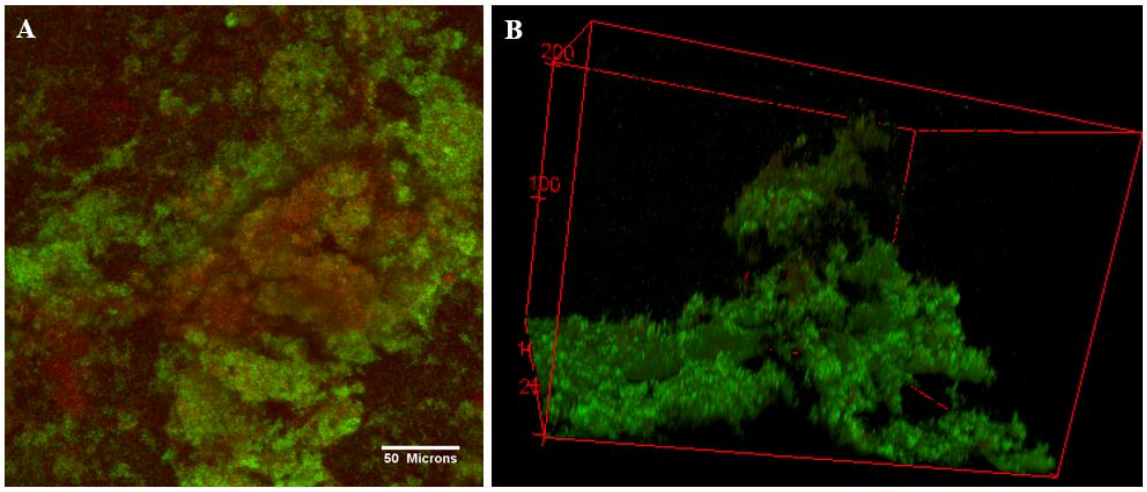

Figure 4.11: Confocal Microscopy Images of a Biofilm Heat Shocked at 60 ºC for 5 Minutes. *Green represents alive bacteria and red represents the dead bacteria. (A) The total biofilm horizontal plane slices compiled on one another into one picture which shows some red demonstrating that the 60ºC heat shock did have an effect on the biofilm's bacterial viability. (B) A three-dimensional rendering of the biofilm demonstrates the morphology of this section of the biofilm, axes are in microns. This also shows that the biofilm's structure is not always columnar in shape and it changes its structure at different distances from the surface.*

The heat shocks done at 70 ºC did show an increase in the amount of dead cells compared to the 60 ºC heat shocks, which had a lot more green, viable cells, present. Figure 4.12 shows a heat shock done at 70 ºC for 2 minutes. The amount of red in Figure 4.12 compared to Figure 4.11, a 60 ºC heat shock for 5 minutes, is significantly more. This visually shows the increase in dead cells when the biofilm is exposed to a higher temperature heat shock. The other trend, a decrease in cell viability with an increased exposure time, can be seen by comparing Figures 4.12 and 4.13. Figure 4.13 is a biofilm that was heat shocked at 70 ºC for 5 minutes, only 3 minutes longer than Figure 4.12's biofilms, but has significant increase in the presence of dead cells.

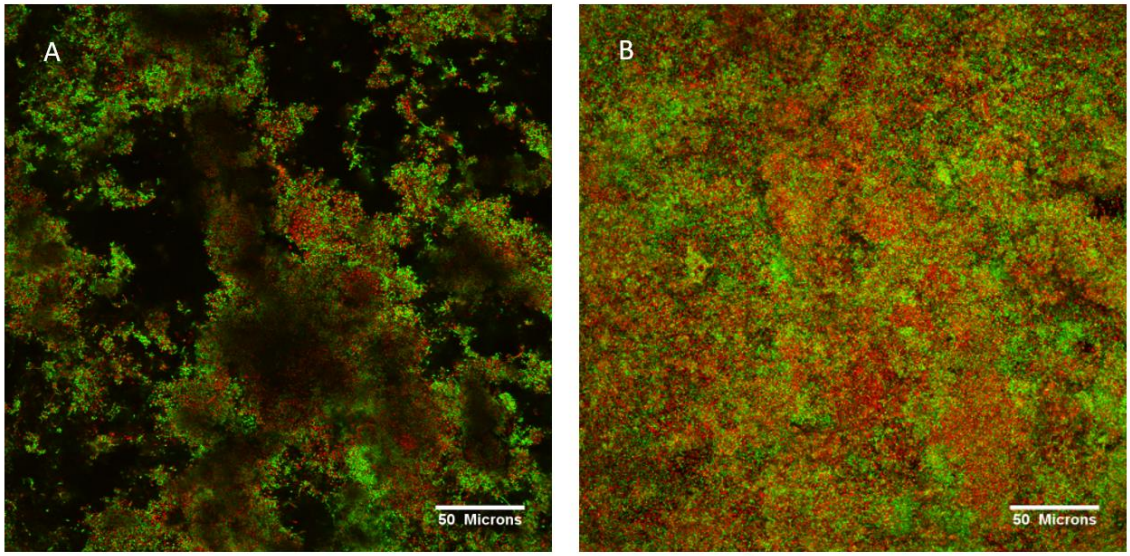

Figure 4.12: Confocal Microscopy Image of a Biofilm Heat Shocked at 70 ºC for 2 Minutes*. Green represents alive bacteria and red represents the dead bacteria. (A) The brightest horizontal plane from the biofilm slices. (B) The total horizontal plane slices from the biofilm compiled on one another into one picture.*

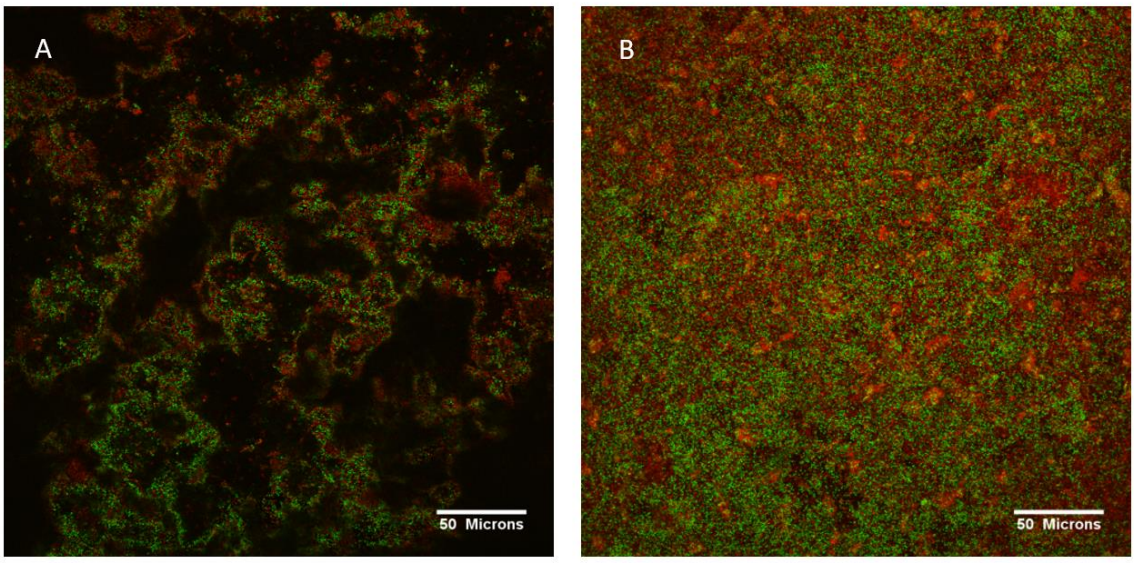

Figure 4.13: Confocal Microscopy Image of a Biofilm Heat Shocked at 70 ºC for 5 Minutes*. Green represents alive bacteria and red represents the dead bacteria. (A) The brightest horizontal plane from the biofilm slices. (B) The total horizontal biofilm plane slices compiled on one another into one picture.*

The heat shocks performed at 80 ºC showed the highest amount of dead bacteria in the biofilms. Figure 4.14 shows a heat shock at 80 ºC for 1 minute and demonstrates a clear increase in the amount of dead cells when compared to all of the previous figures. It also provided a great picture of the morphology seen in these biofilms. Figure 4.14B is a side view of the biofilm and it makes it clear that there is growth above the surface of the microscope slide verifying that these are fully developed, mature biofilms, which is further demonstrated in Figure 4.14C. There are still some green, viable cells present in these pictures, but increasing the exposure time by just one minute increases the amount of dead cells significantly, as seen in Figure 4.15. This further demonstrates that the increase of the time exposure does increase the effectiveness of the heat shock.

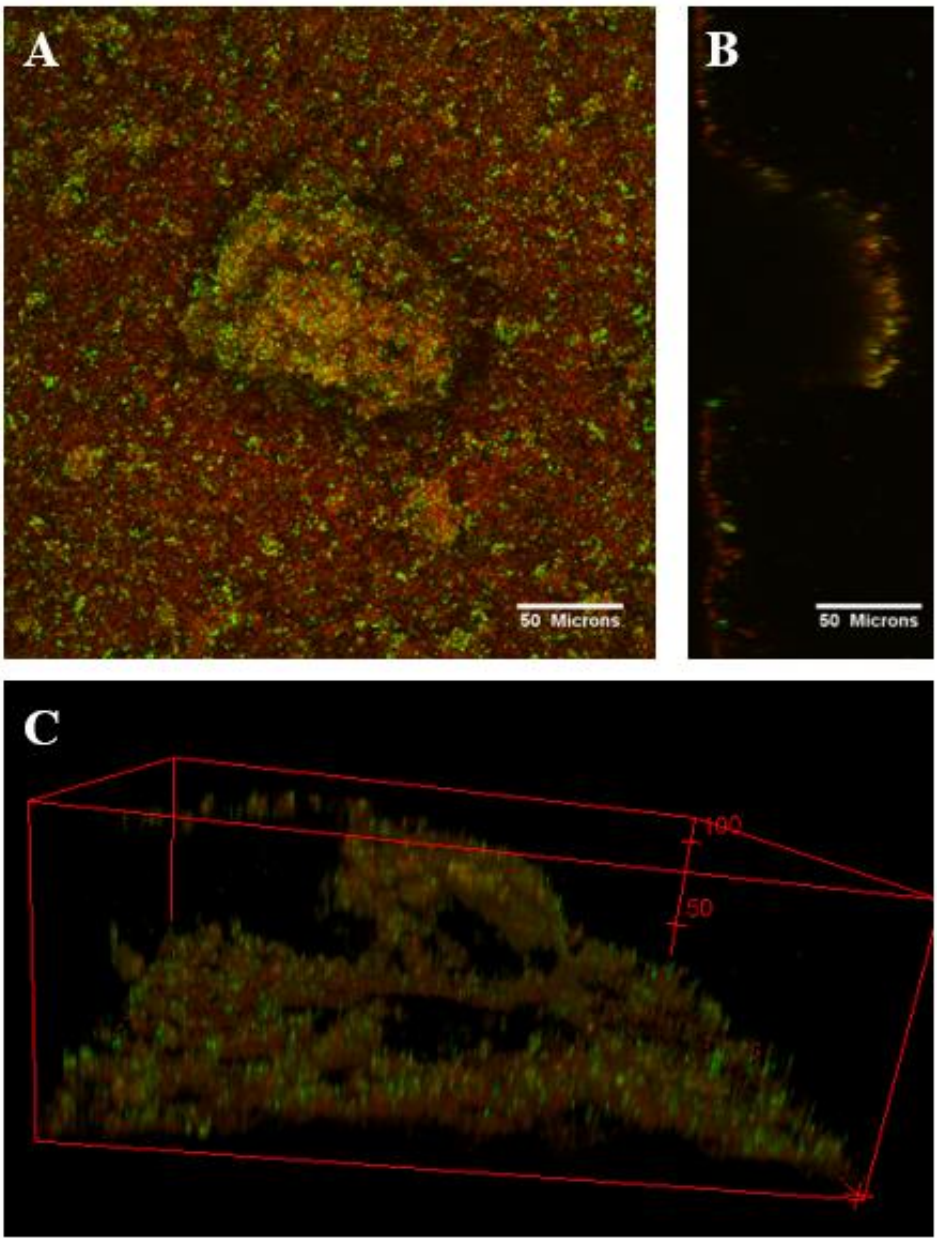

Figure 4.14: Confocal Microscopy Images of a Biofilm Heat Shocked at 80 ºC for 1 Minute*. Green represents alive bacteria and red represents the dead bacteria. (A) The total biofilm horizontal plane slices compiled on one another into one picture. (B) The side view of the series of pictures. This shows an increase in dead cells compared to the controls and (C) demonstrates that the biofilms are mature since they are forming mushroom shaped morphology.*

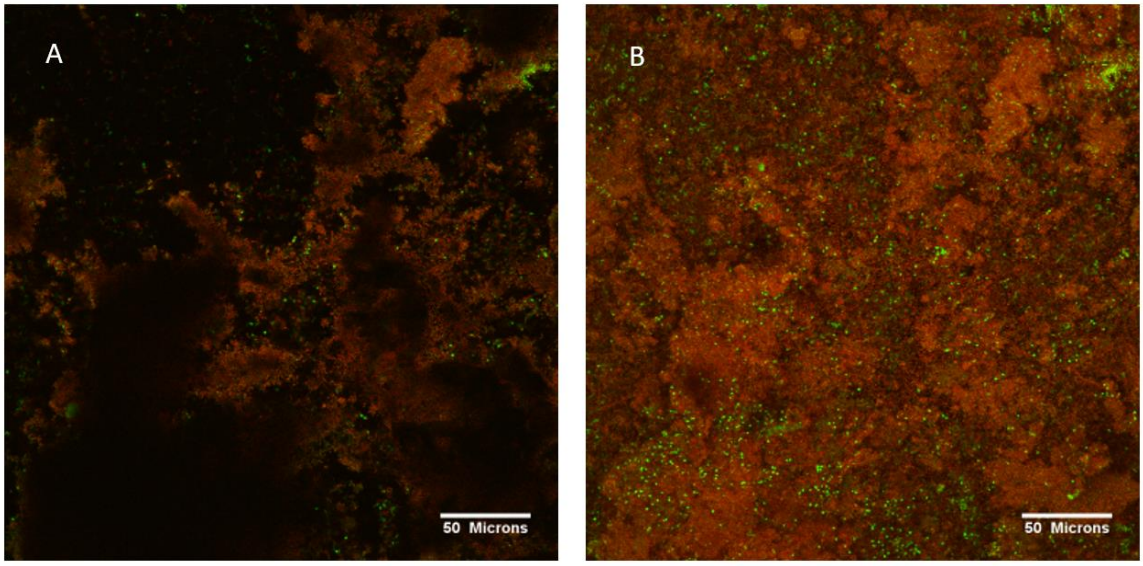

Figure 4.15: Confocal Microscopy Images of a Biofilm Heat Shocked at 80 ºC for 2 Minutes*. Green represents alive bacteria and red represents the dead bacteria. (A) The brightest horizontal plane from the biofilm slices. (B) The total horizontal plane slices from the biofilm compiled on one another into one picture.*

The increase of dead cells as the exposure time to the heat shock increases can be observed from Figures 4.16 and 4.17. Figure 4.16 shows a decrease of viable cells when compared to Figure 4.15. Figure 4.17 shows a further decrease of viable cells when compared to all of the other heat shock times and temperatures since it is the extreme temperature and time, 80 ºC for 30 minutes.

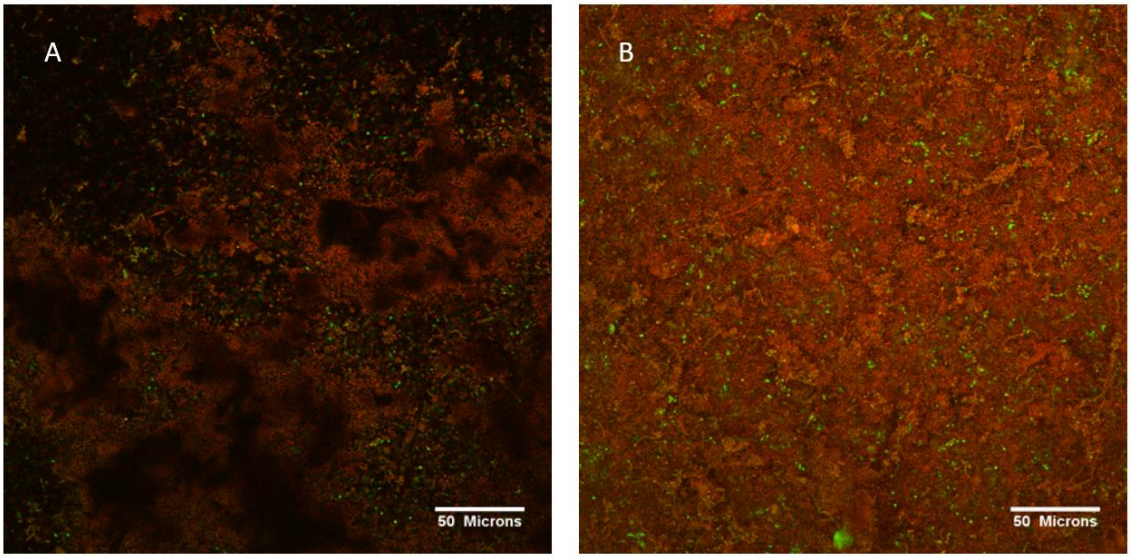

Figure 4.16: Confocal Microscopy Image of a Biofilm Heat Shocked at 80 ºC for 20 Minutes*. Green represents alive bacteria and red represents the dead bacteria. (A) The brightest horizontal plane from the biofilm slices. (B) All the horizontal biofilm plane slices compiled on one another into one picture.*

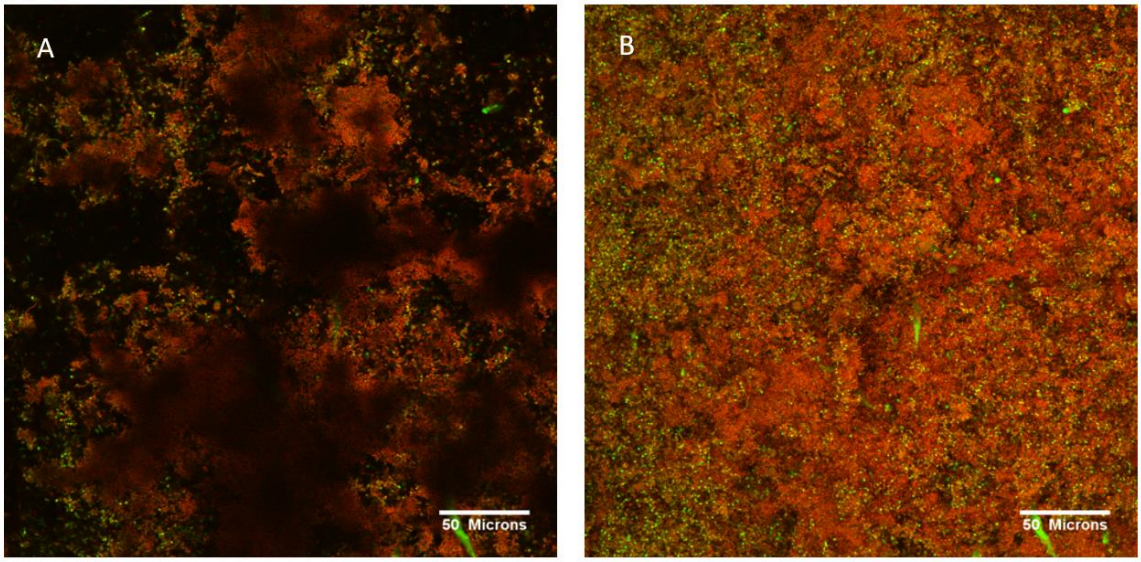

Figure 4.17: Confocal Microscopy Image of a Biofilm Heat Shocked at 80 ºC for 30 Minutes, *the most extreme temperature and exposure time. Green represents alive bacteria and red represents the dead bacteria. (A) The brightest horizontal plane from the biofilm slices. (B) All the biofilm horizontal plane slices compiled onto one another into one picture.*

4.4. Conclusion

The heat shock experiments covered temperatures ranging from 37 ºC to 80 ºC and exposure times ranging from 1 minute to 30 minutes. Since microscopy methods allow for a faster analysis when compared to enumeration two image analysis tools were compared to the enumeration technique utilized in Chapter 3. The two analysis methods did give faster results since the data could be analyzed that same day instead of waiting for the bacteria to grow for a day after plating, as seen in the enumeration technique; however, the results were not comparable to the enumeration. In fact, neither method was able to show the logarithmic decreases observed. Since all the experiments explored showed multiple log reductions, microscopy applications were proven to not be as quantitatively effective as enumeration.

The extensive images of the biofilms taken using CLSM demonstrated the variability of the biofilm morphology and gave visual proof of the heat shocks' efficacy. It was observed that the bacteria further inside a large morphological structure had a larger percent of dead bacteria before heat treatment. This is most likely due to the transport limitations inside those structures creating a nutrient gradient. The heat shocks at the higher temperatures produced images with more dead cells than seen at the lower temperatures, visually demonstrating the effects of the temperatures and exposure times.

CHAPTER 5: EFFECT OF GROWTH CONDITIONS ON THERMAL SHOCK SUSCEPTIBILITY AND REGROWTH OF *PSEUDOMONAS AERUGINOSA* BIOFILMS[†]

5.1. Introduction

Elevated temperature has proven to be a reliable approach for eliminating bacterial populations, as seen in Chapter 3. Heating protocols for planktonic bacteria have long been established at a variety of temperatures and exposure times, and more recently, the decrease in colony forming units (CFU) within a bacterial biofilm has been quantitatively correlated to the degree and duration of thermal shock, according to Equation 5.1:

$$(CFU/cm^2) = (CFU/cm^2)_0 * 10^{-0.079(T-37)} * t^{-0.044(T-37)} \quad \textbf{(Equation 5.1)}$$

where T is the temperature in degrees Celsius, t is the exposure time at that temperature in minutes, and $(CFU/cm^2)_0$ is the original population density of the bacteria in the biofilm.[120] If an implanted medical device has been coated with a magnetically susceptible material, this heat may be delivered wirelessly via an alternating magnetic field to the precise location where the biofilm is growing.[122] The bacterial cell death described by Equation 5.1 covered a temperature range from 37 °C to 80 °C with exposure times ranging from 1 to 30 minutes. In order to quantify the dramatic CFU decrease within this range (up to six orders of magnitude), the biofilms used in that study were grown in tryptic soy broth (TSB) for 1 day in a drip flow reactor to obtain initial CFU loads of nearly 10^9 CFU/cm^2,[120]

[†] Adapted from Ricker, E. B., Bader, T. M., Al-Jaafari, H., Hundley, B. S., and Nuxoll, E. Thermal Shock Susceptibility and Regrowth of *Pseudomonas aeruginosa* Biofilms. Submitted to the International Journal of Hyperthermia.

believed to be far beyond the CFU density typically observed on an infected medical implant.

The literature to-date offers little guidance on the applicability of these findings to biofilms grown *in vivo*, and even less on the magnitude of reduction necessary to eliminate an infection. Additionally, the environmental conditions present are variable depending on the patient and the location of the implant which can dramatically change the biofilm behavior and susceptibility to treatments. The presence of different environmental cues have been observed to change biofilm formation and its subsequent susceptibility to treatments.[26,78,127,136] The development and resistance of biofilms to treatments has proven to be quite dependent on the presence of ions, iron, carbon, nitrogen, and oxygen, among other nutrient sources.[137–142] In the case of a shortage in a nutrient source most biofilm forming bacteria have an increased stress response leading to an increased frequency of biofilm formation and tolerance to treatment.[18,78,143–145] Other stresses placed on the biofilm such as small temperature changes, small pH changes, and the presence of reactive oxygen species have shown an increase in biofilm resistance to treatments.[141,146] The presence of shear stress from agitation, such as an orbital shaker, or from rapid fluid flow over the biofilms while they are forming has demonstrated a change in biofilm morphology.[139,147] These changes in morphology have shown to lead to an increase in tolerance to antibiotics by up to 65% in methicillin resistant *Staphylococcus aureus.*[147] Maturity of the biofilms has also shown to increase a biofilm's tolerance to treatments, such as the case of *Listeria monocytogenes* biofilms which increased their tolerance to quaternary ammonium compound disinfectant by 5 orders of magnitude when grown for just 24 hours longer.[146] There are many contributors from the growth environment that change the biofilm's

behavior which can alter its resistance to treatments making it a unique and interesting aspect to investigate.

To determine whether the growth conditions impact biofilms' thermal susceptibility, thermal shock studies were performed on more mature (4 day) biofilms with significantly lower initial bacterial loads (~10^7 CFU/cm^2) and discontiguous architecture using a shaker table protocol with increased shear stress and decreased nutrient and effluent transport. Moreover, biofilms were investigated using four different growth media: TSB, Mueller Hinton broth (MHB), a minimum glucose medium (GM), and a medium more commonly used for mammalian cell culture (MEM-α). To determine the regrowth potential of thermally shocked biofilms, TSB shaker table biofilms subject to thermal shocks of various intensity were re-incubated. Their population density over time was compared with that of freshly inoculated biofilms. Consistent with prior studies, these trials used biofilms of *Pseudomonas aeruginosa*, a well-studied, model organism. *P. aeruginosa* is the third most common bacterium to cause etiologic infections of orthopedic implants, making up 9.2% of all the medical implant infections,[8] and its systemic infection mortality (38.7%) is at the top of the range for nosocomial infections.[7]

5.2. Materials and Methods

5.2.1. Inoculum

Pseudomonas aeruginosa PAO1 (15692, American Type Culture Collection, Manassas, VA) stores in glycerol were thawed and streaked onto agar plates (Difco Nutrient Agar, Sparks, MD, USA) and incubated inverted for 24 hours at 37 °C. Two colonies were then removed and placed into 5 mL of sterilized (autoclaved at 121 °C and

allowed to cool prior to use) tryptic soy broth (TSB, BD Bacto, Sparks, MD, USA) and grown for 24 hours at 37 °C, obtaining an average of $2.12 \times 10^9 \pm 0.07 \times 10^9$ CFU/mL.

5.2.2. Biofilm Growth and Medium Preparation

Glass microscope slides (75 mm x 25 mm x 1 mm), fully frosted on one side, were placed individually in polystyrene 4-well dishes (Thermo Scientific Nunc, Rochester, NY, USA) along with 333 µL of the inoculum and 5 mL of media per well ($1.32 \times 10^8 \pm 0.04 \times 10^8$ CFU/mL), then the dish was sealed with parafilm. These dishes were placed on an orbital shaker table (VWR 1000, 15 mm orbit, Thorofare, NJ, USA) set at 160 rpm in an incubator at 37 °C for 96 hours. Four different media were used: tryptic soy broth (TSB, BD Bacto, Sparks, MD, USA), Mueller Hinton broth (MHB, Difco, Sparks, MD, USA), a minimum glucose medium (GM), and a mixture containing 90% by volume minimum essential media α with no nucleosides (MEM-α, Gibco Life Technologies) mixed with 10% by volume fetal bovine serum (FBS, Life Technologies) to better simulate the growth anticipated in a mammal.

Thirty grams of TSB powder were dissolved into a liter of de-ionized water and heated for 10 minutes in a 700 W microwave. Powder MHB was dissolved at a concentration of 21 g per liter of de-ionized water and similarly heated for 10 minutes in a 700 W microwave. Both TSB and MHB were then autoclaved at 121 °C to ensure sterility. The minimum glucose medium (GM) was made by mixing 1.44 mg ferrous sulfate heptahydrate, 24 mg magnesium sulfate, 2.7 g potassium phosphate dibasic, 2.7042 g glucose, 4.3 g potassium monophosphate, and 5.232 g 3-(N-morpholino)propanesulfonic acid into 500 mL of de-ionized water (all chemical components purchased from Fisher Scientific, Waltham, MA, USA) and filter sterilized in a VWR, nylon, 0.2 µm pore size

vacuum filter. The 90% MEM-α and 10% FBS (MEM-α/FBS) mixture was made by combining the two components (both liquids) in a 9:1 ratio by volume, MEM-α to FBS, and then filter sterilizing.

5.2.3. Thermal Shock Procedure

After the 96 hour growth period the biofilms and their underlying glass substrates were transferred to a preheated 4-well dish containing 5 mL water per well whose temperature was maintained by a water bath (Isotemp 3013P, Fischer Scientific, Pittsburg, PA, USA) at the target temperature. After the target exposure time the substrate and biofilm were swiftly transferred to the recovery plate, another 4-well dish containing 5 mL water in each well at room temperature. Biofilms were shocked at 50, 60, or 80 °C (plus controls at 37 °C), with exposure times of 1, 5, or 30 minutes. Each condition had at least 12 samples, four parallel replicates of three different plates.

5.2.4. Enumeration

Biofilm population density was quantified via resuspension and plating. After the thermal shock, each 4-well dish of recovered biofilm was wrapped in parafilm and sonicated for 10 minutes at 45 kHz in a VWR Symphony 9.5 L sonicator (Radnor, PA, USA). The homogenized suspension was then serially diluted in tenfold increments and spot plated using 10 µL samples on agar plates (Difco Nutrient Agar, Sparks, MD, USA). After 5 minutes to let the samples adsorb, the plates were inverted and incubated at 37 °C for 20-24 hours before counting the colony forming units (CFU). The CFUs were then converted into a more relevant logarithmic population density, $\log\left(\frac{CFU}{cm^2}\right)$, via Equation 5.2:

$$\log\left(\frac{CFU}{cm^2}\right) = \log\left[\frac{(plate\ count)*10^{dilution\ factor}*\left(\frac{5\ mL}{0.1\ mL}\right)}{18.75\ \frac{cm^2}{slide}}\right] \quad \textbf{(Equation 5.2)}$$

where *plate count* is the number of CFUs in a sample, *dilution factor* is the number of tenfold dilutions to make that sample, *(5 mL / 0.1 mL)* is the ratio of total biofilm suspension to the volume of the plated sampled, and *18.75 cm^2* is the surface area of the biofilm's substrate.[120] Plates with counts from 3 CFU to 30 CFU were the selected dilution set used for calculations. In the case of two dilution sets landing within this range the lower dilution was used. The upper limit, 30 CFU, was chosen based on the ability to reliably count the individual units without overlap issues and the lower limit, 3 CFU, was established to limit the effect of a single CFU skewing the data dramatically. In the case when the direct sample count was lower than the 3 CFU the count was used, but was below the quantification limit.

5.2.5. Confocal Imaging

Biofilm architecture was observed via confocal fluorescent microscopy. Both enumeration and fluorescent microscopy are destructive techniques, so separate biofilms must be used for each. Bacteria were selectively dyed using a Filmtracer LIVE/DEAD Biofilm Viability Kit (Molecular Probes, Inc., Eugene, OR, USA). In this membrane permeability assay SYTO 9 (excitation wavelength 488 nm, emission wavelength 500 nm, green) enters all cells and fluoresces when bound to nucleic acid, while propidium iodide (excitation wavelength 568 nm, emission wavelength 635 nm, red) can only access cells with damaged membranes, displacing SYTO 9 in those cells. With non-overlapping emission and excitation peaks, these dyes allow clear differentiation between the dead and live bacteria via confocal microscopy. Thirty microliters each of SYTO 9 and propidium iodide were added to the recovery well of each biofilm imaged. Biofilms grown in the drip

flow reactor (DFR) were imaged using an upright Bio-Rad Radiance 2100 multiphoton/confocal microscope (Hemel-Hempstead, United Kingdom) with a 40x dip lens, while biofilms grown on the shaker table were inspected using a Zeiss LSM 710 confocal microscope (Oberkochen, Germany) with a 63x dip lens. Both microscopes used confocal settings with an argon laser to excite the propidium iodide and a helium-neon laser to excite the SYTO 9 dye. Biofilms were scanned by horizontal rastering with 1 μm vertical increments from bottom to top. Each row was scanned separately by each laser before advancing to the next row to decrease any overlap in the resulting excitations and emissions. Images were collected in a 1024 × 1024 pixel array and the resulting images were post-processed in the Java-based ImageJ processor (freely available from the NIH website at http://imagej.nih.gov/ij).

5.2.6. Regrowth Trials

An initial growth curve of the biofilms was determined by enumerating biofilms incubated for 1, 2, 4, 24, or 96 hours, then rinsed for 1 minute in sterile, de-ionized water and resuspended by sonication. Post-shock regrowth was investigated by reincubating thermally shocked biofilms in fresh TSB for 2, 4, 12, 24, or 96 hours, then rinsing for 1 minute in sterile, de-ionized water and resuspending for enumeration. The regrowth of biofilms was investigated after heat shocks at 60 °C for 5 and 30 minutes, and 80 °C for 1, 5, and 30 minutes. At least three replicates were performed for each heat shock and regrowth time point.

5.2.7. Statistical Analysis

Statistical analysis of the enumeration results was performed in GraphPad Prism 6. Averages and standard deviations were obtained via arithmetic calculations of log

(CFU/cm^2) values. A two-way ANOVA with a 95% confidence interval set was used to compare the means. The graphs were produced in GraphPad Prism 6 based on the calculated arithmetic mean and standard deviation.

5.3. Results

5.3.1. Difference in Biofilm Architecture and Population

Biofilms grown on a shaker table for 96 hours were starkly different from the biofilms grown in a drip flow reactor (DFR) for 24 hours in both morphology and amount of colony forming units (CFU), even when using the same growth medium, TSB, for the same organism, *P. aeruginosa*. The DFR biofilms had bacteria more densely covering the microscope slides' surface area, typically 100 µm thick with plumes up to 200 µm (Figure 5.1B). The shaker table biofilms were more dispersed across the microscope slides with fewer adhered bacteria in between the biofilm plumes ranging only up to 50 µm in thickness (Figure 5.1A). Figure 5.1 has the two composite confocal image renderings of each biofilm with the live cells fluorescing green with SYTO 9 dye, while the dead cells contain red-fluorescing propidium iodide due to poor membrane integrity. Quantitatively, the CFU population density in the shaker table-grown biofilms was one hundred-fold smaller ($10^{6.64 \pm 0.53}$ CFU/cm^2) than the DFR-grown biofilms ($10^{8.55 \pm 0.32}$ CFU/cm^2).

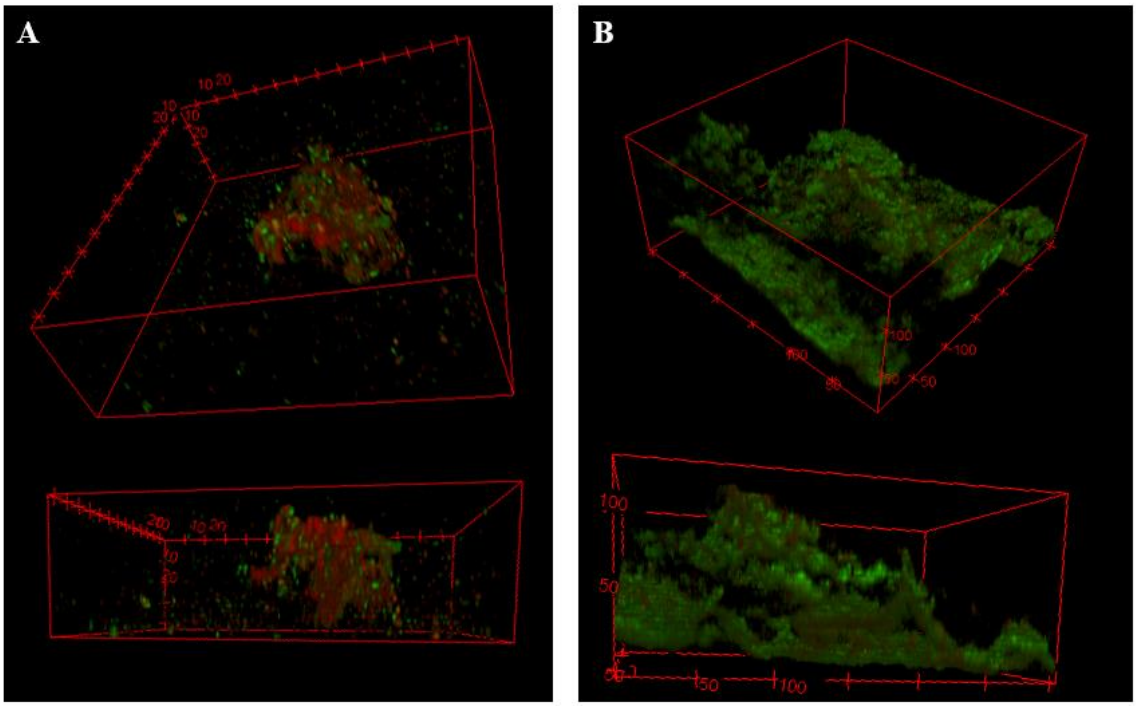

Figure 5.1: Architectural Differences Between a Shaker Plate and DFR-Grown Biofilm. *Confocal fluorescent microscopy images of biofilms grown in A) on a shaker table for 72 hours; and B) a drip flow reactor where the media is applied and drained dripwise for 20 hours following four hours of static incubation. Both biofilms use the same strain of P. aeruginosa and the same tryptic soy broth supply. Green indicating viable bacteria and red indicating dead bacteria with the axes in microns.*

5.3.2. Thermal Susceptibility

The shaker table biofilms also demonstrated significantly different susceptibilities to the thermal shock than seen in the DFR biofilms, as shown in Figure 5.2. While the CFU viability count in DFR biofilms decreased by 0.3-1.7 orders of magnitude depending on exposure time at 50 °C, the shaker table biofilms showed no susceptibility, maintaining the same CFU/cm^2 values even after 30 minutes of exposure time. At 60 °C, however, the shaker table biofilms showed a sharp dependence on exposure time, with no discernable effect at 1 minute of exposure and increased cell death when exposed for longer time periods. At five minutes of exposure to the 60 °C heat the viable bacterial population

dropped by two orders of magnitude and at 30 minutes of exposure time the CFU/cm^2 count dropped by four orders of magnitude. These decreases are comparable in magnitude and more time dependent than those exhibited by DFR-grown biofilms subjected to the same conditions. Similarly, the 80 °C thermal shock on the shaker table biofilms had 3.2 to 5 orders of magnitude decrease in the viable cell counts, below the quantification limit of the experiments, in some cases yielding no CFU at all.

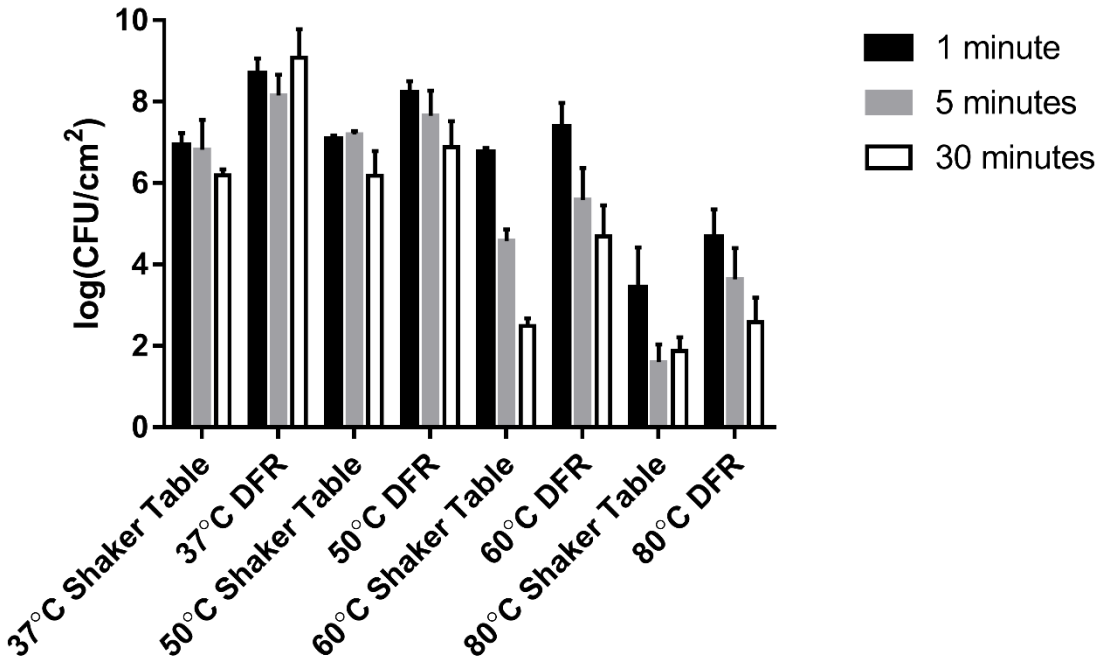

Figure 5.2: Effect of Growth Method on Thermal Susceptibility. *Surviving CFU/cm^2 following thermal shock are compared for biofilms grown on a shaker table versus grown in a drip flow reactor (DFR). All trials used the same tryptic soy broth supply, incubation conditions, and thermal shock protocols, with trials at 37, 50, 60, and 80 °C for 1, 5, or 30 minutes as indicated (n≥12).*

5.3.3. Growth Media Effects

Investigating the effect of various growth media, the MHB and MEM-α/FBS produced shaker table biofilms comparable to the shaker table biofilms grown in TSB, as

determined by two-way ANOVA, with only the glucose media (GM) biofilms differing significantly ($p = 0.05$). These biofilms had a lower bacterial load ($10^{5.94\pm0.49}$ CFU/cm^2) than the other control biofilms by over half an order of magnitude, as shown in Figure 5.3. This figure also indicates the effect of exposure time. For the control biofilms, the thermal shock temperature was the same as the incubation temperature (37 °C), so the duration of the thermal shock (1 to 30 minutes) was not anticipated to have an effect. This is confirmed by the results in Figure 5.3, where biofilms from any given medium show no statistical difference ($p = 0.05$) in CFU/cm^2 regardless of exposure time to the control temperature. The quantification limit indicated in Figure 5.3 ($10^{1.9}$ CFU/cm^2) is based on the criterion that plate counts of undiluted biofilm suspension below 3 CFU are not reliably quantified.

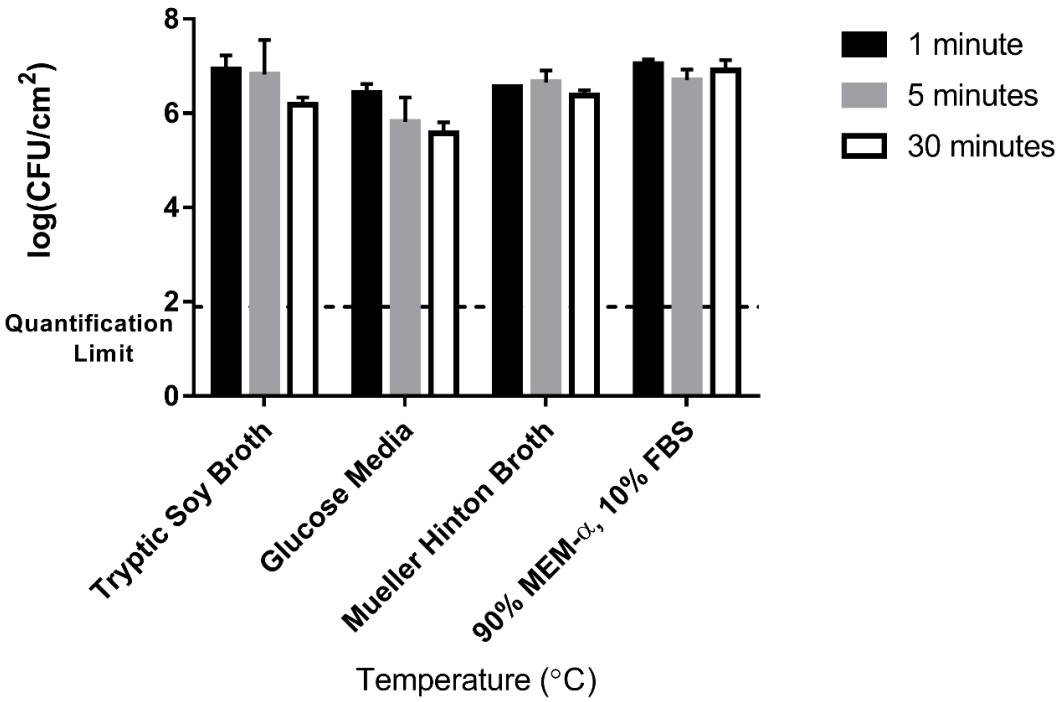

Figure 5.3: Effect of Growth Media on Biofilm Population Density. *Bacterial biofilm population densities are shown for shaker table-grown biofilms cultured in four different media types. In these control trials, all "thermal shocks" were performed at the incubation temperature of 37 °C (i.e., no shock) for the indicated exposure time: 1, 5, or 30 minutes.*

Similar observations were made for each of the different growth media types grown on a shaker table. For all media types, there was no discernable decrease in bacterial viability after exposure to a 50 °C thermal shock regardless of exposure time. The viable cell count from the biofilms exposed to the 60 °C thermal shock for 1 minute also showed no statistical difference from the controls for all but the biofilms grown in MEM-α/FBS ($p=0.05$). All biofilms grown on the shaker table showed decreases at 60 °C for exposure times above 1 minute regardless of growth media. Biofilms grown in TSB and GM showed more of a time dependence with the 60 °C thermal shock than others. Figure 5.4 summarizes these results for each growth medium, again demonstrating that exposure to 80 °C for more than 1 minute decreased the CFU/cm^2 below the quantification limit, sometimes yielding no countable units in the undiluted plated samples.

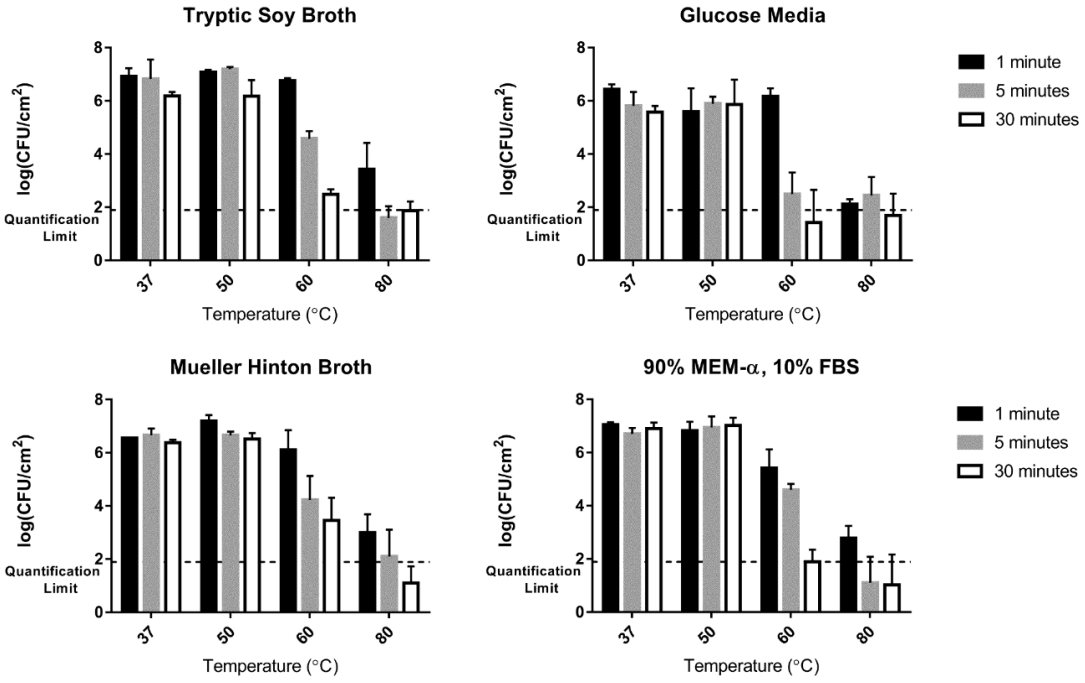

Figure 5.4: Thermal Susceptibility of Shaker Table-Grown Biofilms Based on Growth Media. *At 50 °C, no population decrease is observed regardless of exposure time, while at 60 °C the population drops sharply with time. At 80 °C the decrease is too large to be quantified at exposure times of 5 minute and 30 minute, unlike the exposure time of 1 minute.*

5.3.4. Post Thermal Shock Regrowth

The biofilm growth curve showed rapid attachment and proliferation within the first hour of inoculation, followed by a prompt climb to a plateau population density averaging $10^{6.64 \pm 0.53}$ CFU/cm^2 within four hours, as seen in Figure 5.5. By comparison, thermally shocked biofilms showed no growth during their first four hours of reincubation, and required about 1 day to reach their pre-thermal shock population density. This plateau density was unaffected by the thermal shock.

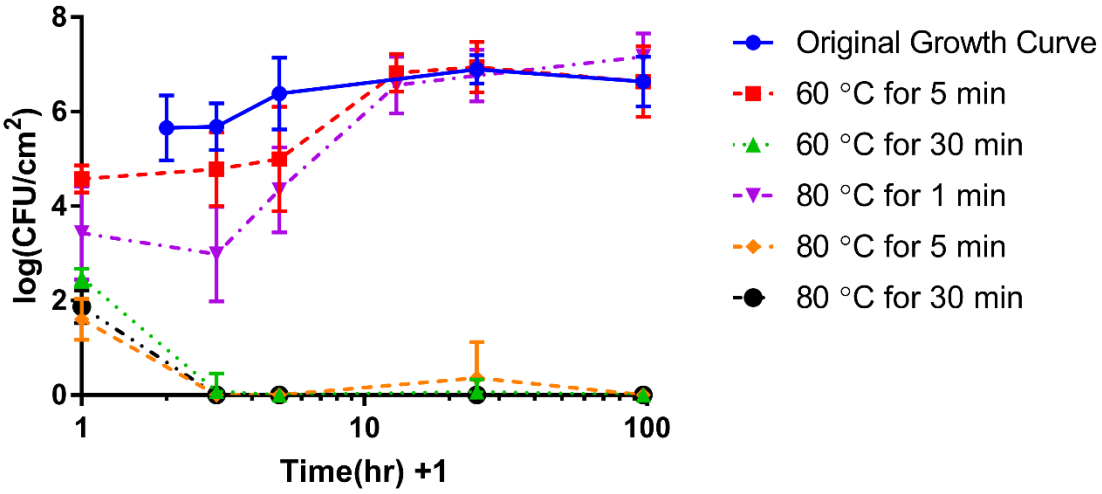

Figure 5.5: TSB Shaker Plate Biofilm Regrowth Post Thermal Shock. *Shaker plate-grown biofilms in TSB were thermally shocked and then regrown and compared to one another and the original growth curve. The 60 °C for 5 minutes and 80 °C for 1 minute regrew to the orginal population size. Thermal shocks of 60 °C for 30 minutes, 80 °C for 5 minutes, and 80 °C for 30 minutes had little to no regrowth.*

Beyond a critical thermal shock intensity, however, the biofilms did not recover. Biofilms shocked at 60 °C for 30 minutes or 80 °C for at least 5 minutes initially showed up to $10^{2.48}$ CFU/cm^2 and $10^{1.87}$ CFU/cm^2 of surviving bacteria, respectively, but two hours later no CFU were observed in almost all cases. Milder thermal shocks of 60 °C for 5 min

or 80 °C for 1 min initially resulted in population densities of at least $10^{4.58}$ CFU/cm^2, and $10^{3.43}$ CFU/cm^2, respectively, and these biofilms recovered as described above.

5.4. Discussion

Coatings which can be heated wirelessly via application of an alternating magnetic field are already under development,[122] raising the possibility of a localized *in situ* thermal shock directly from the biofilm's substrate. This approach, however, requires a clear understanding of the relationship between the thermal shock intensity and its subsequent bacterial population reduction, as well as the degree to which the population must be reduced to be non-viable. Previous studies have demonstrated that these thermal shocks can decrease the bacterial population of a biofilm by up to six orders of magnitude.[120] Even with more labor-intensive enumeration protocol with a quantification limit of $10^{1.1}$ CFU/cm^2, such decreases require initial population densities well exceeding 10^7 CFU/cm^2. Drip flow reactors, in which fresh media is slowly dripped onto a slanted substrate and allowed to drain off, generate biofilms with nearly 10^9 CFU/cm^2, allowing quantification of population decreases over seven orders of magnitude, as correlated in Equation 5.1. It is unclear, however, whether biofilms cultured under such mild conditions would accurately represent *in vivo* biofilms, and if not, the degree to which their thermal susceptibility would be different.

To determine the degree to which growth conditions influence thermal susceptibility, biofilms for this investigation were grown in a variety of chemical environments under starkly different conditions, with a limited supply of nutrients, increased oxygen transport resistance, no waste removal, and shear from the orbital shaker table. By having such a large difference in the growth conditions from the DFR-grown

biofilms a better understanding of the potential range of the biofilm thermal susceptibility could be investigated. Moreover, the biofilms were allowed to mature for several days. Under these conditions, the same bacteria form markedly different biofilms, as demonstrated in Figure 5.1. Quantitatively, these biofilms contained only 1% as many bacteria as the previously reported drip flow biofilms. The chemical environmental composition, however, appeared to have little effect. Even the minimum glucose media produced largely comparable biofilms under the same control conditions.

The thermal susceptibility of these biofilms was also statistically different from the susceptibility quantified in Equation 5.1 for DFR biofilms. Most notably, the 50 °C thermal shock had little to no effect, regardless of exposure time or growth medium. The observed lack of susceptibility to the thermal shock was also seen for biofilms grown in all but the MEM-α/FBS medium when exposed to 60 °C for one minute, indicating that most of the biofilms grown under the shaker table conditions were less susceptible to lower temperature heating than previously seen in the DFR-grown biofilms. This overall increased resistance to mild thermal shock may be attributed to the harsher conditions (*i.e.* shear stress, finite nutrients, and no waste removal) of the shaker table culture, precluding the growth of less robust bacteria. At longer exposure times, however, a 60 °C thermal shock decreased the shaker table-grown biofilms' bacterial viability, in TSB it decreased by two orders of magnitude at five minutes (compared to three orders of magnitude for a DFR-grown biofilm) and four orders of magnitude at 30 minutes (matching a DFR-grown biofilm).

At higher temperatures the decrease in viable cells for the shaker table-grown biofilms more closely mimicked the decrease for DFR-grown biofilms, to the extent that

this could be quantified. TSB shaker table-grown biofilms when exposed to 80 °C for one minute decreased the viable cell count by three orders of magnitude (compared to four orders of magnitude for a DFR-grown biofilm), then the viable cell population dropped below the quantification limit (> 4.7 orders of magnitude decrease) at longer exposures where the DFR-grown biofilms decreased by 5 and 6 orders of magnitude at 5 and 30 minutes of exposure time, respectively.

Unlike the large differences seen between the shaker table-grown biofilms and the DFR-grown biofilms, the overall thermal susceptibility trends were found to be the same irrespective of the growth medium used for the shaker table-grown biofilms. The 50 °C thermal shock had no effect regardless of the chemical composition of the environment, and the 80 °C thermal shock nearly eliminated the bacteria in the biofilms in all but the shortest exposure times. Only at 60 °C was the bacterial reduction quantifiable across the entire exposure time range and the differences based on growth medium evident. Biofilms grown in MHB and TSB had higher viable cell counts after 30 minutes at 60 °C, containing $10^{3.5}$ CFU/cm^2 and $10^{2.5}$ CFU/cm^2, respectively, while biofilms grown in GM and MEM-α/FBS only contained $10^{1.4}$ CFU/cm^2 and $10^{1.9}$CFU/cm^2, respectively, near the quantification limit. Even with a less strict quantification limit, allowing as few as 3 CFU in a quantified plate, only biofilms with a CFU density of $10^{1.9}$ CFU/cm^2 would be considered quantifiable. Many biofilms were below this threshold, however. For instance, the biofilms grown in GM were found to have no growth in over half of the experiments after being exposed to 60 °C for 30 minutes. These data points with a count of zero were included in calculating the overall averages, bringing the mean below the quantification

limit. The frequency of observing no bacterial growth for each experimental set can be viewed in Table 5.1.

Table 5.1: Incidence of Shaker Table Biofilm Bacterial Growth After Heat Shock. *The percent frequency of growth for each experiment post heat shock for the shaker table-grown biofilms.*

Temperature	**Exposure Time**	**Incidence of Bacterial Growth**			
		TSB	GM	MHB	90% MEM-α, 10% FBS
37 °C	1 min	100%	100%	100%	100%
	5 min	100%	100%	100%	100%
	30 min	100%	100%	100%	100%
50 °C	1 min	100%	100%	100%	100%
	5 min	100%	100%	100%	100%
	30 min	100%	100%	100%	100%
60 °C	1 min	100%	100%	100%	100%
	5 min	100%	92%	100%	100%
	30 min	82%	39%	94%	58%
80 °C	1 min	96%	94%	86%	97%
	5 min	42%	61%	75%	47%
	30 min	64%	53%	39%	22%

Equation 5.1 indicates an equivalence between thermal shock temperature and exposure time, with the same degree of population reduction possible across a range of temperatures, each with a corresponding exposure time. Thermal transport modeling based on this relationship suggests that shocks at higher temperature for shorter duration will result in less thermal damage to adjacent tissue than shocks at lower temperature for longer duration. This study indicates that higher temperature, shorter duration heat shocks are also much more universal in their predicted population reduction, regardless of biofilm architecture. The resulting focus on a much narrower parameter space greatly increases the feasibility of investigations on biofilms cultured *in vivo*.

Interestingly, immediate destruction of all bacteria in these biofilms is not necessary for its elimination. Biofilms whose population reduced to ~10^3 CFU/cm^2, by a variety of temperature and exposure time combinations, were not able to propagate and instead died off completely within a few hours. This may indicate that the most thermally resilient bacteria are not reliable biofilm formers, or that these temperatures interrupt or destroy necessary pathways for the bacteria to form a biofilm. They are still able, however, to survive ultrasonic homogenization into suspension and propagate into dense colonies for enumeration, casting doubt on these implications. Alternatively, the thermal shock may alter the EPS environment, rendering it lethal for the surviving bacteria, which could be investigated in the future. The high density of dying cells may create a mass release of autolysins into the EPS, destroying the walls of the remaining cells. Whether shocked at 60 °C for 30 minutes or 80 °C for 5 minutes or more, these biofilms showed no CFU two hours after thermal shock, despite showing up to 10^3 CFU/cm^2 immediately following thermal shock, indicating a threshold population density which a successful treatment must reach beneath.

Thermal shocks resulting in viability counts above 10^3 CFU/cm^2 (60 °C for 5 minutes and 80 °C for 1 minute), on the other hand, did not lead to the biofilm's eventual demise. These biofilms eventually recovered to their previous population plateau, albeit much more slowly than with their original incubation. They demonstrated a longer lag phase followed by steady growth over the following 12 hours. By comparison, the biofilms initially reached their population plateau within four hours of inoculation. This sustained period of slower growth indicates a fundamental change in the bacteria themselves, either directly by the thermal shock or indirectly through selected killing. For the chemical

environment of the EPS to remain altered for that long in a 50 µm thick hydrogel layer, the relevant chemical species must have a diffusion coefficient below 10^9 cm^2/s.[148] Such a species would either be effectively immobile and unable to travel to cells, or would quickly dissipate into the medium.

5.5. Conclusion

Biofilm infections are a daunting problem with limited options for treatment. Generating heat within a biofilm's substrate to deliver a highly localized thermal shock may be an attractive approach, particularly for medical implants, where the current standard of care is explantation of the infected device and the surrounding tissue, followed by additional revision surgeries after the infection has cleared.[2] While the biofilm's nutrient source does not appear to affect its thermal susceptibility significantly, the physical conditions of its growth do significantly impact its susceptibility to modest thermal shocks, such as at 50 °C. The efficacy of more aggressive thermal shocks, such as at 60 °C for 30 minutes or 80 °C for 1 minute, however, appears to be much more uniform, reliably decreasing biofilm population density by five orders of magnitude. That reduction in population density would bring even the most densely populated biofilms below 10^3 CFU/cm^2, and apparently below their viability threshold, effectively killing them. Besides providing an alternative to multiple surgeries with increased infection risk and potentially months without a needed implant,[3] this approach may also be applied to non-medical surfaces that struggle with biofilm fouling but which cannot be subjected to autoclave temperatures (121 °C), such as low glass-transition plastics.

CHAPTER 6: WIRELESS HEATING OF *PSEUDOMONAS AERUGINOSA* BIOFILMS USING IRON OXIDE NANOPARTICLE COATINGS[‡]

6.1. Introduction

Recently there have been studies showing the effect of lower temperatures on biofilms and the exposure times required at these temperatures to kill off the bacteria in the biofilm,[120,149] also discussed in Chapters 3 and 5. Iron oxide nanoparticle composites have demonstrated remote heating up to 7.5 W/cm^2 in both hydrophilic and hydrophobic polymer composites.[122] The use of a magnetic coating to induce thermal shock inside the body will enable a treatment that focuses the energy directly on the implant surface, precisely where the biofilm is growing as seen in Figure 6.1. The power generated by the composite is a result of the nanoparticle's propensity to convert alternating magnetic field (AMF) energy in to thermal energy.[109,122] The current investigation is the first to report wireless heating of a *Pseudomonas aeruginosa* biofilms using energy delivered from a polystyrene (PS) / Fe_3O_4 nanoparticle coating.

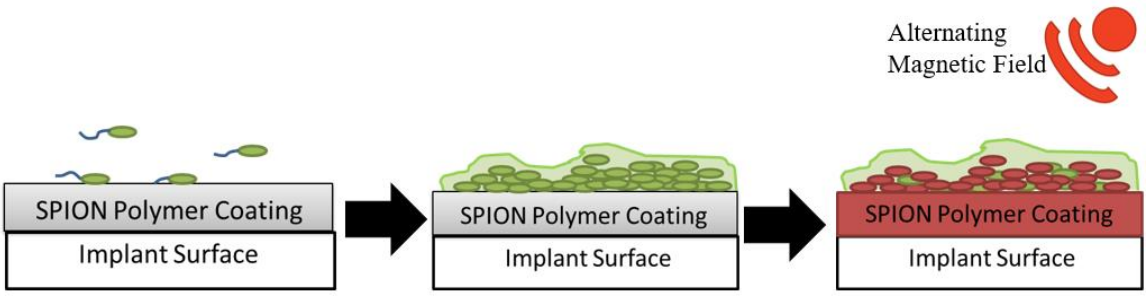

Figure 6.1: Overall Schematic of the SPION Coating Function. *In the unfortunate case of implant infection by planktonic bacteria adhering to the device's surface and forming a biofilm the SPION (superparamagnetic iron oxide nanoparticle) polymer coating can be heated wirelessly to treat the infection in situ.*

[‡] Adapted from Ricker, E. B., Coffel, J., and Nuxoll, E. Wireless Heating of *Pseudomonas aeruginosa* Biofilms Using Iron Oxide Nanoparticle Coatings. In preparation.

Polystyrene was selected as the polymer coating based on its frequency of use in implanted devices, its biocompatibility, and its soft yet relatively robust mechanical nature.[112] The importance of the polymer being mechanically robust stems from the necessity of the polymer to be able to withstand mechanically harsh environments such as a knee replacement or other orthopedic applications. Iron oxide nanoparticles were used in these experiments since these nanoparticles are one of the most heavily studied magnetic nanoparticles and have already been used in the clinical setting.[112,122] *P. aeruginosa* biofilms were used since they are the third most common pathogenic bacterial biofilm found on orthopedic implants[8] and in the case of blood stream infections it is one of the most dangerous with a 38.7% mortality rate.[7]

This chapter investigates the application of the superparamagnetic iron oxide nanoparticle (SPION) coating as the heat source to kill the biofilms. It compares the previous chapter's results of heat shocks done in a water bath to a heat shock coming directly from the coating's surface. This comparison will elucidate the validity of the previous conclusions made based on the water bath heat shocks. The SPION coating did follow the same trends as previously seen in the heat shocks delivered from a water bath, with little deviation. This chapter also explores the heat transfer abilities of the coating and how that changes depending on the position of the coating in the coil which delivers the alternating magnetic field. From these experiments a better understand of the heating potential of the SPION coating for biofilm mitigation was made along with a clearer understanding of necessary precautions for the applications for future studies of this coating.

6.2. Materials and Methods

6.2.1. Iron Oxide Coating

Fe_3O_4 nanoparticles were synthesized via a coprecipitation reaction with $FeCl_3 \cdot H_2O$ and $FeCl_2 \cdot 4H_2O$ (Sigma Aldrich) in a 2:1 mole ratio under basic conditions (KOH, Sigma Aldrich) using previously published methods.[122] Composite coatings were prepared by dissolving 3.2 g of polystyrene (PS) resin (~280,000 MW, Sigma Aldrich) in approximately 40 g of iron oxide nanoparticle slurry (0.082 g/g Fe in toluene) and cast on frosted glass microscope slides to produce 226 ±6 µm-thick coatings. After casting, films were dried at ambient conditions for 8 hr followed by 12 hr of drying at 90 °C to evaporate all remaining solvent. All coatings were made by Joel Coffel in the Nuxoll laboratory.

6.2.2. Biofilm Growth

Stock *Pseudomonas aeruginosa* PAO1 (15692, American Type Culture Collection) was streaked onto a Difco Nutrient Agar plate and allowed to grow for 24 hr at 37 °C. Then two colonies were isolated and placed into 5 mL of Tryptic Soy Broth (TSB, BD Bacto) and allowed to grow for 24 hr at 37 °C until the inoculum reached $2.12 \times 10^9 \pm 0.07 \times 10^9$ colony forming units per milliliter (CFU/mL). The coated slides were wiped down with 70% ethanol and each slide was placed coated side up into a well of a 4-well dish. Five milliliters of TSB were then placed into each well along with 333 mL of the inoculum. The growth plate was then sealed and placed on an orbital shaker set at 160 rmp for 96 hr.

6.2.3. Wireless Heating

The coatings, with the biofilms grown on the surfaces, were remotely heated in a 6-turn AMF generating coil operating at 2.32 kA/m and 302 kHz with feedback control

(operated by an Omega.com iSeries temperature controller) and a fiber optic temperature probe. The coated microscope slides were positioned parallel to AMF lines in a custom, 3D-printed heating chamber with 3 mL of degassed, deionized water; the temperature probe was positioned directly on the coating's surface, see Figure 6.2. Controller tuning parameters were adjusted by Joel Coffel to minimize both the time required to reach the specified set point and the amount of overshoot from the set point.

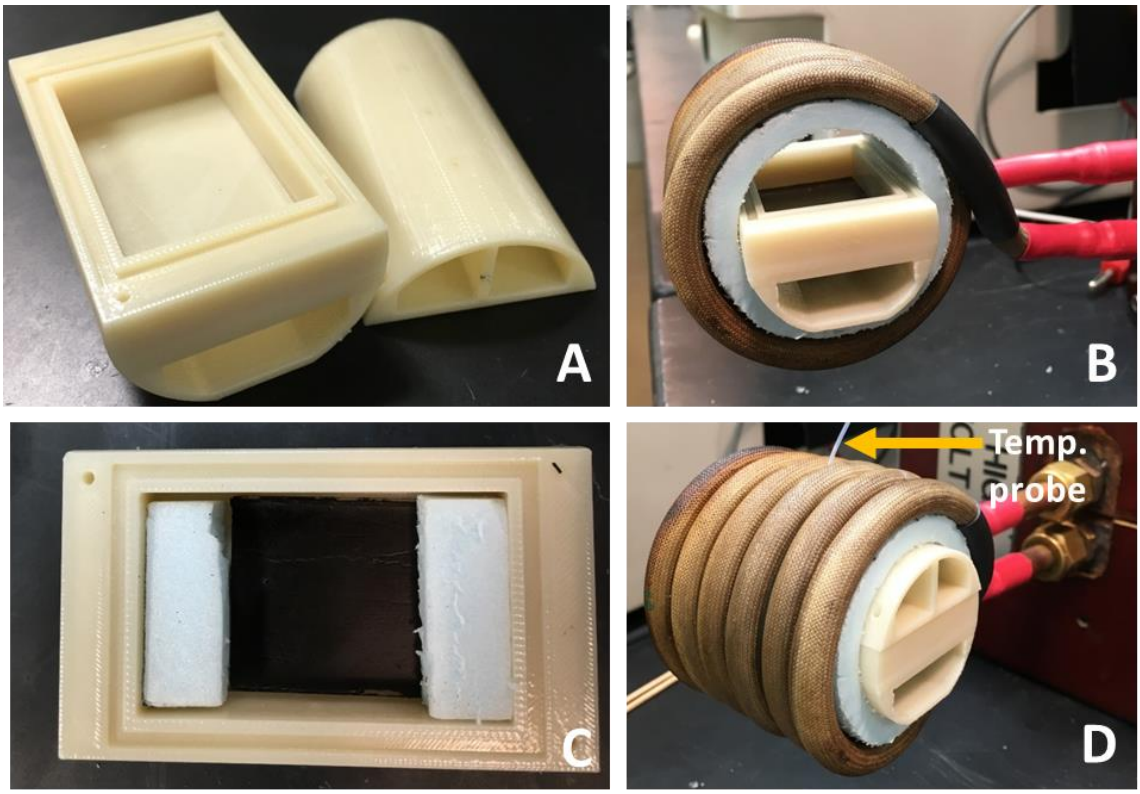

Figure 6.2: Pictures of the Chamber Used to Hold the Biofilm and Substrate for Wireless Heat Shock and The Alternating Magnetic Field Coil. *A) Circular chamber base and lid with hollow voids to insulate chamber from heat loss. B) Chamber placed in 50 mm AMF coil with insulating foam between the coil and chamber. C) 6.5 cm^2 coating in chamber base with foam insulation on both sides of coating. D) Chamber fully assembled in coil with fiber optic temperature probe passed through coil rungs and into the chamber for temperature feedback control at the coating's surface.*

6.2.4. Biofilm Enumeration

After the biofilms were heated using the AMF coil and the coating they were swiftly submerged in a room temperature 4-well dish containing 5 mL deionized water in each well and sonicated (9.5 L VWR Symphony) for 10 min at 45 kHz, creating a homogenized mixture of the dispersed biofilm. The dispersed biofilms were then serially diluted by taking 100 µL of the solution and mixing in 900 µL TSB to then have another 100 µL mixed into the next 900 µL TSB and continued for 8 dilutions total. Each dilution was then spot plated onto an agar plate (Difco Nutrient Agar) and incubated at 37 °C and the colony forming units were counted the next day. The colony forming units were then converted into units of logarithmic density via Equation 6.1:

$$\log\left(\frac{CFU}{cm^2}+1\right)=\log\left[\frac{(plate\ count)*10^{dilution\ factor}*\left(\frac{5\ mL}{0.2\ mL}\right)}{C_{SA}}+1\right] \qquad \textbf{(Equation 6.1)}$$

where the plate count is the counted CFUs, the dilution factor is the corresponding amount of dilutions to the counted CFUs, 5 mL is the amount of liquid the bacteria were sonicated into, 0.2 mL is the amount of plated liquid from the homogenized mixture, C_{SA} is the surface area of the coated slide in cm^2, the added one is to ensure all numbers are defined regardless of count, and $\log\left(\frac{CFU}{cm^2}+1\right)$ is the final reported value. Since in some cases the bacteria appeared countable at multiple dilution sets the dilution that had a CFU count between 3 and 50 was used. To avoid counts that may be skewed from CFUs growing too close to one another, the plate count had to fall below 50 CFUs. In the case that there were two dilutions that had countable CFU sets the less dilute set was used.

6.2.5. Analysis

Using GraphPad Prism 7 the counted colony forming units were analyzed and the two heating systems compared to one another using a two-way ANOVA with 95% confidence. Graphs were produced using the calculated arithmetic mean and standard deviation.

6.2.6. Measurement of Iron Concentration in Solution

To ensure there was no leaching of the iron oxide nanoparticles into the growth media, the iron concentration in the composite films was measured. This was done by digesting them in 8 M HCl for 24 hr, reducing all iron species to Fe^{2+}, and measuring the Fe^{2+} concentration spectrophotometrically (Cary 50, Varian Inc.) using 1,10-phenanthroline monohydrate in a 3.7 M ammonium acetate buffer.

6.2.7. Safety Precautions

Bacterial safety precautions were the same as seen in Chapter 3's safety sections. However, the alternating magnetic field provided an additional safety hazard via its ability to heat up metals nearby. To avoid any potential problem the area surrounding the coil was free of metals and no metal jewelry was worn during the experimental trials. Additionally, the coil could impact electrical units so any computers or other devices were kept outside a five foot radius from the alternating magnetic field coil.

6.3. Results

6.3.1. Magnetic Nanoparticle / Polymer Composite Coating

The iron oxide / polystyrene composite coatings exhibited excellent adhesion to the frosted glass microscope slide as evidence by no film delamination from the substrate

throughout the entire synthesis, biofilm culture, and heat shock. Twelve millimeter diameter coupons were cut from six separate coatings to measure their thickness (229 ± 5 μm, n =6) and iron concentration (30.0 ± 0.4 wt% Fe, n = 6) (work done by Joel Coffel). Their normalized heating rate, SAR, was shown to vary quadratically with respect to AFM power as described by Equation 6.2:

$$SAR = 311.95AMF^2 - 466.13AMF + 172.19 \quad \textbf{(Equation 6.2)}$$

where SAR has units of W/g Fe and AMF is the AMF strength with units of kA/m and the equation has a correlation coefficient of R^2 = 0.9998. The SAR when measured at a maximum AMF of 2.32 kA/m was 675 ± 26 W/g Fe, n = 6, which corresponds to a maximum surface heat flux of 11.1 W/cm^2 assuming a weighted iron composite density of 2.4 g/cm^3.

6.3.2. Wireless Heating

A typical, wireless heat shock requiring an initial, maximum power of 11.1 W/cm^2 was delivered to bring the surface temperature up to an 80 °C set point. Once the temperature approaches this set point, the controller reduced the power delivery dramatically and reached a steady state value near zero after 12 min of heating, suggesting minimal heat losses from the heating chamber to the environment. Transient temperature profiles for the coating under feedback control are shown in Figure 6.3. The most extreme temperature rise (from 21 to 80 °C) was achieved in approximately 30 to 45 s with lower set points reaching their target temperature more quickly. The amount of time the coating was not at its set point was quantified by dividing the area underneath the temperature curve by the ideal area that would be obtained if the coating reached its set point instantaneously at $t > 0$. Values greater than 0.9 were expected for heat shocks lasting

longer than 1 min, *i.e.* the heat shock was at its specified set point for greater than 90% of the total heat shock time. One minute heat shocks had values less than 0.9 due to the amount of time for the temperature to climb to its set point value—greater than 15 secs for most temperature set points from room temperature. Further, the offset (defined as the difference the actual temperature deviated from its set point value) was quantified by time averaging this value over the entire trial period. Negative offset values indicated minimal temperature overshoot which were more desirable to ensure heat shock temperatures did not climb above their specified set point. Demanding a slower temperature rise with less overshoot, or vice versa, for a desired set point can be achieved with this coating and feedback controller by adjusting the controller's PID tuning parameters (done by Joel Coffel).

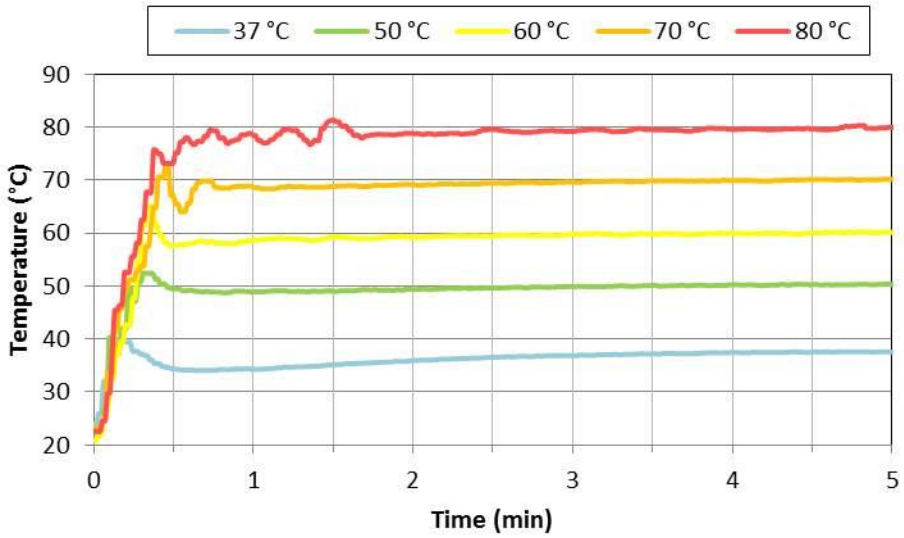

Figure 6.3: Transient Temperature Profiles of Coating Surface*. Set point surface temperatures were achieved in less than 45 s from the time the AMF generator was turned on to begin the heat shock. Less than 0.5 °C offset is observed once steady state was achieved. Figure created by Joel Coffel.*

The polymer coating contained enough iron to quickly ramp-up its surface temperature using a feedback control loop implemented for this system. Set point temperatures were reached within 30 seconds with little to no overshoot, as seen in Figure 6.3.

6.3.3. Biofilm Growth

Control experiments done at body temperature and at the growth temperature, 37 °C, were compared between the water bath heat shocks from Chapter 5 and the SPION coated heat shocks. There were no statistical differences between the two heat shock styles as seen in Figure 6.4, indicating that the biofilms did not form differently due to the coating. All of the SPION coating controls, the 37 °C trials, were found to not be statistically different from one another with an average of 6.72 ± 0.52 log(CFU cm^{-1} +1).

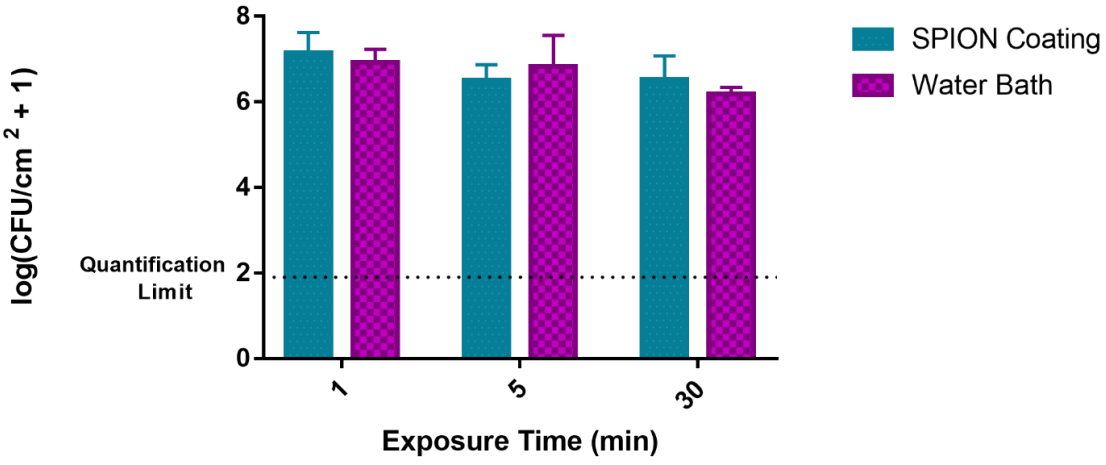

Figure 6.4: Comparison of the Biofilm Growth After the Control Heat Shocks from the Water Bath Heating and the SPION Coating Heating*. Results from the heat shocked biofilms published in the O'Toole et al. paper were compared to the heat shocks done with the SPION coating in these trials to ensure that the biofilms had a similar end population regardless of the heat source at body temperature, 37 °C.*

Iron concentration was measured in the cell culture media used to grow the biofilms and the media used to perform the heat shock. The iron concentration of a fresh media control was subtracted from these measurements and indicated no iron detection observed spectrophotometrically, suggesting little to no iron oxide nanoparticle diffusion from the polystyrene composite matrix into the surrounding environment. The iron concentration results showed that the nanoparticles were not leaching out of the film and therefore not impacting the biofilm.

6.3.4. Biofilm Mitigation

The heated biofilms resulted in similar bacterial cell death to the previously seen water bath thermal shocks in Chapter 5. In all but three cases there was no statistical difference found between the two heating styles. The three cases that were different from the water bath data were the 60 °C for 5 minutes, 70 °C for 1 minute, and 80 °C for 30 minutes. In all of these cases the heating from the SPION coating resulted in more bacterial cell death than seen in the water bath thermal shocks, which can be viewed in Figure 6.5. The 80 °C for 30 minutes thermal shock had the strongest direct statistical significance; however, the SPION coating and the water bath heating results were both below the quantification limit. This indicates that the apparent difference between the two points is not as statistically significant as it appears. The quantification limit is based off of three colony forming units being the lowest reliable count resulting in a quantification limit at 1.9 log(CFU/cm +1).

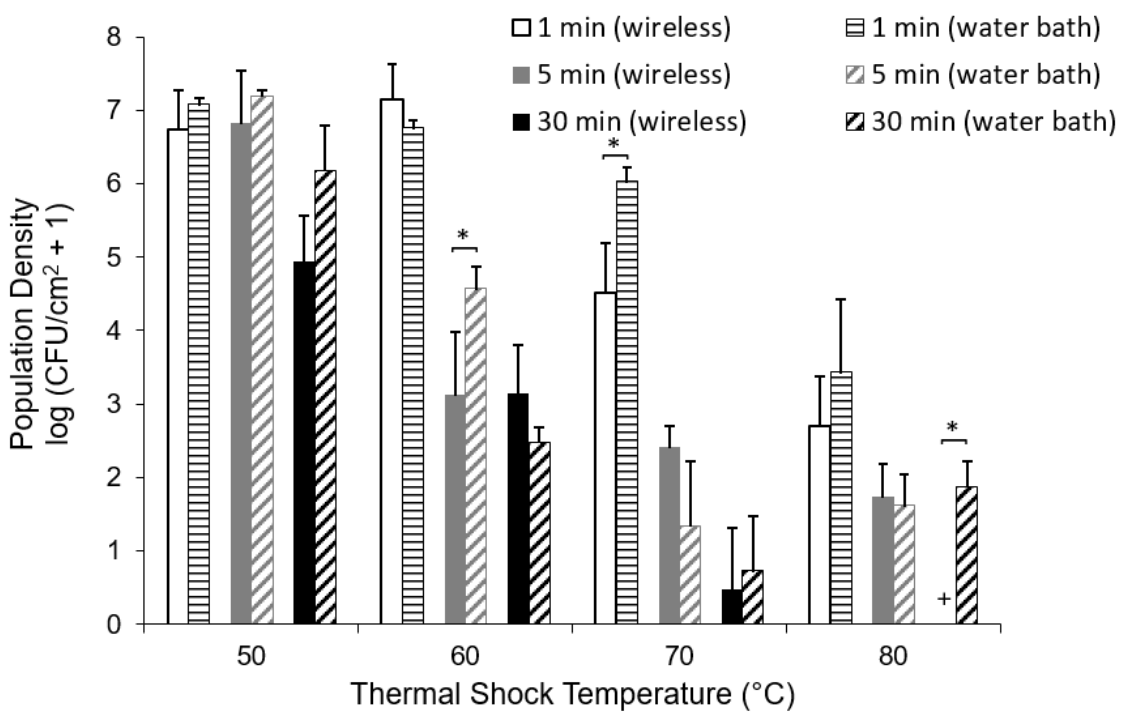

Figure 6.5: Biofilm Thermal Shock Susceptibility Comparison of Water Bath and SPION Coating Heating*. The wireless heating via the SPION coating resulted in similar amounts of viable bacterial cells post thermal shock as the previously seen water bath thermal shocks from Chapter 5. The asterisk denotes a statistical difference and the plus sign denotes when no CFUs were detected.*

The data within the heat shocks achieved via the SPION coating resulted in the lower temperatures having less effect than the higher temperatures and increased in efficacy with lengthened exposure time, shown in Figure 6.5. The 50 °C for 1 minute and 5 minutes were not statistically different from the controls. The same was true for the 60 °C for 1 minute thermal shock that resulted in similar viable counts as the control heat shocks. The 60 °C thermal shocks for 5 minutes and 30 minutes showed a mean decrease of 3.59 log(CFU/cm +1) and 3.58 log(CFU/cm +1), respectively. The 70 °C heated bacteria showed a steady decrease in viability with increased exposure time starting with a two-logarithmic reduction for 1 minute of exposure and another two-logarithmic decrease at

each subsequent exposure time. The 50 °C for 30 minutes heat shock was not significantly different from the 70 °C for 1 minute heat shock. Additional similarities in viable cell counts post thermal shock were observed in the 60 °C for both 5 and 30 minutes, 70 °C for 5 minutes, and the 80 °C for both 1 and 5 minutes. All the 80 °C heat shocks for 30 minutes resulted in no colony forming units indicating that all of the bacteria died in the heat shock.

6.3.5. Heating Uniformity

The original set of thermal shocks in the coil was done on the super paramagnetic iron oxide nanoparticle (SPION) coated microscope slides that were scored down to be 2.5 cm wide and 3.75 cm long. It was found that the edges of these slides did not have similar ampere meter readings as the rest of the microscope slide resulting in slightly lower temperatures along the edge.[112] This is most likely due to the fact that the normalized heating rate (SAR) has a quadratic dependence on field strength, as seen in Equation 6.2 above.

The temperature discrepancy across the SPION coating surface can be observed in Figure 6.6, with the coating on the left side of the field resulting in lower temperatures than the rest of the surface. The smaller slides were more suitably within the AMF field therefore they were investigated for key thermal shocks that showed significant differences between the water bath results and the SPION coating. Since the longer slides with the SPION coating had potential cooler edges, see Figure 6.7, only the data points that had larger amounts of viable cells after the thermal shocks were investigated. The 60 °C for 5 minutes and for 30 minutes, the 70 °C for 1 minute, and the 80 °C for 1 minute thermal shocks were all identified as having larger viable cell counts after the thermal shock that were significantly different from the water bath data seen in Chapter 5. These temperatures and

exposure times were then repeated with slides of 2.5 cm by 2.5 cm instead to ensure that the surface had a uniform field, see Figure 6.8. The shorter slides showed a significant decrease in viable cell counts after heating than the longer slides for the majority of the thermal shocks. The 70 °C for 1 minute did not show a significant difference between the two lengths.

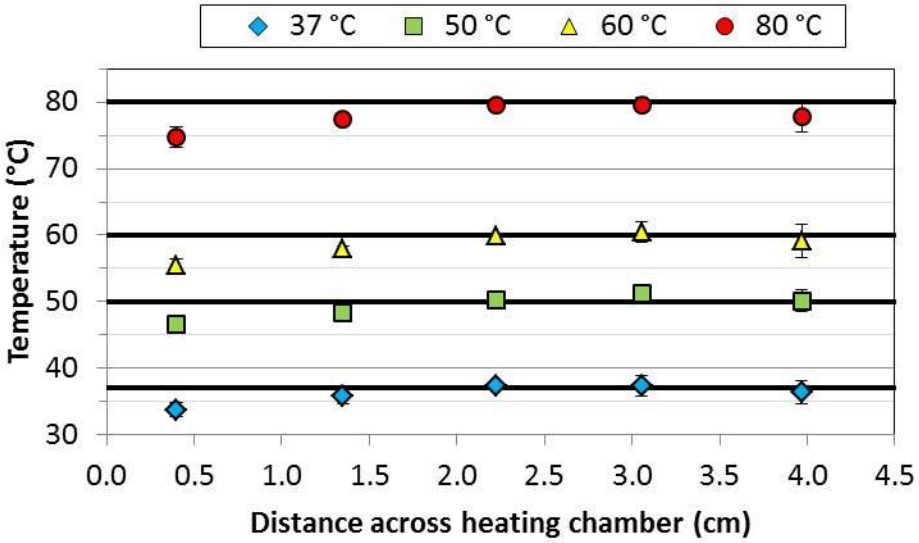

Figure 6.6*: *Temperature Across the SPION Coating Surface. *Temperature measurements across coating surface correspond to deficiencies in the magnetic field strength near the left end of the coil/heating chamber which result in parts of the coating being heated to lower temperatures than the desired set point value. Figure created by Joel Coffel.*

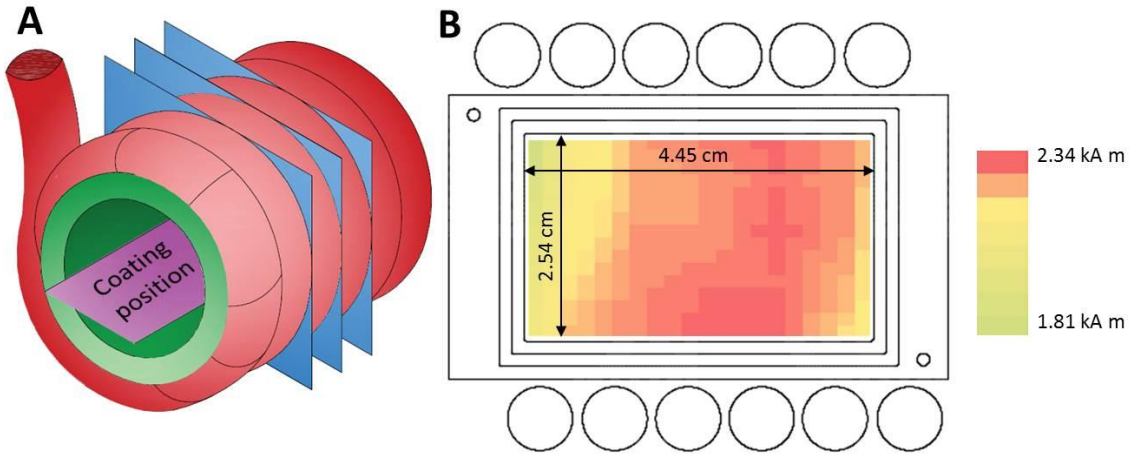

Figure 6.7: Schematic of the SPION Coating Position in the Alternating Magnetic Field's Coil and the Resulting Power Output Heat Map. *A) The position of the alternating magnetic field coil to the coating were parallel to one another. B) The heating effect towards the edge of the slide's surface was affected by the lower magnetic power towards the edge of the coil due to decreased alternating magnetic field strength at the ends. Figure created by Joel Coffel.*

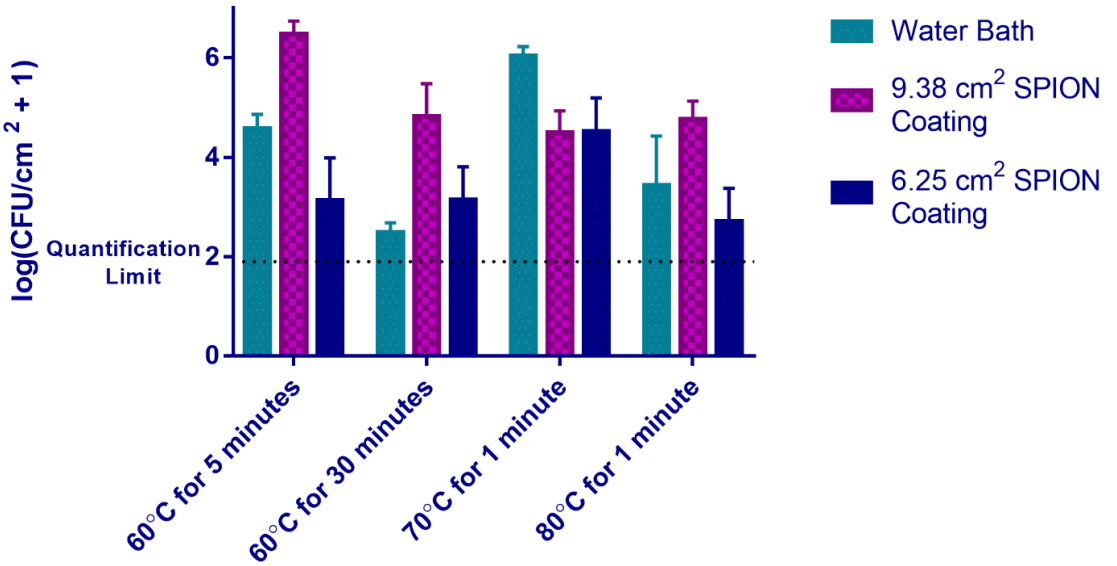

Figure 6.8: Effect of Slide Length on Bacterial Viability Under Various Heat Shock Conditions*. Due to the lower heat transfer at the ends of the slides, shorter slides were investigated to determine the overall effect on bacterial viability post heat shock. In all cases the bacterial population decreased or stayed the same when the length of the coating was decreased.*

6.4. Discussion

Biofilm infections on implanted devices affect hundreds of thousands of patients in the United State annually, leading to painful and long recoveries for these patients.[2,9] The superparamagnetic iron oxide nanoparticle (SPION) coating developed proved that wireless heating can not only be achieved, it killed 100% of the bacteria in the biofilm on a surface as seen by the most extreme case, 80 °C heat shock for 30 minutes. Previous research has shown the effect of heat on biofilms and the possibility of wireless heating applied to a surface;[122] however, this is the first case where a coating has been shown to wirelessly heat a surface and successfully kill bacteria in a biofilm.

It was demonstrated that the temperature of the device can be tuned to reach a given temperature and hold that temperature for a specific amount of time. This allows for specific parameters to be achieved based on the needs of the patient, implant, and infection. The heating achieved via the SPION coating was not statistically different overall from the viable cell count reductions previously reported in Chapter 5 using a water bath showing that the means of heat delivery is independent of the actual amount of bacterial cell death. Heat shocks delivered via a water bath were the same as the heat shocks delivered via the SPION coating for all the control temperature, 37 °C, trials regardless of exposure time. In both the SPION coating heated cases and the water bath heated cases there was little to no effect at 50 °C for 1 and 5 minutes nor at 60 °C for 1 minute. At extended exposure times at 60 °C the population steadily decreased. With the 80 °C heat shocks showing huge population drops, 70 °C was added to the temperature points to explore the effects between the 80 °C heat shocks resulting in high efficacy and the 60 °C which had a large time dependence. For the 5 minutes and 30 minutes of heat shock exposure there was little

difference observed between the 70 °C and 80 °C heat shocks. This indicates that if a longer exposure time is needed at lower temperature a heat shock at 70 °C might be a good alternative to the 80 °C heat shocks.

Overall trends were very similar between the water bath and SPION coating heating systems. Similar to the previously reported heat shocks the wireless heating still showed the biofilms to be more resistant to the lower temperatures, such as 50 °C for 1 and 5 minutes and the 60 °C thermal shock for 1 minute. The 60 °C and 70 °C heat shocks were more effective against the bacteria and the 70 °C thermal shocks dropped the viable cell count by 2 log (CFU/cm +1) with each time step explored indicating a stronger time dependence than seen in the water bath heating trials. The temperature still proved to be the most effective factor with the exposure time to that temperature having a secondary effect. Another similarity between the two heating styles showed that a lower temperature can be maintained for longer to achieve the same amount of bacterial cell death as seen at a higher temperature held for a shorter amount of time. An example of this was the 50 °C for 30 minutes was not statistically different from the 70 °C heat shock for 1 minute. This was also seen for heat shocks at 60 °C held for 30 minutes mitigating a similar amount of bacterial cells as seen by the 80 °C heat shock for 1 minute. Using these similarities will allow for biofilm infected implants to be treated at lower temperatures for longer periods of time or higher temperatures for brief periods of time depending on many factors, such as heat transfer and the type of implant material used.

Previously it was found that the thermal loading can be increased by simultaneously increasing the iron concentration and film thickness, and maintaining a parallel orientation to the magnetic field.[122] Using this information a large amount of iron oxide nanoparticles

was used in the coating to quickly ramp-up the surface temperature. The coating was always placed in the same location in the magnetic field with a parallel orientation to the field for each trial. The temperature ramp-up time was brief for the SPION coating, but when compared to the water bath which has a large thermal inertia resulting in a negligible period of time to reach the set temperature there were some differences. Despite these differences the SPION coating heat shocks resulted in very similar bacterial reduction to the previously found water bath heat shocks for these biofilms.

There were, however, a few cases that resulted in statistically different results than what was seen in the water bath trials occurring in the transition temperatures and the most variation in results appeared when the length of the coating was changed. The differences observed were most likely due to the coating not reaching a uniformly heated surface, which is a possible scenario with any AMF coil and a medical device coating combination and must be taken into account. There were three statistically different points, the 60 °C for 5 minutes, 70 °C for 1 minute, and 80 °C for 30 minutes, seen in Figure 6.8. The mismatch in the data is a direct result of cooler areas on the coating as a result of areas of the coating extending into a weaker AMF as seen in Figure 6.7. Even though 90% of the larger surface area coating is in a uniform field with an average AMF strength of 2.31 ±0.02 kA/m, and the remaining 10% is exposed to a field strength that is only 9.4% lower than the average (2.09 ±0.1 kA/m), due to the quadratic dependence of AMF energy conversion to thermal energy, using Equation 6.2, the heating rate would be 26% less in this weaker area. This results in cold spots which are, at most, 5-6 °C cooler than the rest of the coating as shown in Figure 6.6. Dramatic differences can be observed at these heat shocks with

different coating to AMF field ratios indicating that a larger AMF field with a smaller coated surface will result in a more uniform heating across the entire surface.

6.5. Conclusion

Currently the procedure used for treating patients with biofilm infected implants is incredibly invasive, requires many surgeries, has a long recovery time, and has a low patient quality of life.[2,9] The introduction of a SPION coating that can be heated wirelessly and kill the bacterial biofilm *in situ* without needing additional surgeries could greatly improve patient quality of life. The data obtained were similar to the previous findings of heat shocks on biofilms done in a water bath suggesting that the biofilm will respond to heat similarly regardless of the source. This research proved that the wireless heating via the SPION coating can be achieved and can kill 100% of the bacteria at the most extreme case and 99.9999% of the bacteria if heated at 80 °C for 5 minutes. It was demonstrated that the amount of bacterial cell death has the most variation between 60 °C and 80 °C. In this transition range it was observed to have a maximum efficacy when the coating was smaller than the AMF field due to a more uniform heating of the surface. Progress could be made to ensure a uniformly heated coating by using a larger coil than the patient, or mirroring variances in magnetic field strength with corresponding variances in iron loading or coating position relative to the applied AMF. The more extreme temperatures resulted in the most reduction of the biofilm's bacteria, even at the shorter exposure times, suggesting that the higher temperatures at shorter exposure times should be a focus in the future to maximize the bacterial reduction and minimize the heat penetration into the surrounding tissue. The next chapter explores the heating of these biofilms in conjunction with antibiotics to determine if there are additive or synergistic effects between the two

therapy options since most patients will be treated with antibiotics regardless of additional heat shock treatment.

CHAPTER 7: SYNERGISTIC EFFECTS OF HEAT AND ANTIBIOTICS ON *PSEUDOMONAS AERUGINOSA* BIOFILMS[§]

7.1. Introduction

Persister cells are bacteria in a biofilm that have low metabolic rates and low division rates, which are more resistant to the effects of the antibiotics that typically target either a metabolic pathway or a replication process.[18,61,145] The presence of persister cells results in a population of bacteria that are inherently more resistant to antibiotic treatment.[145] The application of a mild temperature increase, 5 °C increase or less, has enhanced antibiotic efficacy against biofilms in some cases,[150,151] though the decrease in population density was still modest. With the ability to wirelessly deliver localized heat directly at an implant surface *in situ*, more aggressive temperature increases can be achieved,[122] prompting the need to investigate the combined effect of these two orthogonal mitigation strategies together.

This study investigated the combined effect of antibiotics with heat using *Pseudomonas aeruginosa* biofilms. *P. aeruginosa* is a common model organism and is the third most common biofilm former on joint implants.[8] The antibiotics ciprofloxacin, tobramycin, and erythromycin were investigated due to their different mechanisms of action, different sizes, their resistance to higher temperatures, and their frequency of use in patients. The differences in their structural make up and size can be viewed in Figure 7.1. Ciprofloxacin is the smallest of these antibiotics, 331 g/mol, and has been shown to dehydrate at 120 °C, but remains stable below 100 °C.[152–154] It inhibits DNA gyrase and

[§] Ricker, E. B. and Nuxoll, E. Synergistic Effects of Heat and Antibiotics on *Pseudomonas aerugionosa* Biofilms. In preparation.

topoisomerase IV which in turn hinders the cell's ability to replicate.[69] Tobramycin is slightly larger than ciprofloxacin at 468 g/mol and has no appreciable decomposition until 164 °C.[155] Tobramycin binds to the 30S ribosomal subunit in the 16S rRNA A-site preventing protein synthesis.[156–158] Erythromycin is the largest of these antibiotics, 734 g/mol, and does not experience dehydration until reaching 105.6 °C.[159] Erythromycin hinders protein synthesis by binding to the 50S ribosomal subunit in the exit tunnel and causes addition defects.[160–162] The effect of each antibiotic on both planktonic and biofilm bacteria was determined across a concentration range of 0.25 µg/mL to 32 µg/mL for each antibiotic, with further concentrations investigated as needed. Select concentrations were then added to heat shock trials ranging from 37 °C to 80 °C and 1 min to 30 min exposure time. Population reductions for these combined treatments were then compared with reductions by corresponding mono-treatments to identify and quantify synergistic activity.

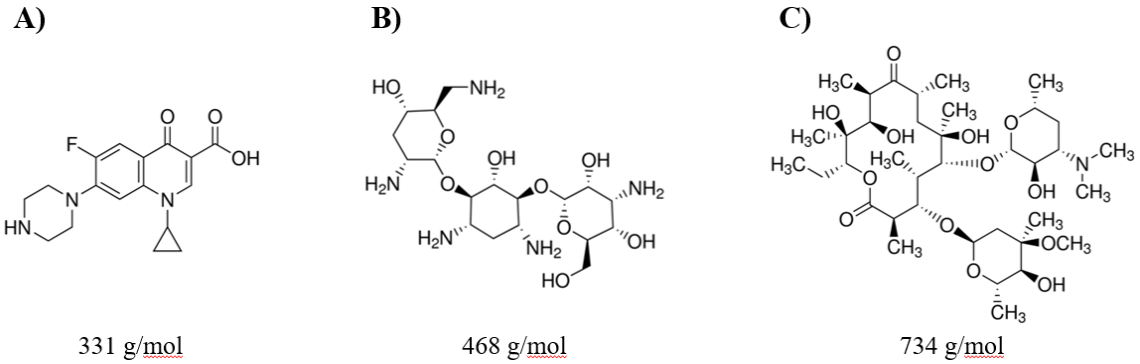

Figure 7.1: Antibiotic Structures and Their Molecular Weight*. The structure of (A) ciprofloxacin, (B) tobramycin, and (C) erythromycin and their corresponding molecular weights.*

7.2. Materials and Methods

7.2.1. Biofilm Growth

Cryogenically preserved *Pseudomonas aerugiona* PAO1 (15692, American Type Culture Collection, Manassas, VA) was thawed and streaked on an agar plate (Difco Nutrient Agar, Sparks, MD, USA). The agar plates were inverted and incubated at 37 °C for 24 hours. An inoculum was made by suspending two colony forming units (CFUs) from the agar plate in five milliliters of sterile tryptic soy broth (TSB, BD Bacto, Sparks, MD, USA) made as directed and incubated at 37 °C for 24 hours, achieving an average concentration of $2.12 \times 10^9 \pm 0.07 \times 10^9$ CFU/mL. One milliliter of inoculum was then diluted into 15 mL TSB and mixed gently. One hundred fifty microliters of the diluted mixture was then placed into each well of the 96-well plate, except for the negative control wells which received 150 µL of TSB. The plate was part of an MBEC™ assay (Innovotech, Edmonton, AB, Canada) in which a corresponding array of 96 pegs protrudes from the plate lid into the wells, providing a convenient array of substrates for biofilm growth which are then readily transferred to new wells.[163] The peg lid was placed onto the 96-well plate then sealed using Parafilm and placed on an orbital shaker table (VWR 1000, 15 mm orbit, Thorofare, NJ, USA) at 160 rpm and incubated at 37 °C for 24 hours.

7.2.2. Antibiotic Preparation

A stock of 5 mg/mL ciprofloxacin in sterile, de-ionized water was prepared with ciprofloxacin hydrochloride (MP Biomedicals, Santa Ana, CA, USA) and mixed thoroughly. Tobramycin stock was made in a similar fashion by mixing 5 mg/mL tobramycin sulfate salt (Sigma-Aldrich, St. Louis, MO, USA) in sterile, de-ionized water. Erythromycin was obtained from MP Biomedicals and the stock was prepared by mixing

5 mg/mL erythromycin into ethanol. Each antibiotic mixture was then filter sterilized through a 0.22 µL PES membrane sterile filter (Millex®GP filter unit) and stored at 2 °C. Each antibiotic was then diluted from the stock solution into sterile TSB at an array of concentrations serially diluted in a 96-well challenge plate used that day.

7.2.3. Antibiotic Exposure

After 24 hours of growth, the array of biofilm-covered pegs was transferred into a 96-well rinse plate (Costar® 96 well flat bottom cell culture, Corning Incorporated, NY, USA) containing 200 µL/well de-ionized, sterile water at ambient temperature for 2 min to remove bacteria not incorporated in the biofilm. The peg lid was then transferred to a 96-well challenge plate of wells containing 200 µL of various concentrations of ciprofloxacin, tobramycin, or erythromycin diluted in TSB. The range of antibiotic concentration was determined from the degree of efficacy the antibiotic had on the biofilm with a range of 0.032 µg/mL to 32 µg/mL for ciprofloxacin, 0.25 µg/mL to 32 µg/mL for tobramycin, and 0.25 µg/mL to 128 µg/mL for erythromycin. For the antibiotic experiments without heat shock the peg lid was exposed to a single challenge plate for 24 hours in an incubator at 37 °C before rinsing again for 2 min in a new rinse plate. The peg lid was then transferred to a recovery plate containing 200 µL/well fresh, sterile TSB for resuspension and enumeration.

7.2.4. Antibiotic and Heat Exposure

To investigate the combined effect of antibiotics and heat shock, three antibiotic concentrations were selected based on the antibitiotic treatment results. A concentration with little to no effect was selected, along with a transition concentration where an effect on the biofilm was observed, and the bloodstream concentration of each antibiotic when

used in a patient. These concentrations allowed for any synergism present to be observed and for the observation of the most applicable concentration, the bloodstream concentration, to be compared at the same combined treatment parameters. The bloodstream concentration may be higher than the concentration at the implant's surface, however, it is likely that the antibiotics are saturated in the tissue, thereby obtaining similar concentrations as the bloodstream. Biofilms cultured and exposed to antibiotics as discussed above were removed from their antibiotic challenge plate after only four hours. The four hours of antibiotic exposure before heating would give the antibiotics time to diffuse through the EPS, if they are capable of doing so, before the heating step and would simiuate the real world application more closely since people will be treated with antibiotics prior to, throughout, and post heat treatment. They were quickly tranferred to a challenge plate with the same array of antibiotic concentrations, preheated to the target temperature by a thermostatted water bath. Temperatures of 37 °C, 50 °C, 60 °C, 70 °C, and 80 °C were studied at exposure times of 1, 5, and 30 min. The pegs were left in the heated challenge plate for the desired exposure time, then transferred to a new challenge plate with the same antibiotic concentrations at 37 °C and incubated for the remainder of the total 24 hour antibiotic exposure time. Following 24 total hours of antibiotic exposure time the peg lid was rinsed once again for two minutes in a new rinse plate and placed into a recovery plate for re-suspension and enumeration. Each growth and challenge plate step is shown in Figure 7.2.

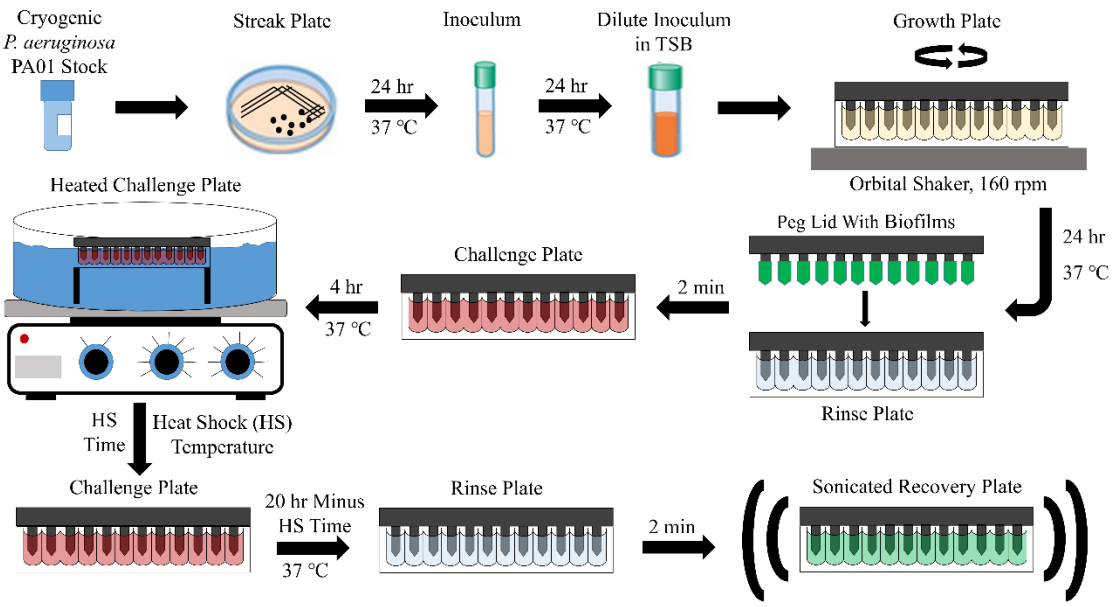

Figure 7.2: Schematic of the Biofilm Growth and the Combined Heat Shock and Antibiotic Treatment. *Stock P. aeruginosa PAO1 bacteria was prepared to grow biofilms which were grown in an MBEC™ assay on an orbital shaker table. The biofilms were then transferred via the peg lid to a rinse plate to rinse off any loosely adhered bacteria then moved over to the challenge plate containing antibiotics and controls in different wells. After 4 hours of the initial challenge plate the biofilms were heat shocked in a heated water bath. The biofilms were then swiftly transferred over to a new challenge plate for the remainder of the total 24 hours of antibiotic exposure. The biofilms were rinsed once again and then placed in a recovery plate for sonication, dilution, and enumeration.*

7.2.5. Biofilm Enumeration

To disrupt the biofilm and re-suspend the bacteria in a homogenous solution for serial dilution, each recovery plate with biofilm covered pegs was sonicated for ten minutes at 45 kHz in a VWR Symphony 9.5 L sonicator (Radnor, PA, USA). The sonicated recovery plates were serially diluted tenfold in a 96-well flat bottom culture plate. Twenty microliters of each dilution were spot plated on agar plates and allowed to absorb for approximately 20 minutes before the agar plates were inverted and incubated at 37 °C for 20 to 24 hours. The resulting colony forming units (CFUs) were then counted and recorded.

The logarithmic population density, $\log\left(\frac{CFU}{peg}\right)$, was calculated using Equation 7.1:

$$\log\left(\frac{CFU}{peg}\right) = \log\left[\frac{(plate\ count)*10^{dilution\ factor}*\left(\frac{200\ \mu L}{20\ \mu L}\right)}{peg} + 1\right] \qquad \textbf{(Equation 7.1)}$$

where the *dilution factor* is the number of tenfold dilutions corresponding to the sample counted and the *plate count* is the number of CFUs counted in that sample. The *(200 µL / 20 µL)* is the ratio of the total recovery suspension to the amount that was sampled. Dilutions showing 3 to 50 CFUs were used for analysis; when two dilutions fit this range, the less dilute sample was used. The upper bound (50) prevents counting error due to overlapping CFUs and the lower bound (3) prevents a single CFU from altering the $\log\left(\frac{CFU}{peg}\right)$ value by more than 0.125 by chance. By this rubric, population densities below $\log\left(\frac{CFU}{peg}\right) = 1.49$ cannot be quantified. In cases where the undiluted recovery well sample yielded less than 3 CFUs, lower $\log\left(\frac{CFU}{peg}\right)$ were calculated but should be considered below the quantification limit. For samples with no CFU evident, the "+1" in Equation 7.1 ensured that the $\log\left(\frac{CFU}{peg}\right)$ value was 0 rather than mathematically undefined; its effect on values above the quantification limit is negligible.

7.2.6. Optical Density Measurements of Planktonic Bacteria

The planktonic bacteria that had escaped the biofilm via dispersion after the heat treatment were optically observed to better understand the biofilm's dispersion post heat treatment while antibiotics were still present. To estimate the free-swimming bacteria following the antibiotic treatment, the optical density (BioTek Gen5 Microplate Reader, Winooski, Vermont, USA) at 600 nm was measured for each well in the second challenge

plate. The negative controls in the challenge plate contained only TSB and were used to calculate an average background.

7.2.7. Statistical Analysis

The statistical analysis of both the planktonic optical density reads and the logarithmic CFU counts were reported via their arithmetic mean and standard deviation. The reported optical density numbers had a measured average background of 0.8 subtracted from their original raw values. Statistical analysis was performed in GraphPad Prism 7 using the two-way ANOVA with a confidence interval of 95%. The antibiotic and heat treatments were only considered synergistic when the antibiotic treatment and the heat treatment had no effect on their own while the combined treatment showed a decrease in viable bacterial cells post treatment.

7.3. Results

7.3.1. Antibiotic Biofilm Trials

None of the antibiotics reduced the biofilm below quantifiable population density at physiologically relevant concentrations, as indicated in Figure 7.3, which shows biofilm population densities after 24 hours of 37 °C exposure to antibiotic concentrations ranging from 128 µg/mL to 0.032 µg/mL in twofold dilutions. Ciprofloxacin and tobramycin did show a power-law decrease in biofilm population density with increasing antibiotic concentration up to 32 µg/mL, with ciprofloxacin prompting consistently lower populations. Erythromycin showed little effect at any concentration.

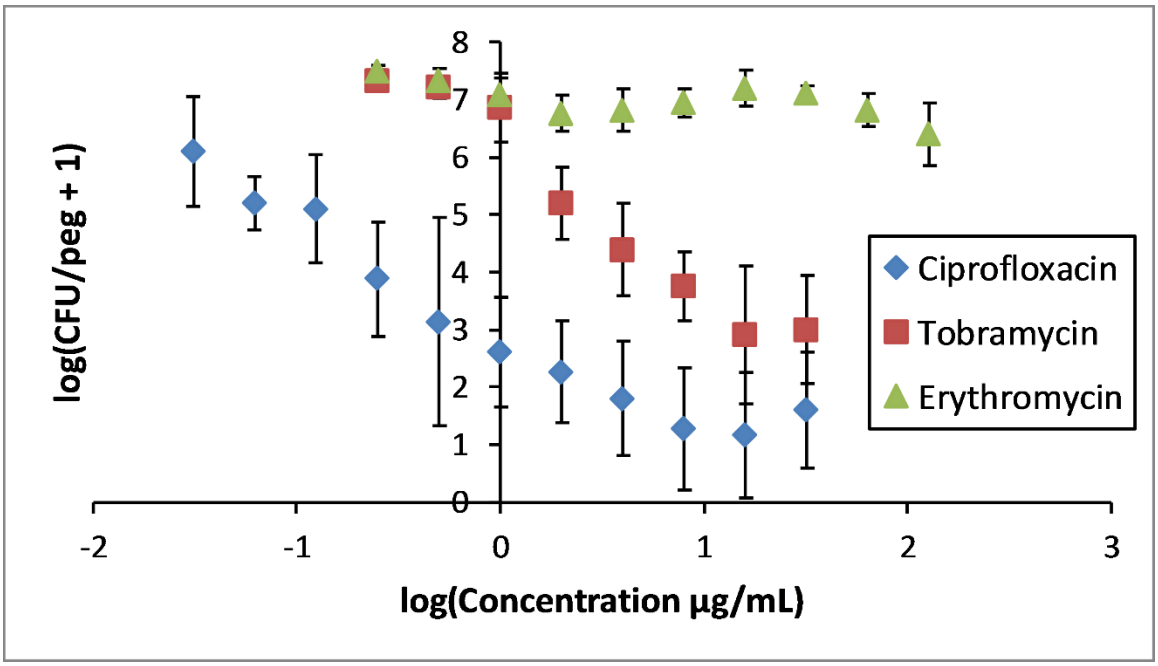

Figure 7.3: Antibiotic Effect on Biofilm Viability. *The ciprofloxacin and tobramycin followed a power-law decrease for a discrete concentration range before reaching an asymptote, with ciprofloxacin having a larger effect on the biofilms than tobramycin. Erythromycin showed no statistical differences for each concentration tested.*

These results were used to select the concentrations for the combined antibiotic and heat-shock trials. Intravenously, ciprofloxacin, tobramycin, and erythromycin are administered at concentrations of 4, 4, and 2 µg/mL, respectively.[69] As these concentrations ciprofloxacin and tobramycin had significant population effects on their own, lower concentrations, 0.125 and 1.0 µg/mL for ciprofloxacin and 1.0 and 2.0 µg/mL for tobramycin, were also used for the combined treatment trials so that increased bacterial death from combined activity could be better quantified. The lower concentrations had little impact on biofilm population density by themselves (discernable for ciprofloxacin) while the intermediate concentrations had a clear power-law effect. Larger concentrations, 64 and 128 µg/mL, of erythromycin were used to increase the likelihood of observing any antibiotic effect at all.

7.3.2. Effects of Antibiotics and Heat on Biofilms

The biofilms were more resistant to both heat and antibiotics than their planktonic counterparts. Without antibiotics, the heat treatment alone resulted in a binary effect, killing all the biofilm bacteria at 60 °C for 30 min, 70 °C for 5 min, and 80 °C for 1 min, while milder treatments had no statistically significant effect, as seen in Figures 7.4 through 7.6. Without heat shock, the biofilm reductions agree with Figure 7.3, showing that the transfer of the biofilms to fresh 37 °C wells had little impact on biofilm viability. These results reconfirm that while ciprofloxacin and tobramycin at higher concentrations significantly reduce biofilm populations, they cannot, on their own, reliably eliminate them as seen with the more aggressive heat shocks. Even at low concentrations, however, those antibiotics have a significant synergistic impact within a key window of heat shock conditions.

Ciprofloxacin at the bloodstream concentration, 4 µg/mL, and at 1 µg/mL substantially reduced biofilms with at least a five-order magnitude decrease in viable bacteria regardless of the heating, seen in Figure 7.4. Combined with 70 °C, 1 min heat shocks, these ciprofloxacin concentrations left no viable bacteria, however, despite the fact that the 70 °C 1 min heat shock by itself had no discernable effect. Even the 0.125 µg/mL ciprofloxacin concentration, which had little effect on biofilms by itself, reduced biofilm populations by five orders of magnitude when combined with otherwise ineffective heat shocks at 60 °C for 5 min and 70 °C for 1 min.

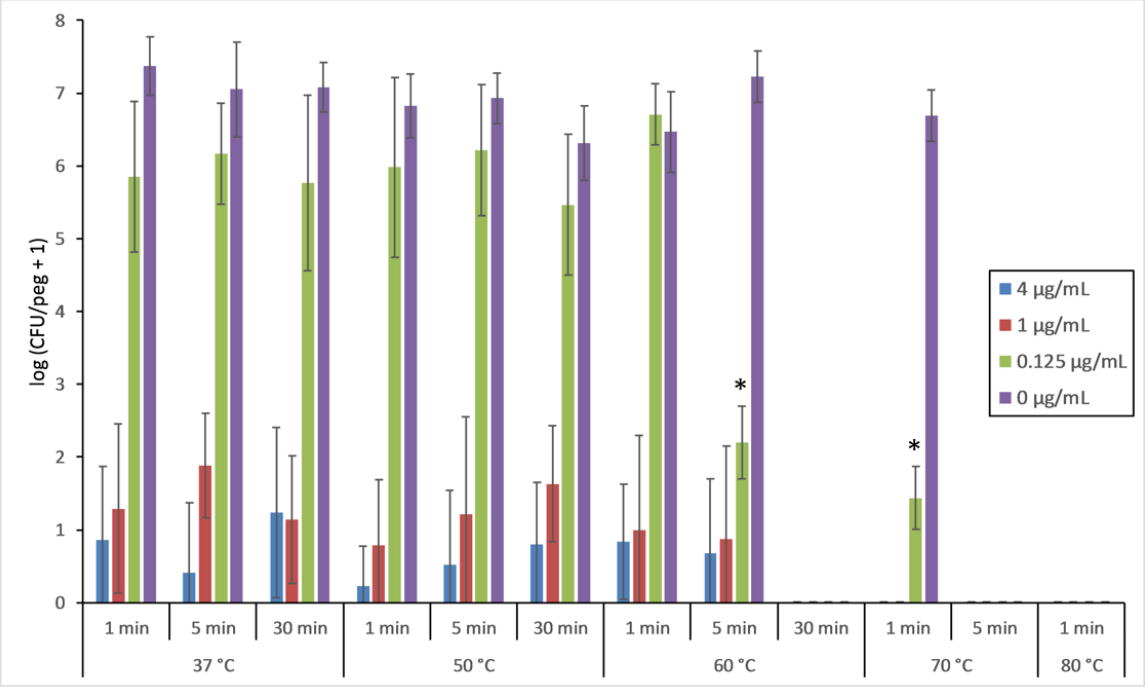

Figure 7.4: Effect of Heat and Ciprofloxacin on Biofilm Viability. *The heat on its own had no effect except at 60 °C for 30 min, 70 °C for 5 min, and 80 °C for 1 min where it effectively eradicated all the bacteria. At the other temperature and exposure times the ciprofloxacin showed no statistical difference from the controls except at 60 °C for 5 min and 70 °C for 1 min where the viable cell counts dropped dramatically for the 0.125 µg/mL concentrations. The asterisks denote significant differences from the corresponding controls (37 °C).*

Tobramycin was the second most effective antibiotic on its own and demonstrated this synergy with heat more clearly than either of the other two antibiotics. Figure 7.5 shows the trend of prolonged heat exposure time increasing the overall efficacy of biofilm mitigation at all non-zero tobramycin concentrations, regardless of temperature. No trend is seen at the control temperature (37 °C) nor is this trend observed without tobramycin, except for complete elimination at 60 °C for 30 min, 70 °C for 5 min, and 80 °C for 1 min as mentioned earlier. Within each of the concentration sets for tobramycin the 50 °C for 30 min and the 60 °C for 5 min exposures resulted in similar mitigation amounts. At 50 °C for

30 min, 60 °C for 5 min, and 70 °C for 1 min the effect of the combined heat and antibiotics was larger than either treatment by itself.

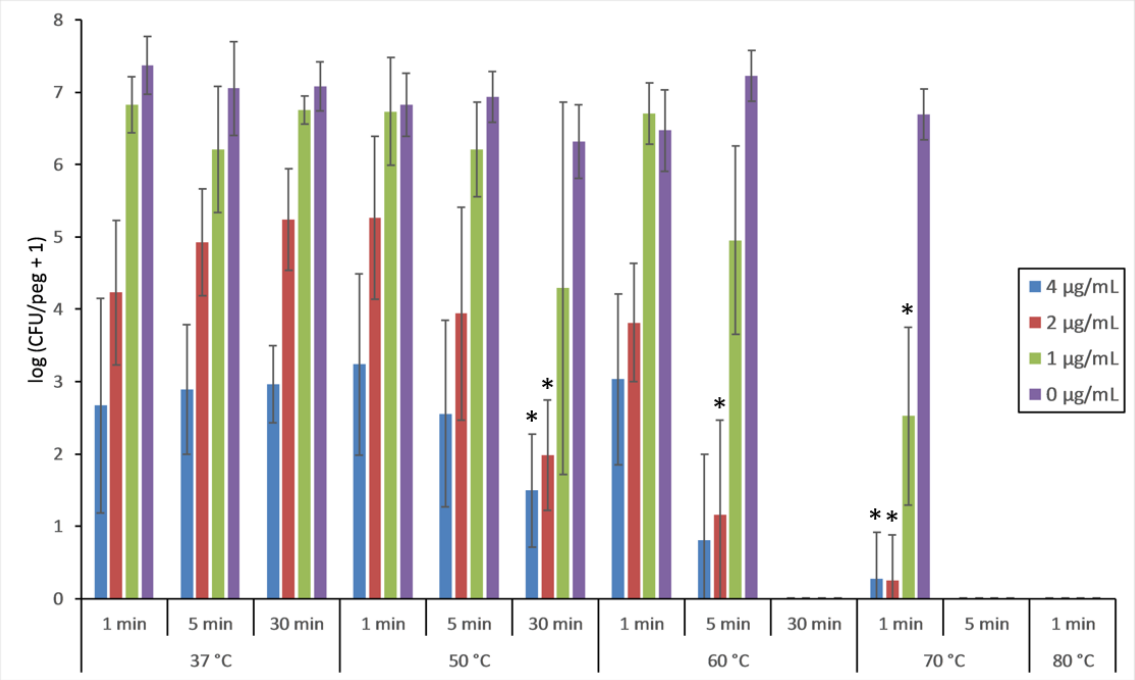

Figure 7.5: Effect of Heat and Tobramycin on Biofilm Viability. *An observable increase in treatment efficacy can be seen at 60 °C for 5 min and 70 °C for 1 min regardless of tobramycin concentration. A subtler increase in treatment efficacy was observed at 50 °C for 30 min. Otherwise there were no statistical differences between the controls and the 50 °C for 1 and 5 min regardless of tobramycin concentration. Heat treatments of 60 °C for 30 min, 70 °C for 5 min, and 80 °C for 1 min eradicated the biofilm independently of the tobramycin concentration. The asterisks denote significant differences from the corresponding controls (37 °C).*

Erythromycin showed no effect at any concentration for the control temperature, 37 °C, nor in combination with 50 °C heat treatments as seen in Figure 7.6. However, biofilms heated at 60 °C for 5 min and treated with 64 µg/mL or 128 µg/mL erythromycin decreased in viable bacteria by an average of 1.5 log(CFU/peg) and 2.7 log(CFU/peg), respectively. At 70 °C for 1 min the biofilms exposed to 64 µg/mL decreased by 2.3 log(CFU/peg) and when exposed to 128 µg/mL the number of viable bacteria decreased by

6.0 log(CFU/peg). Similar to the other antibiotics, the combined antibiotics and heat shock approach showed the greatest increase in efficacy over either individual treatment in the heat shock window of 60 °C for 5 min to 70 °C for 1 min.

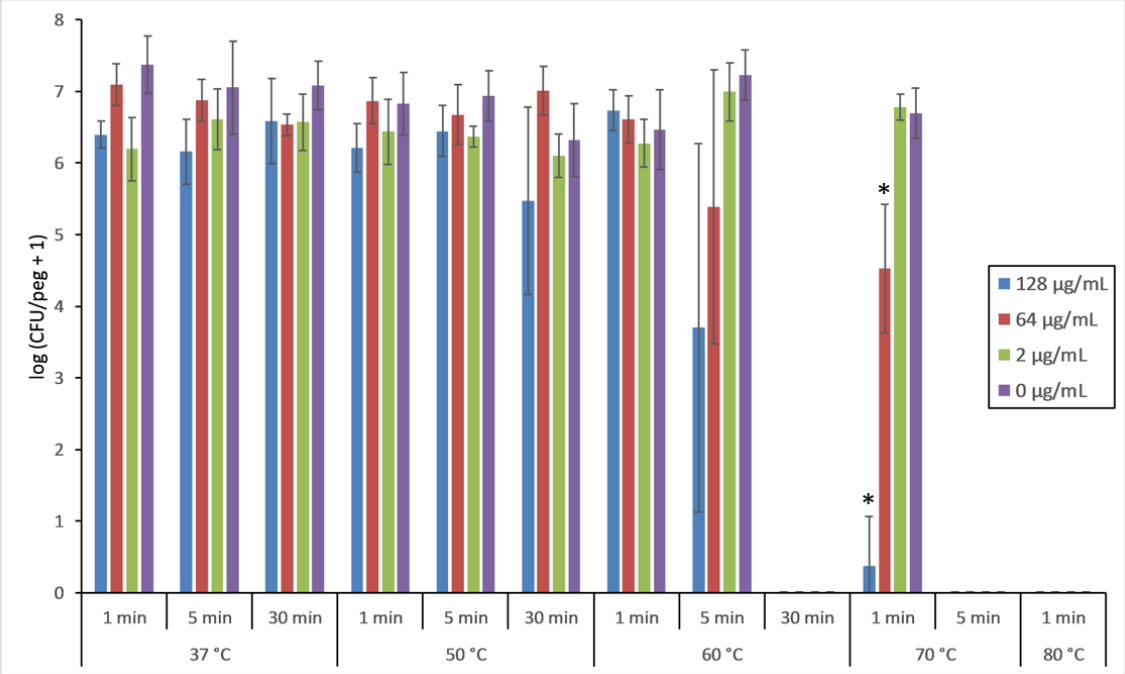

Figure 7.6: Effect of Heat and Erythromycin on Biofilm Viability. *No statistical differences were seen between any of the erythromycin concentrations for temperatures of 37 °C and 50 °C. At 60 °C for 5 min an observable difference appears at concentrations of 128 and 64 µg/mL and again at 70 °C for 1 min. Biofilms treated with 2 µg/mL erythromycin proved to be no different than the biofilms not exposed to antibiotics. The heat killed off all the bacteria regardless of antibiotic treatment at the higher temperatures and prolonged exposure times. The asterisks denote significant differences from the corresponding controls (37 °C).*

7.3.3. Effects of Antibiotics and Heat on Dispersed Planktonic Bacteria

Further confirming the biofilm measurements, the media in which the biofilms incubated after heat shock resulted in optical density measurements with virtually no bacteria for treatments in which the corresponding biofilm was destroyed. Moreover, in antibiotic free trials the heat shock had no apparent effect on the bacteria's ability to

disperse from the biofilm and repopulate a fresh well. However, the presence of antibiotics strongly inhibited planktonic bacterial growth regardless of the presence of heat shock. All three concentrations of ciprofloxacin, 0.125, 1.0, and 4.0 µg/mL seen in Figure 7.7, and tobramycin, 1.0, 2.0, and 4.0 µg/mL seen in Figure 7.8, were effective against the planktonic bacteria with the higher two of the three concentrations killing off almost all the free-swimming bacteria regardless of heat shock. Erythromycin had no discernable effect at 2 µg/mL as seen in Figure 7.9. However, at 64 µg/mL there was a reduction in population even without heat shock, and a further decrease in viable planktonic bacterial cells at 128 µg/mL. Notably, while a 60 °C heat shock for 5 min had no effect by itself, in the presence of erythromycin the bacteria population was significantly reduced from the non-heat-shocked values, this effect was even more pronounced with a heat shock at 70 °C for 1 min. The synergistic effect of antibiotics with heat shocks at 60 °C for 5 min and 70 °C for 1 min were observed with all the antibiotics, but most prominent with erythromycin.

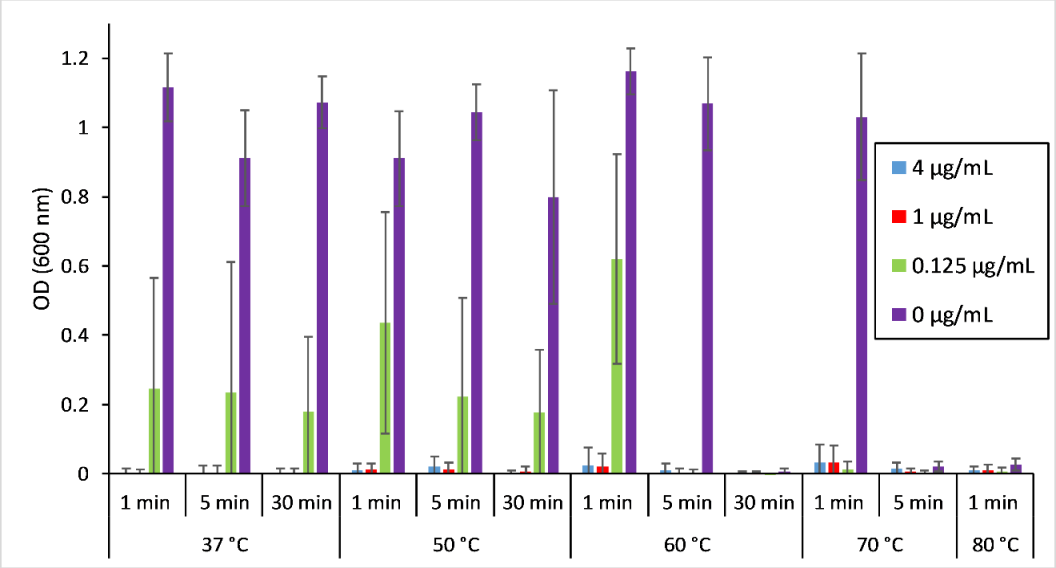

Figure 7.7: Effect of Heat and Ciprofloxacin on the Remaining Planktonic Bacteria Viability. *The optical density of the dispersed planktonic bacteria from the biofilm proved to only be present for concentrations of 0.125 µg/mL ciprofloxacin or when there was no antibiotic present. Heat treatments of 60 °C for 30 min, 70 °C for 5 min, and 80 °C for 1 min had no growth regardless of ciprofloxacin concentration. Ciprofloxacin at 0.125 µg/mL when combined with 60 °C for 5 min or 70 °C for 1 min completely eradicated the planktonic bacteria.*

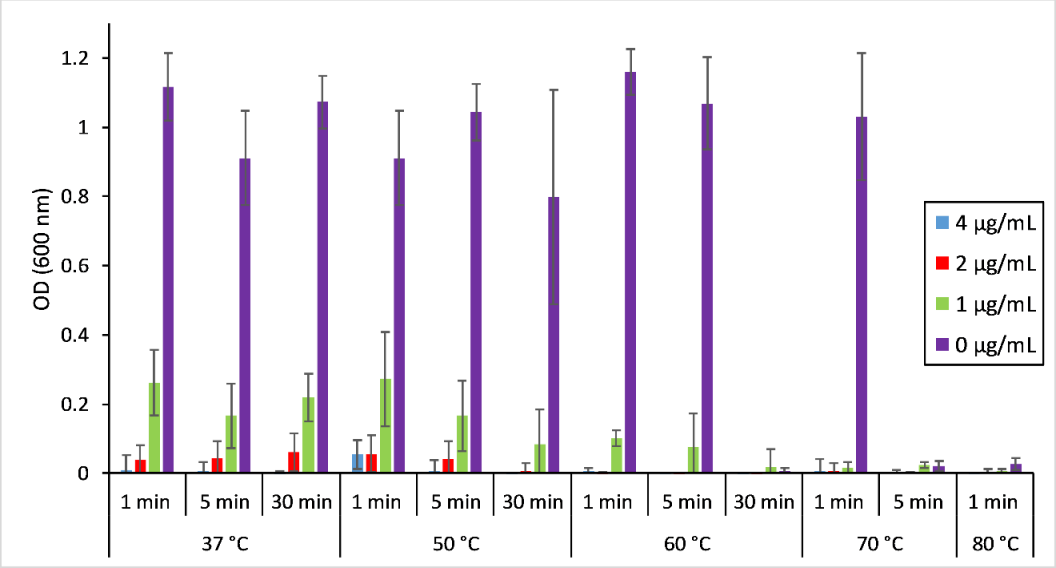

Figure 7.8: Effect of Heat and Tobramycin on the Remaining Planktonic Bacteria Viability. *Tobramycin was quite effective against the bacteria that dispersed from the biofilm and showed complete eradication of the planktonic bacteria at all concentrations of tobramycin at 70 °C, 80 °C and 60 °C for 30 min. At concentrations of 1 µg/mL and 2 µg/mL when combined with heat shocks of 50 °C for 30 min or 60 °C for any exposure time resulted in no planktonic growth.*

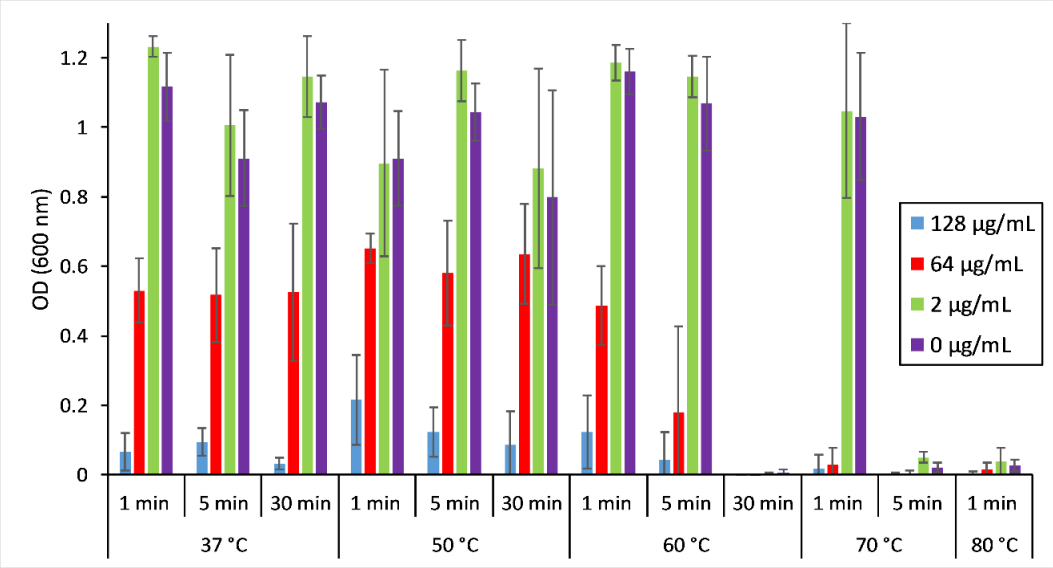

Figure 7.9: Effect of Heat and Erythromycin on the Remaining Planktonic Bacteria Viability. *No difference was observed between the biofilms treated with an erythromycin concentration of 2 µg/mL and the biofilms not treated with erythromycin. However, the higher concentrations of erythromycin did have an improved efficacy in the presence of heat against the planktonic bacteria.*

7.4. Discussion

Biofilms are present in many locations, from the plaque on teeth to the bottom of ship hulls. On implanted medical devices a biofilm infection can be life threatening and often requires surgical explantation followed by intensive antibiotic treatment before surgical implantation of a replacement device.[2] This stems from biofilms' much higher resistance to antibiotics than their planktonic counterparts,[16,17,19] a phenomenon demonstrated again in this study, with all three antibiotics showing more efficacy against free-swimming bacteria than their biofilms. In the most extreme case, erythromycin at 37 °C had no effect against the biofilm at any concentration, but decreased the optical density of the planktonic bacteria by 90% at 128 µg/mL. Tobramycin and ciprofloxacin had some efficacy against the biofilms, but in each case reached an asymptote where they could not

further reduce the bacteria population below about 3 log(CFU/peg) or 1 log(CFU/peg), respectively, while virtually eliminating planktonic bacteria. Heat shock, on the other hand, appears to effectively mitigate biofilms, though conduction of heat to the tissue may cause significant damage which must be minimized[57,120,149] and the combination of antibiotics with the heat could lower those required temperatures.

As antibiotics are typically administered to infected patients as a first line of defense, their effect on the efficacy of heat shock is of prime interest. It was hypothesized that synergistic effects would be observed from improved transport of the antibiotics through the EPS or increased bacterial metabolism from the heat increasing the vulnerability of the bacteria. The heat shock window for such observations is limited on one end by shocks effective enough to eradicate the bacterial biofilms on their own (60 °C for 30 min, 70 °C for 5 min, and 80 °C for 1 min) and on the other end by shocks so weak that even amplified effects are not discernible. This synergistic window was observed at 70 °C for 1 min and at 60 °C for 5 min for all the antibiotics and additionally at 50 °C for 30 min for tobramycin. At these temperatures and exposure time the biofilms were not affected by either heat shock or antibiotics alone, but when combined these treatments had a substantial effect on the biofilm population.

One potential contribution to the synergism is the increased transport of the antibiotics through the EPS in the presence of heat. Some antibiotics such as aminoglycosides like tobramycin have been shown to have slow transport across the EPS, while other antibiotics such as ciprofloxacin appear to have little transport limitation across the EPS.[61,164] This aligns with these results that ciprofloxacin was more effective against the biofilms than tobramycin, with little to no effect seen from erythromycin. This trend

also follows the molecular masses of the antibiotics closely which may influence the diffusivity of the molecules based on their sizes. The limited duration of the elevated temperature (1 to 30 min) compared to the overall exposure time (24 hr) suggests that this contribution was limited, as the diffusivity should only increase about 50% according to the Wilke-Chang diffusivity model.[165] Chemical reactions or physical adsorption of the antibiotics by the EPS would also effectively limit their transport;[66] however, the change of antibiotics at the 4 hr point should increase the efficacy regardless of temperature and that was not observed.

Many researchers have suggested that the limiting factor for antibiotic efficacy in biofilms is not transport, but rather the low metabolism of many of the bacteria in the biofilm.[61] The decreased metabolism of bacteria based on their locations in the biofilm is well documented[61,145,166] and likely contributes to the observed synergism in this study. With little baseline metabolic activity, inhibition of replication or protein synthesis has little consequence on bacterial viability, severely limiting the antibiotics' efficacy in biofilms. Thermal stimulation of metabolic activity would increase this efficacy dramatically. This study supports this hypothesis and identified a temperature and exposure time thresholds at which the metabolism increases. All antibiotics showed synergistic efficacy at 70 °C for 1 min and at 60 °C for 5 min, with tobramycin also synergistically effective at 50 °C for 30 min. Tobramycin can also cause bacteria wall damage[156,167,168] which may increase its synergy with heat shock. A further implication of this hypothesis is that heat shocks at those conditions without antibiotics may increase the activity of the bacteria in the biofilm.

In practice, it is unlikely that any biofilm infection therapy would be implemented without concurrent systemic antibiotics. This study indicates that with these antibiotics in combination with a heat shock treatment, biofilms may be eliminated at lower temperatures and exposure times than previously observed, significantly reducing the damage to surrounding tissue. Reduced heat shocks also require less heating power. With a decreased demand for heating power a wirelessly heated coating via induction from an alternating magnetic field would require a lower magnetic field strength and would improve the ability to localize the field.

7.5. Conclusion

An elegant solution to biofilm infection and biofouling is the use of heat. However, heat is not always a viable option at the needed high temperatures and exposure times to kill the bacteria in the biofilm such as the case of an implanted device. This study showed that the use of antibiotics in conjunction with heat can have a synergistic mitigation effect against *P. aeruginosa* biofilms. Heat shocks of 70 °C for 1 min and 60 °C for 5 min, which had no mitigation effect on their own, prompted a sharp decrease in biofilm population density when combined with any of the three antibiotics with different mechanisms of action, even at concentrations that have no effect on their own. While heat shock likely does increase antibiotic transport through the EPS, the results of this study suggest transport is not the limiting factor in antibiotic efficacy in these biofilms. More consistent with these results is the theory that metabolic activity is severely limited in a fraction of biofilm bacteria, and that heat shocks of 70 °C for 1 min and 60 °C for 5 min, or in some cases, 50 °C for 30 min, will stimulate activity for antibiotic efficacy. This synergism

significantly reduces the required thermal load and the negative impacts of this load on the surrounding tissue and materials.

CHAPTER 8: CONCLUSIONS AND RECOMMENDATIONS

Biofilms cause infections and biofouling in a wide range of scenarios from implanted medical devices to industrial plants, spurring the development of many innovative antibiofouling techniques. The use of a polymer coating containing superparamagnetic iron oxide nanoparticles, or a SPION coating, is an elegant solution to achieve wireless heating of a surface to mitigate a biofilm. The work done in this thesis achieved a better understanding of how effective heat is against *Pseudomonas aeruginosa* biofilms by investigating the required temperatures and exposure times to kill the bacteria and the combined treatment with antibiotics for a variety of biofilms grown in different growth conditions.

8.1. Drip Flow Reactor Grown Biofilm Thermal Mitigation

Biofilms grown in a drip flow reactor, DFR, were very high in population density most likely due to the abundance of nutrients flowing over the biofilm, easier oxygen exchange, and constant waste removal. The DFR biofilms' high population counts allowed for quantitative correlations of the degree of bacterial cell death to the shock temperature and exposure time across the entire parameter space (50-80 °C and 1-30 minutes). When the DFR biofilms were heat shocked they exhibited significant population reduction at every point within the heat shock parameter space. The effect of the thermal shock on the bacteria followed a modified Arrhenius dependence on temperature and a Weibull-style relationship to the exposure time, as seen in Equation 3.3 and Equation 3.4. Various time and temperature combinations resulted in similar population decreases, such as 60 °C for 30 minutes and 80 °C for 1 minute, allowing for different types of heat shocks to be applied depending on which would be more beneficial for that application. For a polymer that

cannot safely heat above 70 °C the lower temperature for a longer exposure time may be desirable, while an implanted bone pin would want a shorter exposure time to the heat to decrease the overall heat transfer to the body by minimizing the duration of heating. Up to six orders of magnitude drop in viable bacterial cells in the biofilms were observed with the thermal treatment, which appears to be a viable way to mitigate biofilms.

8.2. Analysis Tools

Two ways of analyzing the resulting bacteria after the heat shocks were investigated, enumeration and microscopy. Sonicating the bacteria into a homogenous suspension and then serially diluting this liquid and plating each dilution (*i.e.* enumeration) provided a consistent set of results and is commonly used in the microbiology world. However, these results did not show the biofilm morphology nor the spatial information about the heat shock's effect across the biofilm. Via confocal scanning laser microscopy and dyes the morphology of the biofilms could be observed. It was found that the biofilms grown in the DFR grew across the microscope slide surface with thicknesses from 50 μm to plumes up to 150 μm. The heat shocks did not kill just the outermost bacteria nearest the heat source, but killed bacteria throughout the biofilm indicating that the heat transfer limitations were negligible through these thin films. Two analysis techniques were used to determine the amount of live bacteria after a heat shock via objective thresholding of the microscope images and the results were not as consistent as the enumeration results. Therefore, it was determined that serial dilution and plating was the most reliable way to quantify the population reduction while using the confocal scanning laser microscope to visually observe the biofilm morphology and bacterial viability after the heat shocks.

8.3. Growth Condition Effects on Thermal Mitigation

The growth conditions of the biofilms greatly dictated the response the bacteria had to the thermal shocks. For the bacterial biofilms grown in a DFR the bacteria had a fairly steady decrease over a logarithmic scale while the biofilms grown on a shaker table were more resilient to the heat treatment at the lower temperatures. The biofilms from the shaker table had no significant difference ($p \leq 0.05$) whether they were heat shocked at 50 °C or at their incubation temperature of 37 °C. The same was true for the shaker table-grown biofilms heat shocked at 60 °C for 1 minute. This indicates that the biofilms grown on the shaker table were more robust than the DFR-grown biofilms. The observed difference is most likely due to the harder growth conditions that the shaker table-grown biofilms experienced. These biofilms had a limited amount of nutrient, constant shear forces, no removal of waste products, and were grown for 4 days. The harder growth conditions are believed to be the cause of the difference in thermal susceptibility with the nutrient sources having little effect since the different growth media showed only subtle differences in the 60 °C thermal shocks. However, at the higher temperatures, 80 °C and at 60 °C for 30 minutes, the biofilms had a consistent amount of viable cell reduction of at least five orders of magnitude, more closely following the predictive model discussed in Chapter 3. This indicates that for a more consistent mitigation the higher temperatures will provide a more reliable treatment and if coupled with a shorter exposure time the surrounding tissue will have limited damage from the heat.

8.4. Regrowth After Heat Shock

With the growth media showing little difference and the shaker table-grown biofilms proving to be the hardest biofilms to kill the TSB shaker table-grown biofilms

were regrown after the heat shock to determine the effects after the heat shock. The biofilms were re-incubated from a heat shock and enumerated after 2, 4, 12, 24, or 96 hours of regrowth time. The heat shocks investigated were 60 °C for 5 and 30 minutes, 70 °C for 5 minutes, and 80 °C for 1, 5, and 30 minutes since they had bacterial cell death post heat shock What was observed was that the biofilms that had population density that decreased to below 10^3 CFU/cm^2 did not grow back, in fact they failed to thrive while the biofilms that did not decrease below this population density eventually grew back to the original population. The regrowth study identified the 10^3 CFU/cm^2 as a threshold population density below which a treatment would need to bring the population in order to be successful.

8.5. Wireless Heat Treatment

Biofilms heat shocked via the SPION coating and an alternating magnetic field proved to be similar to the results observed from water bath heat shocks indicating that the source of the heat does not affect the results. Additionally, the wireless heating of the biofilms proved that the SPION coating could be effective when used to mitigate a hard to reach biofilm infection. A valuable observation found during these trials was the sensitivity of the nanoparticle coating's location to the local magnetic field strength. As the generation of heat varies quadratically with the field strength and the population of surviving bacteria vary logarithmically with the heat generation, small biofilm regions in a slightly weaker field can change the overall population reductions achieved across the rest of the biofilm. importance of the ratio between the coated surface length and the length of the alternating magnetic field coil. The coated surface should be about half the length of the coil that is

delivering the alternating magnetic field and should be placed centrally into the coil. This will insure constant and reliable heating across the entire surface.

8.6. Combined Heat and Antibiotic Treatment

Three antibiotics were screened for their efficacy against both the biofilm and planktonic bacteria. Ciprofloxacin[152–154], tobramycin[155], and erythromycin[159] are three antibiotics typically effective against *P. aeruginosa* and thermally stable up to 100 ºC. Each of the antibiotics had a different mechanism of action and each were different in size with ciprofloxacin being the smallest and erythromycin being the largest. When the biofilms were treated with just antibiotics ciprofloxacin was the most effective followed by tobramycin, with no effects observed with erythromycin treatments. The ciprofloxacin and tobramycin could kill off much of the bacteria in the biofilm but would reach an asymptote where they showed no difference in effect with increasing antibiotic concentration. The high concentrations did show a large effect on the biofilms, however, these concentrations far surpass the safe dosage levels for a patient.

The combined therapy of antibiotics with heat showed a significant improvement of the treatment efficacy within a specific temperature and exposure time window. All three antibiotics increased in their efficacy at 60 °C for 5 minutes and 70 °C for 1 minute. At these two points neither heat nor antibiotics on their own had an observable effect; however, together they had up to six orders of magnitude decrease in viable cells post treatment. Two theories were discussed as to the reasoning behind the synergism, increased transportation of the antibiotics through the EPS in the presence of heat, or the increase in metabolic activity of more dormant cells in the presence of heat. Increased diffusion when systems are heated is a well-known process; however, not as likely to be a large factor

when the thickness of the EPS is so small. Further into the biofilm, bacteria tend to take on a more dormant state, decreasing their metabolism and division rates. Since most antibiotics require binding sites from an active metabolic pathway or an actively dividing cell the dormant cells are not affected by the antibiotics. It was concluded that the transport limitation was not as likely to be a significant factor for the observed synergism as the metabolism increase due to the behavior observed. This synergistic behavior will allow for lower temperatures and shorter exposure times for patients currently on an antibiotic and further increase the efficacy of the treatment by combining heat and antibiotics.

8.7. Recommendations

8.7.1. Effect of Shear on Biofilm Growth and Thermal Susceptibility

Shear stress has been shown to have a significant effect on biofilms[28,82,147,169] and is physiologically inherent, especially for implants such as a heart stent, making it imperative to study. Through flow cell studies the effect of shear on the biofilm's growth and therefore susceptibility to heat can be investigated along with the presence of a convective heat sink which could greatly change the heating dynamics of the biofilm. There is also the possibility that the bacteria may try and flee the biofilm into the cooler flow and this potential can be observed via a flow cell experiment. An initial set of flow cell experiments were conducted, but further investigation would elucidate the effects shear stress may have on the biofilm and how that may change the effect heat has on the biofilm. The flow cell was set up with insulated walls and an electroresistive heating coating made of nichrome foil placed in the center of the floor of the flow cell. The biofilms were grown on the coating in a DFR. The flow cell had water flowing through at 37 ºC at 1 L/min, but varying rates should be investigated. The outlet of the flow cell was collected to determine

if any viable bacteria had been sheared off or dispersed. The biofilms were heated through the substrate at 50 °C and 80 °C to determine the effect of heat when combined with a fluid flow. As seen in Figure 8.1 the shear stress of the flow over the biofilm did remove quite a few bacteria from the biofilm, most of which were viable, regardless of temperature. However, the higher temperature, 80 °C did appear to cause more bacteria to disperse than the other temperatures. This initial data set, however, requires more time and data collection to have a thorough conclusion drawn.

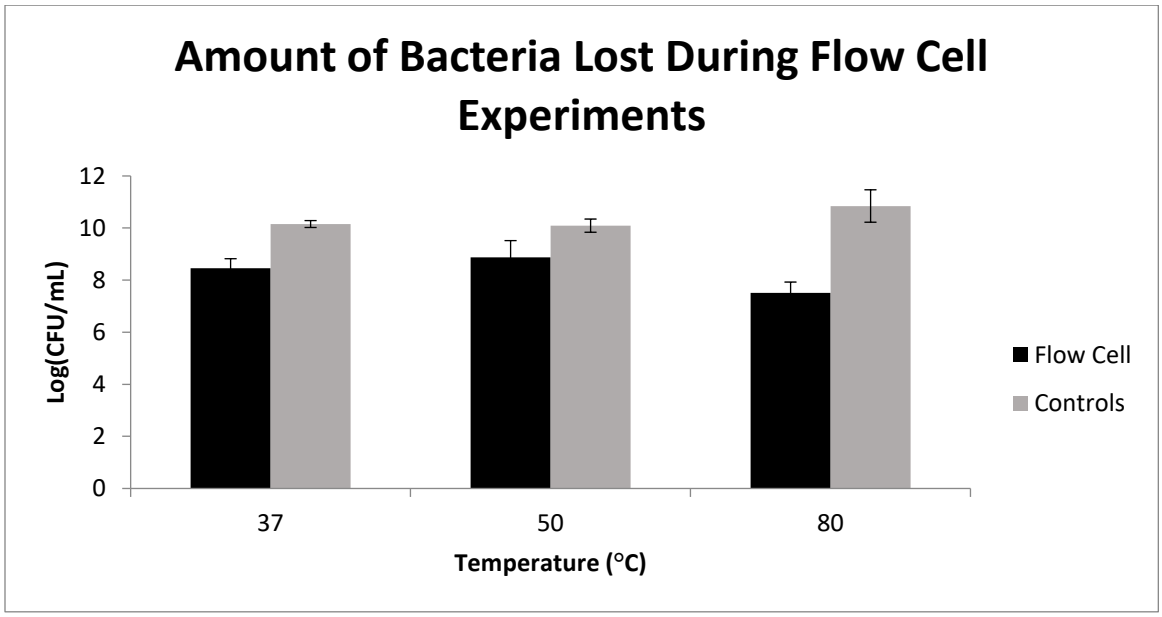

Figure 8.1: Initial Flow Cell Data on the Amount of Bacteria Lost During the Flow Cell Experiments*. Flow of body temperature water was run at 1 L/min over the biofilm while its substrate was heated. Controls were heat shocks in the flow cell without any flow.*

Further experiments conducted with temperatures of 50 ºC, 60 ºC, 70 ºC, and 80 ºC along with controls of 37 ºC should be conducted to get a better understanding of the effect fluid flow may have on the biofilm. The use of thermistors placed throughout the biofilm surface could give insight into where the heating is most intense and how the convective flow of the media impacts the biofilm temperatures. It is hypothesized that some bacteria

will leave the biofilm to go into the flowing 37 ºC water as a means to escape the heat. To determine the amount of bacteria disassociating from the biofilm solely from the heating at lower temperatures, the flow cell should be run at similar speeds as the drip flow reactor. It is hypothesized that since the biofilm was grown at these speeds, the shear stress will have negligible effects on the bacteria and therefore eliminate that variable. Once the amount of bacteria leaving the biofilm due to heating is determined, the synergistic effects of heating and shear can be determined. The flow cell experiments should also be closely monitored to determine convective heat sink potentials for any biofilm treatments that may have a flow of liquids adjacent to it. It is hypothesized that with shear the biofilms will be thinner and contain less bacteria making it more susceptible to the heat treatment. These experiments will also indicate if fleeing bacteria from the biofilm will be a factor in the treatment since they could cause a more systemic infection once they leave the biofilm. It is also possible that if the bacteria flee the biofilm during the heating that the antibiotics and the immune system will be able to be more effective against the infection since it will then be in its more susceptible form, the planktonic state.

8.7.2. Regrowth

Chapter 5 discusses the regrowth of the shaker plate biofilms grown in TSB; however, more information could be obtained from regrowth studies. Only one heat shock was applied during the regrowth studies investigated and it is possible that the efficacy of the heat treatments may change with repeated heat shocks. Multiple heat shocks may result in more resistant bacteria to the heat since the remaining bacteria may become more adept to the higher temperature environment. It is also possible that the repeated heat shocks may yield a more effective result with the bacteria that did not die in the first treatment dying in

the second treatment. The regrown biofilms did show a decrease in their growth rate after the heat shock and the timing of a second heat shock in that slow regrowth time may be a vitally important differentiation between success and failure for repeated heat shocks. Therefore, investigations into the specific timing of a follow up heat shock may bring to light more information about the effect of heat on the biofilms and how to best design a treatment plan.

8.7.3. Wireless Heating

The wireless heating experiments seen in Chapter 6 were completed with polystyrene polymers with iron oxide nanoparticles embedded into the polymer. Further investigations into effective polymers will expand the potential use of this technology and allow for the implementation of the most biocompatible coating. This could be further investigated by measuring the retention of the polymer coating when in an animal and through longevity trials. Additionally, the control of the wireless heating via the SPION coating could be improved so that pulsatile heating could be applied to the surface. Pulsatile heating may decrease the heat transfer to the surrounding tissue while effectively killing the bacteria in the biofilm.

8.7.4. Analyze Bacterial Changes

The bacteria behavior is likely to have changed in the presence of heat as discussed in Chapter 7. This change was hypothesized to be from the heat increasing the metabolism of the bacteria and therefore increasing the efficacy of the antibiotics, however, this still has to be investigated. The metabolism changes from the heat and antibiotic treatment could be better understood using MTT and mass spectrometry analysis. MTT, 3-(4,5-dimethylthiazol-2-yl)-2,5-diphenyltetrazolium bromide indicates the amount of metabolic

activity of cells and could be used to determine the overall change in metabolic behavior. Enzymes in viable cells will break down the MTT to formazan, thereby changing the color of the wells from a yellow color to a purple color, this reaction can be seen in Figure 8.2. The larger quantity of purple present indicates a larger amount of metabolically active cells. This can be observed quantitatively via an absorbance plate reader at 570 nm with a reference read at 630 nm. Initial trials of MTT were performed with 100 µL removed from each well and 5 µL of MTT added to each well. The MTT was then left to be converted to formazan for a determined amount of time and then the reaction stopped by adding 100 µL of 0.04N HCl in isopropanol. Once the reaction was completed, the microtiter plates were read in a plate reader at 570 nm and 630 nm. A percent viability can be calculated by comparing to blank wells and control growth wells. It was found that the biofilm bacteria have a slower metabolic rate so they need to be exposed to the MTT longer; this time exposure was determined by creating an MTT exposure curve.

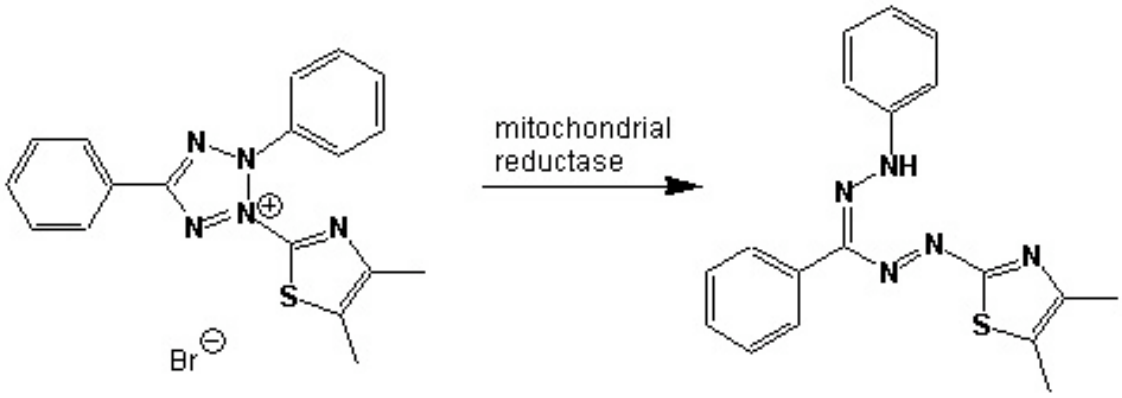

Figure 8.2: Schematic of MTT Chemical Reaction. *MTT breaks down to formazan using the hydrogen group cleaved from an NADH in the mitochondria.*

It was found that just a half hour of exposure to MTT was efficient for the planktonic bacteria, but very little of the MTT was converted to formazan for the biofilm bacteria after a half hour, presumably due to slowed metabolic rates. Therefore, to get a comparable amount of MTT conversion to formazan a set of time trials with biofilms needed to be performed to determine the best conversion time for the MTT with biofilms. This was conducted by allowing the biofilms to grow on the peg lid as described above and then after rinsing and sonicating the bacteria into a recovery plate the bacteria were transferred to another plate and diluted into a set of ten-fold dilutions. MTT was added and the reaction stopped at different time intervals. Figure 8.3 shows the data collected for the best MTT conversion trials.

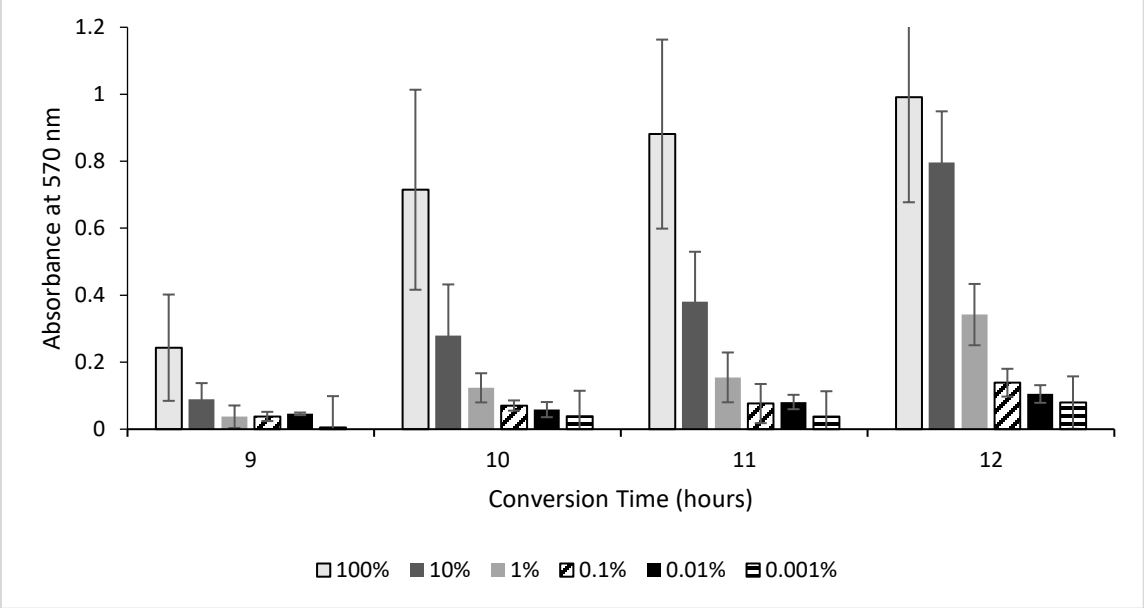

Figure 8.3: MTT Conversion to Formazan Timing Experiments for Biofilms*. MTT was allowed time to convert to formazan and then the reaction was stopped and the absorbance read at 570 nm.*

From the timing data collected, the time steps of 11 hours and 12 hours were singled out since they showed the most distinction between one dilution to the next. Leaving MTT

in the biofilm's recovery plate for 12 hours resulted in the higher absorbance readings, but maintained very similar trends seen in the 11 hour trials. The 11 hour trials had absorbance readings closer to the planktonic readings at a half hour; therefore, a conversion time of 11 hours was used for the biofilm readings and a conversion time of a half hour for the planktonic readings. Now that the MTT timing trial has been determined the effect of overall metabolism changes can be observed for the heated trials, antibiotic trials, and the combined trials. The observation of an increase in metabolism would support the hypothesis that the heat is increasing the metabolism and therefore increasing the efficacy of the antibiotics.

Another method that could be used to analyze the changes in the bacteria in the presence of these treatments would be a combined analysis using high pressure liquid chromatography, HPLC, and a dual mass spectrometry, MS/MS, approach. The metabolites that are produced from the biofilm can be separated via the HPLC and more thoroughly analyzed via a MS/MS to determine which metabolites are present and in what quantities.[31,170–173] Using the information gathered from these instruments a better understanding of the reaction the bacterial cells are having, whether it is a decrease in communication molecules, an increase in toxin production, or a number of other possibilities, can be determined. This information will help guide the correct treatment to decrease the toxin output from the bacteria while increasing the efficacy of the treatments.

8.7.5. In Vivo Trials

To better understand the potential of the SPION coating the coating should be used in an animal model, starting with a mouse model, to better understand the effect of the treatment *in vivo* and to ensure the efficacy of the treatment. The immune response,

infection prevalence, amount of viable cells post treatment, and the effects of the implant should all be studied to determine the overall efficacy of this biofilm treatment strategy. Toxicity tests of the implant and its coating should be performed *in vitro* before any trials *in vivo* to ensure minimum damage to the mouse and the host cells due to the foreign body's presence. Once a material is identified and the toxicity is known, a mouse model can then be explored. Biofilms can be grown on implantable SPION coated coupons and placed into neutropenic mice to ensure less variability in the experiments. The mice will need to have several days of antibiotic treatment before implanting the device. Once implanted the coating can be heated while the mouse is under anesthesia. Initial post treatment should end with the mouse euthanized and the implant removed. The implanted device should be sonicated and enumerated to determine biofilm viability post heat shock and the surrounding mouse cells should be removed for histology measurements to determine the necrosis and inflammation effects of the treatment and bacteria. This will elucidate the effect of the heating on the surrounding tissue and determine if there are different parameters that need to be met to move the technology to the clinical setting.

8.7.6. Investigate the Effects on Other Bacterial Species

All of the experiments investigated thus far and future research should be repeated with other common bacteria found on implanted infections, such as *Staphylococcus aureus*, *Staphylococcus epidermidis*, and *Escherichia coli* to better understand the effect of the SPION coating treatment for a variety of potential biofilm forming species. The parameters determined to be the best for *P. aeruginosa* indicated that the higher temperatures for shorter periods of time may be the most effective treatment strategy and the experiments done with the other bacterial species could concentrate primarily on those treatment

strategies. Co-cultured biofilms, or biofilms composed of multiple species of bacteria may result in very different treatment requirements and should also be heavily investigated for a better understanding of the requirements needed for treating an infected implant device. A good starting point would be to investigate the co-culture of *P. aeruginosa* and *S. aureus* since most of the ground work on the *P. aeruginosa* biofilm has already been investigated and *S. aureus* is one of the most common implant biofilm formers.

8.8. Closing Remarks

Biofilm infections on implanted devices lead to many complications such as systemic infections that can cause the mortality of otherwise healthy individuals. These individuals who develop a biofilm infection have very few options since biofilms are resistant to antibiotics. Removal of the implant is the current procedure and includes invasive surgery, loss of implant function during recovery, and twice the likelihood of infection on the new implanted device. This billion-dollar problem in the U.S. causes thousands of patients to suffer each year. Using a superparamagnetic iron oxide nanoparticle coating on implanted devices will allow doctors to treat the implant wirelessly, without invasive surgery, by using an alternating magnetic field to heat the surface, killing the biofilm infection *in situ.* The results thus far have indicated that the biofilms should be heated to a higher temperature for a short amount of time to thoroughly kill the bacteria and minimize the damage to the surrounding host tissue. Combined effects of heat and antibiotics have proven to be synergistic and can improve efficacy. The use of the SPION coating technology can be utilized for other applications as well, such as pipes with biofouling problems or improved ship hull cleaning to prevent cross sea contamination.

Additionally, the knowledge of biofilms obtained in this work furthers the understanding of biofilms and their thermal susceptibility from a variety of circumstances.

APPENDIX

Iterative Selection MATLAB Code

```
[filename,path] = uigetfile('*.tif', 'Select the .tif files',
'MultiSelect','on');

    % 'MultiSelect','on' allows you to select multiple files at once
Obviously with the uigetfile, the user is selecting all the files to
wants to include in the upload

    % However, when using MultiSelect, MATLAB stores the filenames as
an array. Which means if you select 10 files, it will create a 10x1
cell

    % array, where each cell (i,1) contains a filename. If you try to
select one file when referencing cell arrays, your program won't

    % work. So if you do it this way, *ALWAYS SELECT MORE THAN ONE
FILE* .


L = length(filename);   % Alert user to number of files selected

offset=1;

prompt = ('Enter the name you wish to assign the Excel file which
\nwill store image data. For example entering "data" \nwill save as
data.xsls\n');

str = input(prompt, 's');

Efilename = strcat(str,'.xlsx');

K = {'Image', 'Threshold', 'Background Sum', 'Foreground Sum',
'Minimum', 'Maximum'};
```

```
xlswrite(Efilename,K,3);

offset=2;

set = ischar(filename); % Send through while loop if false send through
single pass if false




if set==0

    % Cycle through the different files in the array

    for i=1:1:L

    A = imread(strcat(path,filename{i}));

    G=A;

    J=A;

    Z = min(min(A));

    Y = max(max(A));



    %Thresholding method

    I=0;   % Set initial value of moving index to zero

    T=255; % Set upper limit to threshold



    while I<=T

    B=A>I; % B is logic matrix true/false 1/0 dependent upon
comparision to threshold

    A(~B)=0; % Restores A with only numbers greater than threshold
```

```
    H=G<=I; % H is logic matrix true/false 1/0 dependent upon
comparision to threshold

    J=G-A; % Overrides original matrix with only numbers less than
threshold

    M = sum(sum(J))+1; % SUMM: (Nsubi*Isubi) BG

    N = sum(sum(H))+1; % SUMM: (Nsubi) BG

    O = sum(sum(A)); % SUMM: (Nsubi*Isubi) FG

    P = sum(sum(B)); % SUMM: (Nsubi) FG

    T = (M/N + O/P)/2; % Calculates threshold

    I = I+1; % Increase moving index by one

    end

    T  %prints final value of T in command window

    T = num2str(T); %Convert float to string

    [D, B] = strread(filename{i}, '%s %s','delimiter','.'); % The
original file name is stored as column A file extension is stored in
column B

    imwrite(A, [filename{i} '-', T, '.tif']) % Writes new image upon
calculation of Threshold Value (T)

    E = [D, T, N, P, Z, Y]; % Compiles values in preparation to write
as a row to excel file

    xlswrite(Efilename,E, 3, sprintf('A%d',offset)); % Writes row to
excel

    offset = offset + 1;
```

```
    end



else
    % Cycle through when only a single image is selected
    A = imread(strcat(path,filename));
    G=A;
    J=A;
    Z = min(min(A));
    Y = max(max(A));


    %Thresholding method
    I=0;   % Set initial value of moving index to zero
    T=255; % Set upper limit to threshold


    while I<=T
    B=A>I; % B is logic matrix true/false 1/0 dependent upon
comparision to threshold
    A(~B)=0; % Restores A with only numbers greater than threshold
    H=G<=I; % H is logic matrix true/false 1/0 dependent upon
comparision to threshold
    J=G-A; % Overrides original matrix with only numbers less than
threshold
```

```
    M = sum(sum(J))+1; % SUMM: (Nsubi*Isubi) BG

    N = sum(sum(H))+1; % SUMM: (Nsubi) BG

    O = sum(sum(A)); % SUMM: (Nsubi*Isubi) FG

    P = sum(sum(B)); % SUMM: (Nsubi) FG

    T = (M/N + O/P)/2; % Calculates threshold

    I = I+1; % Increase moving index by one

    end

    T  %prints final value of T in command window

    T = num2str(T); %Convert float to string

    [D, B] = strread(filename, '%s %s','delimiter','.'); % The original
file name is stored as column A file extension is stored in column B

    imwrite(A, [filename '-', T, '.tif']) % Writes new image upon
calculation of Threshold Value (T)

    E = [D, T, N, P, Z, Y]; % Compiles values in preparation to write
as a row to excel file

    xlswrite(Efilename,E, 3, sprintf('A%d',offset)); % Writes row to
excel    offset = offset + 1;

end


'End Program'
```

REFERENCES

1. Tran, N. & Tran, P. A. Nanomaterial-based treatments for medical device-associated infections. *Chemphyschem* **13,** 2481–2494 (2012).
2. Darouiche, R. O. Treatment of infections associated with surgical implants. *N. Engl. J. Med.* **350,** 1422–1429 (2004).
3. Moran, E., Byren, I. & Atkins, B. L. The diagnosis and management of prosthetic joint infections. *J. Antimicrob. Chemother.* **65,** iii45-iii54 (2010).
4. Harro, J. M., Peters, B. M., O'May, G. A., Archer, N., Kerns, P., Prabhakara, R. & Shirtliff, M. E. Vaccine development in Staphylococcus aureus: taking the biofilm phenotype into consideration. *FEMS Immunol. Med. Microbiol.* **59,** 306–323 (2010).
5. Ehrlich, G. D., Stoodley, P., Kathju, S., Zhao, Y., McLeod, B. R., Balaban, N., Hu, F. Z., Sotereanos, N. G., Costerton, J. W., Stewart, P. S., Post, J. C. & Lin, Q. Engineering approaches for the detection and control of orthopaedic biofilm infections. *Clin Orthop Relat Res* **437,** 59–66 (2006).
6. Ammerlaan, H. S. M., Harbarth, S., Buiting, A. G. M., Crook, D. W., Fitzpatrick, F., Hanberger, H., Herwaldt, L. A., van Keulen, P. H. J., Kluytmans, J. A. J. W., Kola, A., Kuchenbecker, R. S., Lingaas, E., Meessen, N., Morris-Downes, M. M., Pottinger, J. M., Rohner, P., dos Santos, R. P., Seifert, H., Wisplinghoff, H., *et al.* Secular trends in nosocomial bloodstream infections: Antibiotic-resistant bacteria increase the total burden of infection. *Clin. Infect. Dis.* **56,** 798–805 (2013).
7. Wisplinghoff, H., Bischoff, T., Tallent, S. M., Seifert, H., Wenzel, R. P. & Edmond, M. B. Nosocomial bloodstream infections in US hospitals: analysis of 24,179 cases from a prospective nationwide surveillance study. *Clin. Infect. Dis.* **39,** 309–317 (2004).
8. Montanaro, L., Speziale, P., Campoccia, D., Ravaioli, S., Cangini, I., Pietrocola, G., Giannini, S. & Arciola, C. R. Scenery of Staphylococcus implant infections on orthopedics. *Future Microbiol.* **6,** 1329–1349 (2011).
9. Metsemakers, W. J., Kuehl, R., Moriarty, T. F., Richards, R. G., Verhofstad, M. H. J., Borens, O., Kates, S., Morgenstern, M. & Morgenstern, M. Infection after fracture fixation: Current surgical and microbiological concepts. *Inj. Int. J, Care Inj.* (2016). doi:http://dx.doi.org/10.1016/j.injury.2016.09.019
10. Fernandes, A. & Dias, M. The microbiological profiles of infected prosthetic implants with an emphasis on the organisms which form fiofilms. *J. Clin. Diagnostic Res.* **7,** 219–223 (2013).
11. Rohde, H., Burandt, E. C., Siemssen, N., Frommelt, L., Burdelski, C., Wurster, S., Scherpe, S., Davies, A. P., Harris, L. G., Horstkotte, M. A., Knobloch, J. K.-M., Ragunath, C., Kaplan, J. B. & Mack, D. Polysaccharide intercellular adhesin or protein factors in biofilm accumulation of Staphylococcus epidermidis and Staphylococcus aureus isolated from prosthetic hip and knee joint infections. *Biomaterials* **28,** 1711–1720 (2007).
12. Lentino, J. R. Prosthetic joint infections : bane of orthopedists, challenge for infectious disease specialists. *Clin. Infect. Dis.* **36,** 1157–1161 (2003).

13. Wisplinghoff, H., Ewertz, B., Wisplinghoff, S., Stefanik, D., Plum, G., Perdreau-Remington, F. & Seifert, H. Molecular evolution of methicillin-resistant Staphylococcus aureus in the metropolitan area of Cologne, Germany, from 1984 to 1998. *J. Clin. Microbiol.* **43,** 5445–5451 (2005).
14. Burke, J. P. Infection control — a problem for patient safety. *N. Engl. J. Med.* **348,** 651–656 (2003).
15. Jarvis, W. R. Infection control and changing health-care delivery systems. *Emerg. Infect. Dis.* **7,** 170–173 (2001).
16. Piddock, L. J. V. Multidrug-resistance efflux pumps - not just for resistance. *Nat. Rev. Microbiol.* **4,** 629–636 (2006).
17. Costerton, J. W., Stewart, P. S. & Greenberg, E. P. Bacterial biofilms: a common cause of persistent infections. *Science (80-.).* **284,** 1318–1322 (1999).
18. Anderl, J. N., Zahller, J., Roe, F. & Stewart, P. S. Role of nutrient limitation and stationary-phase existence in Klebsiella pneumoniae biofilm resistance to ampicillin and ciprofloxacin. *Antimicrob. Agents Chemother.* **47,** 1251–1256 (2003).
19. Anwar, H., Strap, J. L. & Costerton, J. W. Susceptibility of biofilm cells of Pseudomonas aeruginosa to bactericidal actions of whole blood and serum. *FEMS Microbiol. Lett.* **92,** 235–242 (1992).
20. Abdallah, M., Benoliel, C., Drider, D., Dhulster, P. & Chihib, N.-E. Biofilm formation and persistence on abiotic surfaces in the context of food and medical environments. *Arch. Microbiol.* **196,** 453–472 (2014).
21. Olszewska, M. A. Microscopic findings for the study of biofilms in food environments. *ACTA Biochim. Pol.* **60,** 531–537 (2013).
22. Bridier, A., Sanchez-Vizuete, P., Guilbaud, M., Piard, J.-C. & Naïtali, M. Biofilm-associated persistence of food-borne pathogens. *Food Microbiol.* **45,** 167–178 (2015).
23. CDC. Foodborne germs and illnesses. *Center for Disease Control and Prevention* (2016). Available at: https://www.cdc.gov/foodsafety/foodborne-germs.html. (Accessed: 27th February 2017)
24. Coughlan, L. M., Cotter, P. D., Hill, C. & Alvarez-Ordóñez, A. New weapons to fight old enemies: novel strategies for the (bio)control of bacterial biofilms in the food industry. *Front. Microbiol.* **7,** 1–21 (2016).
25. Momba, M. N. B. & Binda, M. A. Combining chlorination and chloramination processes for the inhibition of biofilm formation in drinking surface water system models. *J. Appl. Microbiol.* **92,** 641–648 (2002).
26. Breidenstein, E. B. M., de la Fuente-Núñez, C. & Hancock, R. E. W. Pseudomonas aeruginosa: all roads lead to resistance. *Trends Microbiol.* **19,** 419–426 (2011).
27. Center for Biofilm Engineering, M. Biofilm Basics. (2013). Available at: http://www.biofilm.montana.edu/node/2390.
28. Clontz, L. *Microbial Limit and Bioburden Tests: Validation Approaches and Global Requirements*. Second Edition. Taylor & Francis Group, LLC, Boca Raton, FL (2009).
29. Willey, J. M., Sherwood, L. M. & Woolverton, C. J. *Prescott's Microbiology*. Eighth Edition. MacGraw Hill, New York, NY (2008).
30. Francolini, I. & Donelli, G. Prevention and control of biofilm-based medical-device-related infections. *FEMS Immunol. Med. Microbiol.* **59,** 227–238 (2010).

31. Zhang, B. & Powers, R. Analysis of bacterial biofilms using NMR-based metabolomics. *Future Med. Chem.* **4,** 1273–1306 (2012).
32. Haussler, S. & Fuqua, C. Biofilms 2012: new discoveries and significant wrinkles in a dynamic field. *J. Bacteriol.* **195,** 2947–2958 (2013).
33. Holt, J. G., Krieg, N. R., Sneath, P. H. A., Staley, J. T. & Williams, S. T. *Bergey's Manual of Systematic Bacteriology*. Nineth Edition. Lippincott Williams & Wilkins, Philadelphia, PA (2000).
34. Srivastava, S. & Bhargava, A. Biofilms and human health. *Biotechnol. Lett.* **38,** 1–22 (2016).
35. Sauer, K., Camper, A. K., Ehrlich, G. D., Costerton, J. W. & Davies, D. G. Pseudomonas aeruginosa displays multiple phenotypes during development as a biofilm. *J. Bacteriol.* **184,** 1140–1154 (2002).
36. Majik, M. S., Naik, D., Bhat, C., Tilve, S., Tilvi, S. & D'Souza, L. Synthesis of (R)-norbgugaine and its potential as quorum sensing inhibitor against Pseudomonas aeruginosa. *Bioorg. Med. Chem. Lett.* **23,** 2353–2356 (2013).
37. Parsek, M. R. & Greenberg, E. P. Acyl-homoserine lactone quorum sensing in Gram-negative bacteria: A signaling mechanism involved in associations with higher organisms. *PNAS* **97,** 8789–8793 (2000).
38. Kalia, V. C. Quorum sensing inhibitors: an overview. *Biotechnol. Adv.* **31,** 224–245 (2013).
39. Cady, N. C., McKean, K. A., Behnke, J., Kubec, R., Mosier, A. P., Kasper, S. H., Burz, D. S. & Musah, R. A. Inhibition of biofilm formation, quorum sensing and infection in Pseudomonas aeruginosa by natural products-inspired organosulfur compounds. *PLoS One* **7,** e38492 (2012).
40. Shrout, J. D., Chopp, D. L., Just, C. L., Hentzer, M., Givskov, M. & Parsek, M. R. The impact of quorum sensing and swarming motility on Pseudomonas aeruginosa biofilm formation is nutritionally conditional. *Mol. Microbiol.* **62,** 1264–1277 (2006).
41. Moore, J. D., Gerdt, J. P., Eibergen, N. R. & Blackwell, H. E. Active efflux influences the potency of quorum sensing inhibitors in Pseudomonas aeruginosa. *ChemBioChem* **15,** 435–442 (2014).
42. Horswill, A. R., Stoodley, P., Stewart, P. S. & Parsek, M. R. The effect of the chemical, biological, and physical environment on quorum sensing in structured microbial communities. *Anal. Bioanal. Chem.* **387,** 371–380 (2007).
43. Pearson, J. P., van Delden, C. & Iglewski, B. H. Active efflux and diffusion are involved in transport of Pseudomonas aeruginosa cell-to-cell signals. *J Bacteriol* **181,** 1203–1210 (1999).
44. Sawada, I., Maseda, H., Nakae, T., Uchiyama, H. & Nomura, N. A quorum-sensing autoinducer enhances the mexAB-oprM efflux-pump expression without the MexR-mediated regulation in Pseudomonas aeruginosa. *Microbiol. Immunol.* **48,** 435–439 (2004).
45. Watrous, J. D., Phelan, V. V, Hsu, C.-C., Moree, W. J., Duggan, B. M., Alexandrov, T. & Dorrestein, P. C. Microbial metabolic exchange in 3D. *ISME J.* **7,** 770–780 (2013).

46. Kaufmann, G. F., Sartorio, R., Lee, S.-H., Rogers, C. J., Meijler, M. M., Moss, J. A., Clapham, B., Brogan, A. P., Dickerson, T. J. & Janda, K. D. Revisiting quorum sensing: discovery of additional chemical and biological functions for 3-oxo-N-acylhomoserine lactones. *PNAS* **102,** 309–314 (2005).
47. Charlton, T. S., de Nys, R., Netting, A., Kumar, N., Hentzer, M., Givskov, M. & Kjelleberg, S. A novel and sensitive method for the quantification of N-3-oxoacyl homoserine lactones using gas chromatography-mass spectrometry: application to a model bacterial biofilm. *Environ. Microbiol.* **2,** 530–541 (2000).
48. Paharik, A. E. & Horswill, A. R. The staphylococcal biofilm: adhesins, regulation, and host response. *Microbiol Spectr.* **4,** 1–27 (2016).
49. Mah, T.-F., Pitts, B., Pellock, B., Walker, G. C., Stewart, P. S. & O'Toole, G. A. A genetic basis for Pseudomonas aeruginosa biofilm antibiotic resistance. *Lett. to Nat.* **426,** 1–5 (2003).
50. Poole, K. Pseudomonas aeruginosa: resistance to the max. *Front. Microbiol.* **2,** 1–13 (2011).
51. Nickel, J. C., Ruseska, I., Wright, J. B. & Costerton, J. W. Tobramycin resistance of Pseudomonas aeruginosa cells growing as a biofilm on urinary catheter material. *Antimicrob. Agents Chemother.* **27,** 619–624 (1985).
52. Andrews, J. M. Determination of minimum inhibitory concentrations. *J. Antimicrob. Chemother.* **48 Suppl S,** 5–16 (2001).
53. Bundtzen, R. W., Gerber, A. U., Cohn, D. L. & Craig, W. A. Postantibiotic suppression of bacterial growth. *Rev. Infect. Dis.* **3,** 28–37 (1981).
54. Meng, Z., Chongjin, S., You, X., Xing, D., Wang, W. & Du, L. Characteristics of baicalin synergy with penicillin or Notopterygium ethanol extracts against Staphylococcus aureus. *Tsinghua Sci. Technol.* **11,** 459–461 (2006).
55. Ceri, H., Olson, M. E., Stremick, C., Read, R. R., Morck, D. & Buret, A. The calgary biofilm device: new technology for rapid determination of antibiotic susceptibilities of bacterial biofilms. *J. Clin. Microbiol.* **37,** 1771–1776 (1999).
56. Abdi-Ali, A., Mohammadi-Mehr, M. & Agha Alaei, Y. Bactericidal activity of various antibiotics against biofilm-producing Pseudomonas aeruginosa. *Int. J. Antimicrob. Agents* **27,** 196–200 (2006).
57. Hengzhuang, W., Wu, H., Ciofu, O., Song, Z. & Høiby, N. Pharmacokinetics/ pharmacodynamics of colistin and imipenem on mucoid and nonmucoid Pseudomonas aeruginosa biofilms. *Antimicrob. Agents Chemother.* **55,** 4469–4474 (2011).
58. Harimawan, A. & Ting, Y.-P. Investigation of extracellular polymeric substances (EPS) properties of P. aeruginosa and B. subtilis and their role in bacterial adhesion. *Colloids Surfaces B Biointerfaces* **146,** 459–467 (2016).
59. Gunn, J. S., Bakaletz, L. O. & Wozniak, D. J. What's on the outside matters: the role of the extracellular polymeric substance of Gram-negative biofilms in evading host immunity and as a target for therapeutic intervention. *J Biol. Chem.* **291,** 12538–12546 (2016).

60. Jennings, L. K., Storek, K. M., Ledvina, H. E., Coulon, C., Marmont, L. S., Sadovskaya, I., Secor, P. R., Tseng, B. S., Scian, M., Filloux, A., Wozniak, D. J., Howell, P. L. & Parsek, M. R. Pel is a cationic exopolysaccharide that cross-links extracellular DNA in the Pseudomonas aeruginosa biofilm matrix. *PNAS* **112,** 11353–11358 (2015).
61. Walters III, M. C., Roe, F., Bugnicourt, A., Franklin, M. J. & Stewart, P. S. Contributions of antibiotic penetration, oxygen limitation, and low metabolic activity to tolerance of Pseudomonas aeruginosa biofilms to ciprofloxacin and tobramycin. *Antimicrob. Agents Chemother.* **47,** 317–323 (2003).
62. Gellatly, S. L. & Hancock, R. E. W. Pseudomonas aeruginosa: new insights into pathogenesis and host defenses. *Pathog. Dis.* **67,** 159–173 (2013).
63. Davies, D. Understanding biofilm resistance to antibacterial agents. *Nat. Rev. Drug Discov.* **2,** 114–122 (2003).
64. Yu, F. P. & McFeters, G. A. Physiological responses of bacteria in biofilms to disinfection. *Appl. Environ. Microbiol.* **60,** 2462–2466 (1994).
65. Huang, C.-T., Yu, F. P., McFeters, G. A. & Stewart, P. S. Nonuniform spatial patterns of respiratory activity within biofilms during disinfection. *Appl. Environ. Microbiol.* **61,** 2252–2256 (1995).
66. Stewart, P. S. Theoretical aspects of antibiotic diffusion into microbial biofilms. *Antimicrob. Agents Chemother.* **40,** 2517–2522 (1996).
67. de Beer, D., Stoodley, P., Roe, F. & Lewandowski, Z. Effects of biofilm structures on oxygen distribution and mass transport. *Biotechnol. Bioeng.* **43,** 1131–1138 (1994).
68. Kaprelyants, A. S. & Kell, D. B. Dormancy in stationary-phase cultures of Micrococcus luteus: flow cytometric analysis of starvation and resuscitation. *Appl. Environ. Microbiol.* **59,** 3187–3196 (1993).
69. *AHFS Drug Information 2008*. 2008 Edition. American Society of Health-System Pharmacists, Inc., Bethesda, MD (2008).
70. Poole, K. Efflux-mediated multiresistance in Gram-negative bacteria. *Clin. Microbiol. Infect.* **10,** 12–26 (2004).
71. Dupont, P., Hocquet, D., Jeannot, K., Chavanet, P. & Plésiat, P. Bacteriostatic and bactericidal activities of eight fluoroquinolones against MexAB-OprM-overproducing clinical strains of Pseudomonas aeruginosa. *J. Antimicrob. Chemother.* **55,** 518–522 (2005).
72. Poonsuk, K., Tribuddharat, C. & Chuanchuen, R. Simultaneous overexpression of multidrug efflux pumps in Pseudomonas aeruginosa non-cystic fibrosis clinical isolates. *Can. J. Microbiol.* **60,** 437–443 (2014).
73. Arabestani, M. R., Rajabpour, M., Mashouf, R. Y., Alikhani, M. Y. & Mousavi, S. M. Expression of efflux pump MexAB-OprM and OprD of Pseudomonas aeruginosa strainsIsolated from clinical samples using qRT-PCR. *Arch. Iran. Med.* **18,** 102–108 (2015).
74. Aeschlimann, J. R. The role of multidrug efflux pumps in the antibiotic resistance of Pseudomonas aeruginosa and other Gram-negative bacteria: insights from the society of infectious diseases pharmacists. *Pharmacotherapy* **23,** 916–924 (2003).

75. Evans, K. & Poole, K. The MexA-MexB-OprM multidrug efflux system of Pseudomonas aeruginosa is growth-phase regulated. *FEMS Microbiol. Lett.* **173,** 35–39 (1999).
76. de Kievit, T. R., Parkins, M. D., Gillis, R. J., Srikumar, R., Ceri, H., Poole, K., Iglewski, B. arbara H. & Storey, D. G. Multidrug efflux pumps: expression patterns and contribution to antibiotic resistance in Pseudomonas aeruginosa biofilms. *Antimicrob. Agents Chemother.* **45,** 1761–1770 (2001).
77. Ghosh, S., Cremers, C. M., Jakob, U. & Love, N. G. Chlorinated phenols control the expression of the multidrug resistance efflux pump MexAB-OprM in Pseudomonas aeruginosa by interacting with NalC. *Mol. Microbiol.* **79,** 1547–1556 (2011).
78. Poole, K. Stress responses as determinants of antimicrobial resistance in Pseudomonas aeruginosa: multidrug efflux and more. *Can. J. Microbiol.* **60,** 783–791 (2014).
79. Starr, L. M., Fruci, M. & Poole, K. Pentachlorophenol induction of the Pseudomonas aeruginosa mexAB-oprM efflux operon: involvement of repressors NalC and MexR and the antirepressor ArmR. *PLoS One* **7,** e32684 (2012).
80. Vakulenko, S. B. & Mobashery, S. Versatility of aminoglycosides and prospects for their future. *Clin. Microbiol. Rev.* **16,** 430–450 (2003).
81. Driffield, K., Miller, K., Bostock, J. M., O'Neill, A. J. & Chopra, I. Increased mutability of Pseudomonas aeruginosa in biofilms. *J. Antimicrob. Chemother.* **61,** 1053–1056 (2008).
82. Vadillo-Rodríguez, V., Pacha-Olivenza, M. A., Gónzalez-Martín, M. L., Bruque, J. M. & Gallardo-Moreno, A. M. Adsorption behavior of human plasma fibronectin on hydrophobic and hydrophilic Ti6Al4V substrata and its influence on bacterial adhesion and detachment. *J. Biomed. Mmaterials Res. Part A* **101A,** 1397–1404 (2013).
83. Morones-Ramirez, J. R., Winkler, J. A., Spina, C. S. & Collins, J. J. Silver enhances antibiotic activity against Gram-negative bacteria. *Sci. Transl. Med.* **5,** 1–11 (2013).
84. Roehling, S., Astasov-frauenhoffer, M., Hauser-Gerspach, I., Braissant, O., Woelfler, H., Waltimo, T., Kniha, H. & Gahlert, M. In vitro biofilm formation on titanium and zirconia implant surfaces. *J. Periodontol.* **88,** 298–307 (2017).
85. Gosau, M., Haupt, M., Thude, S., Strowitzki, M., Schminke, B. & Buergers, R. Antimicrobial effect and biocompatibility of novel metallic nanocrystalline implant coatings. *J. Biomed. Mater. Res. B Appl. Biomater.* **104B,** 1571–1579 (2016).
86. Kim, J., Kwon, S. & Ostler, E. Antimicrobial effect of silver-impregnated cellulose: potential for antimicrobial therapy. *J. Biol. Eng.* **3,** 20–29 (2009).
87. Wang, B., Xu, Q., Ye, Z., Liu, H., Lin, Q., Nan, K., Li, Y., Wang, Y., Qi, L. & Chen, H. Copolymer brushes with temperature-triggered, reversibly wwitchable bactericidal and antifouling properties for biomaterial surfaces. *ACS Appl. Mater. Interfaces* **8,** 27207–27217 (2016).
88. Busscher, H. J., van der Mei, H. C., Subbiahdoss, G., Jutte, P. C., van den Dungen, J. J. A. M., Zaat, S. A. J., Schultz, M. J. & Grainger, D. W. Biomaterial-associated infection: locating the finish line in the race for the surface. *Sci. Transl. Med.* **4,** 153rv10 (2012).

89. Campoccia, D., Montanaro, L., Speziale, P. & Arciola, C. R. Antibiotic-loaded biomaterials and the risks for the spread of antibiotic resistance following their prophylactic and therapeutic clinical use. *Biomaterials* **31,** 6363–6377 (2010).
90. Campoccia, D., Montanaro, L. & Arciola, C. R. A review of the biomaterials technologies for infection-resistant surfaces. *Biomaterials* **34,** 8533–8554 (2013).
91. Gbejuade, H. O., Lovering, A. M. & Webb, J. C. The role of microbial biofilms in prosthetic joint infections. *Acta Orthop.* **86,** 147–158 (2015).
92. Howlin, R. P., Brayford, M. J., Webb, J. S., Cooper, J. J., Aiken, S. S. & Stoodley, P. Antibiotic-loaded synthetic calcium sulfate beads for prevention of bacterial colonization and biofilm formation in periprosthetic infections. *Antimicrob. Agents Chemother.* **59,** 111–120 (2015).
93. Kiran, S., Sharma, P., Harjai, K. & Capalash, N. Enzymatic quorum quenching increases antibiotic susceptibility of multidrug resistant Pseudomonas aeruginosa. *Iran. J. Microbiol.* **3,** 1–12 (2011).
94. Bryers, J. D., Jarvis, R. A., Lebo, J., Prudencio, A., Kyriakides, T. R. & Uhrich, K. Biodegradation of poly(anhydride-esters) into non-steroidal anti-inflammatory drugs and their effect on Pseudomonas aeruginosa biofilms in vitro and on the foreign-body response in vivo. *Biomaterials* **27,** 5039–5048 (2006).
95. Koul, S., Prakash, J., Mishra, A. & Kalia, V. C. Potential emergence of multi-quorum sensing inhibitor resistant (MQSIR) bacteria. *Indian J. Microbiol.* **56,** 1–18 (2016).
96. Glover, A. L., Bennett, J. B., Pritchett, J. S., Nikles, S. M., Nikles, D. E., Nikles, J. A. & Brazel, C. S. Magnetic heating of iron oxide nanoparticles and magnetic micelles for cancer therapy. *IEEE Trans. Magn.* **49,** 231–235 (2013).
97. Abdelghany, S. M., Quinn, D. J., Ingram, R. J., Gilmore, B. F., Donnelly, R. F., Taggart, C. C. & Scott, C. J. Gentamicin-loaded nanoparticles show improved antimicrobial effects towards Pseudomonas aeruginosa infection. *Int. J. Nanomedicine* **7,** 4053–4063 (2012).
98. Aparna, V., Dineshkumar, K., Mohanalakshmi, N., Velmurugan, D. & Hopper, W. Identification of natural compound inhibitors for multidrug efflux pumps of Escherichia coli and Pseudomonas aeruginosa using in silico high-throughput virtual screening and in vitro validation. *PLoS One* **9,** e101840 (2014).
99. Nakayama, K., Ishida, Y., Ohtsuka, M., Kawato, H., Yoshida, K., Yokomizo, Y., Ohta, T., Hoshino, K., Otani, T., Kurosaka, Y., Yoshida, K., Ishida, H., Lee, V. J., Renau, T. E. & Watkins, W. J. MexAB-OprM specific efflux pump inhibitors in Pseudomonas aeruginosa. Part 2: achieving activity in vivo through the use of alternative scaffolds. *Bioorg. Med. Chem. Lett.* **13,** 4205–4208 (2003).
100. Nakayama, K., Ishida, Y., Ohtsuka, M., Kawato, H., Yoshida, K., Yokomizo, Y., Hosono, S., Ohta, T., Hoshino, K., Ishida, H., Yoshida, K., Renau, T. E., Léger, R., Zhang, J. Z., Lee, V. J. & Watkins, W. J. MexAB-OprM-specific efflux pump inhibitors in Pseudomonas aeruginosa. Part 1: discovery and early strategies for lead optimization. *Bioorg. Med. Chem. Lett.* **13,** 4201–4204 (2003).
101. Sugimura, M., Maseda, H., Hanaki, H. & Nakae, T. Macrolide antibiotic-mediated downregulation of MexAB-OprM efflux pump expression in Pseudomonas aeruginosa. *Antimicrob. Agents Chemother.* **52,** 4141–4144 (2008).

102. Damestani, Y., de Howitt, N., Halaney, D. L., Garay, J. E. & Aguilar, G. Evaluation of laser bacterial anti-fouling of transparent nanocrystalline yttria-stabilized-zirconia cranial implant. *Lasers Surg. Med.* **48,** 782–789 (2016).
103. Carmen, J. C., Roeder, B. L., Nelson, J. L., Robison Ogilvie, R. L., Robison, R. A., Schaalje, G. B. & Pitt, W. G. Treatment of biofilm infections on implants with low-frequency ultrasound and antibiotics. *Am. J. Infect. Control* **33,** 78–82 (2005).
104. Howlin, R. P., Fabbri, S., Offin, D. G., Symonds, N., Kiang, K. S., Knee, R. J., Yoganantham, D. C., Webb, J. S., Birkin, P. R., Leighton, T. G. & Stoodley, P. Removal of dental biofilms with an ultrasonically activated water stream. *J. Dent. Res.* **94,** 1303–1309 (2015).
105. van der Borden, A. J., Maathuis, P. G. M., Engels, E., Rakhorst, G., van der Mei, H. C., Busscher, H. J. & Sharma, P. K. Prevention of pin tract infection in external stainless steel fixator frames using electric current in a goat model. *Biomaterials* **28,** 2122–2126 (2007).
106. van der Borden, A. J., van der Werf, H., van der Mei, H. C. & Busscher, H. J. Electric current-induced detachment of Staphylococcus epidermidis biofilms from surgical stainless steel. *Appl. Environ. Microbiol.* **70,** 6871–6874 (2004).
107. van der Borden, A. J., van der Mei, H. C. & Busscher, H. J. Electric block current induced detachment from surgical stainless steel and decreased viability of Staphylococcus epidermidis. *Biomaterials* **26,** 6731–6735 (2005).
108. Chmielewski, R. A. N. & Frank, J. F. A predictive model for heat inactivation of Listeria monocytogenes biofilm on buna-N rubber. *LWT* **39,** 11–19 (2006).
109. Li, C. H., Hodgins, P. & Peterson, G. P. Experimental study of fundamental mechanisms in inductive heating of ferromagnetic nanoparticles suspension (Fe3O4 Iron Oxide Ferrofluid). *J. Appl. Phys.* **110,** 1–10 (2011).
110. Park, H., Park, H.-J., Kim, J. A., Lee, S. H., Kim, J. H., Yoon, J. & Park, T. H. Inactivation of Pseudomonas aeruginosa PA01 biofilms by hyperthermia using superparamagnetic nanoparticles. *J. Microbiol. Methods* **84,** 41–45 (2011).
111. Guo, Z., Zhang, D., Wei, S., Wang, Z., Karki, A. B., Li, Y., Bernazzani, P., Young, D. P., Gomes, J. A., Cocke, D. L. & Ho, T. C. Effects of iron oxide nanoparticles on polyvinyl alcohol: interfacial layer and bulk nanocomposites thin film. *J. Nanoparticle Res.* **12,** 2415–2426 (2010).
112. Coffel, J. *Implementation and Modeling of in Situ Magnetic Hyperthermia*. University of Iowa, Iowa City, (2016).
113. Sturtevant, R. A., Sharma, P., Pavlovsky, L., Stewart, E. J., Solomon, M. J. & Younger, J. G. Thermal augmentation of vancomycin against staphylococcal biofilms. *Shock* **44,** 121–127 (2015).
114. Polla, B. S., Mariéthoz, E., Hubert, D. & Barazzone, C. Heat-shock proteins in host-pathogen interactions: implications for cystic fibrosis. *Trends Microbiol.* **3,** 392–396 (1995).
115. Singh, V. & Aballay, A. Heat shock and genetic activation of HSF-1 enhance immunity to bacteria. *Cell Cycle* **5,** 2443–2446 (2006).
116. Llanes, C., Hocquet, D., Vogne, C., Benali-Baitich, D., Neuwirth, C. & Plésiat, P. Clinical strains of Pseudomonas aeruginosa overproducing MexAB-OprM and MexXY efflux pumps simultaneously. *Antimicrob. Agents Chemother.* **48,** 1797–1802 (2004).

117. Weiner, L. M., Webb, A. K., Limbago, B., Dudeck, M. A., Patel, J., Kallen, A. J., Edwards, J. R. & Sievert, D. M. Antimicrobial-resistant pathogens associated with healthcare-associated infections: summary of data reported to the national healthcare safety network at the centers for disease control and rrevention, 2011 – 2014. *Infect. Control Hosp. Epidemiol.* **37,** 1288–1301 (2016).
118. Parkins, M. D. & Floto, R. A. Emerging bacterial pathogens and changing concepts of bacterial pathogenesis in cystic fibrosis. *J. Cyst. Fibros.* **14,** 293–304 (2015).
119. Luna, C. M., Rodriguez-Noriega, E., Bavestrello, L. & Guzmán-Blanco, M. Gram-negative infections in adult intensive care units of Latin America and the Caribbean. *Crit. Care Res. Pract.* **2014,** 480463 (2014).
120. O'Toole, A., Ricker, E. B. & Nuxoll, E. Thermal mitigation of Pseudomonas aeruginosa biofilms. *Biofouling* **31,** 665–675 (2015).
121. O'Toole, A. M. *Thermal Deactivation of Pseudomonas aeruginosa Biofilms*. University of Iowa, Iowa City, IA (2015).
122. Coffel, J. & Nuxoll, E. Magnetic nanoparticle/polymer composites for medical implant infection control. *J. Mater. Chem. B* **3,** 7538–7545 (2015).
123. Hassani, M., Mañas, P., Pagán, R. & Condón, S. Effect of a previous heat shock on the thermal resistance of Listeria monocytogenes and Pseudomonas aeruginosa at different pHs. *Int. J. Food Microbiol.* **116,** 228–238 (2007).
124. Bolte, S. & Cordelières, F. P. A guided tour into subcellular colocalization analysis in light microscopy. *J. Microsc.* **224,** 213–232 (2006).
125. Heidrich, M., Kühnel, M. P., Kellner, M., Lorbeer, R.-A., Lange, T., Winkel, A., Stiesch, M., Meyer, H. & Heisterkamp, A. 3D imaging of biofilms on implants by detection of scattered light with a scanning laser optical tomograph. *Biomed. Opt. Express* **2,** 2982–2994 (2011).
126. Yang, X., Beyenal, H., Harkin, G. & Lewandowski, Z. Evaluation of biofilm image thresholding methods. *Wat. Res.* **35,** 1149–1158 (2001).
127. Harrison, J. J., Ceri, H., Yerly, J., Stremick, C. A., Hu, Y., Martinuzzi, R. & Turner, R. J. The use of microscopy and three-dimensional visualization to evaluate the structure of microbial biofilms cultivated in the Calgary Biofilm Device. *Biol. Proced. Online* **8,** 194–215 (2006).
128. Beyenal, H., Donovan, C., Lewandowski, Z. & Harkin, G. Three-dimensional biofilm structure quantification. *J. Microbiol. Methods* **59,** 395–413 (2004).
129. Yang, X., Beyenal, H., Harkin, G. & Lewandowski, Z. Quantifying biofilm structure using image analysis. *J. Microbiolical Methods* **39,** 109–119 (2000).
130. Xavier, J. B., Schnell, A., Wuertz, S., Palmer, R., White, D. C. & Almeida, J. S. Objective threshold selection procedure (OTS) for segmentation of scanning laser confocal microscope images. *J. Microbiol. Methods* **47,** 169–180 (2001).
131. Ji, Z., Card, K. J. & Dazzo, F. B. CMEIAS JFrad: a digital computing tool to discriminate the fractal geometry of landscape architectures and spatial patterns of individual cells in microbial fiofilms. *Microb. Ecol.* **69,** 710–720 (2015).
132. Lepanto, P., Lecumberry, F., Rossello, J. & Kierbel, A. A confocal microscopy image analysis method to measure adhesion and internalization of Pseudomonas aeruginosa multicellular structures into epithelial cells. *Mol. Cell. Probes* **28,** 1–5 (2014).

133. Yerly, J., Hu, Y., Jones, S. M. & Martinuzzi, R. J. A two-step procedure for automatic and accurate segmentation of volumetric CLSM biofilm images. *J. Microbiol. Methods* **70,** 424–433 (2007).
134. Larimer, C., Winder, E., Jeters, R., Prowant, M., Nettleship, I., Addleman, R. S., Addleman, R. S. & Bonheyo, G. T. A method for rapid quantitative assessment of biofilms with biomolecular staining and image analysis. *Anal. Bioanal. Chem.* **408,** 999–1008 (2016).
135. Yuan, X., Martínez, J.-F., Eckert, M. & López-Santidrián, L. An improved Otsu threshold segmentation method. *Sensors* **16,** 1–31 (2016).
136. Kavanaugh, J. S. & Horswill, A. R. Impact of environmental cues on Staphylococcal quorum sensing and biofilm development. *J. Biol. Chem.* **291,** 12556–12564 (2016).
137. Shukla, S. K. & Rao, T. S. Effect of calcium on Staphylococcus aureus biofilm architecture: A confocal laser scanning microscopic study. *Colloids Surfaces B Biointerfaces* **103,** 448–454 (2013).
138. Lin, M.-H., Shu, J.-C., Huang, H.-Y. & Cheng, Y.-C. Involvement of iron in biofilm formation by Staphylococcus aureus. *PLoS One* **7,** e34388 (2012).
139. Stoodley, P., Dodds, I., Boyle, J. D. & Lappin-Scott, H. M. Influence of hydrodynamics and nutrients on biofilm structure. *J. Appl. Microbiol.* **85,** 19S–28S (1999).
140. Xu, Z., Islam, S., Wood, T. K. & Huang, Z. An integrated modeling and experimental approach to study the influence of environmental nutrients on biofilm formation of Pseudomonas aeruginosa. *Biomed Res. Int.* **2015,** 1–12 (2015).
141. Cerca, N. & Jefferson, K. K. Effect of growth conditions on poly-N-acetylglucosamine expression and biofilm formation in Escherichia coli. *FEMS Microbiol. Lett.* **283,** 36–41 (2008).
142. Cornelis, P. & Dingemans, J. Pseudomonas aeruginosa adapts its iron uptake strategies in function of the type of infections. *Front. Cell. Infect. Microbiol.* **3,** 1–7 (2013).
143. Rode, T. M., Langsrud, S., Holck, A. & Møretrø, T. Different patterns of biofilm formation in Staphylococcus aureus under food-related stress conditions. *Int. J. Food Microbiol.* **116,** 372–383 (2007).
144. Cowell, B. A., Willcox, M. D. P., Herbert, B. & Schneider, R. P. Effect of nutrient limitation on adhesion characteristics of Pseudomonas aeruginosa. *J. Appl. Microbiol.* **86,** 944–954 (1999).
145. Nguyen, D., Joshi-Datar, A., Lepine, F., Bauerle, E., Olakanmi, O., Beer, K., McKay, G., Siehnel, R., Schafhauser, J., Wang, Y., Britigan, B. E. & Singh, P. K. Active stravation responses mediate antibiotic tolerance in biofilms and nutrient-limited bacteria. *Science (80-.).* **334,** 982–986 (2011).
146. Nilsson, R. E., Ross, T. & Bowman, J. P. Variability in biofilm production by Listeria monocytogenes correlated to strain origin and growth conditions. *Int. J. Food Microbiol.* **150,** 14–24 (2011).
147. Kostenko, V., Salek, M. M., Sattari, P. & Martinuzzi, R. J. Staphylococcus aureus biofilm formation and tolerance to antibiotics in response to oscillatory shear stresses of physiological levels. *FEMS Immunol. Med. Microbiol.* **59,** 421–431 (2010).

148. Seader, J. D., Henley, E. J. & Roper, D. K. *Separation Process Principles*. Third Edition. John Wiley & Sons, Danvers, MA (2011).
149. Wahlen, L., Parker, A., Walker, D., Pasmore, M. & Sturman, P. Predictive modeling for hot water inactivation of planktonic and biofilm-associated Sphingomonas parapaucimobilis to support hot water sanitization programs. *Biofouling* **32,** 751–761 (2016).
150. Hassani, M., Mañas, P., Pagán, R. & Condón, S. Effect of a previous heat shock on the thermal resistance of Listeria monocytogenes and Pseudomonas aeruginosa at different pHs. *Int. J. Food Microbiol.* **116,** 228–238 (2007).
151. Allan, B., Linseman, M., MacDonald, L. A., Lam, J. S. & Kropinski, A. M. Heat shock response of Pseudomonas aeruginosa. *J. Bacteriol.* **170,** 3668–3374 (1988).
152. Zupančič, M., Korošec, R. C. & Bukovec, P. The thermal stability of ciprofloxacin complexes with magnesium(II), zinc(II) and cobalt(II). *J. Therm. Anal. Calorim.* **63,** 787–795 (2001).
153. El-Gamel, N. E. A., Hawash, M. F. & Fahmey, M. A. Structure characterization and spectroscopic investigation of ciprofloxacin drug. *J. Therm. Anal. Calorim.* **108,** 253–262 (2012).
154. Turel, I. & Bukovec, P. Comparison of the thermal stability of ciprofloxacin and its compounds. *Thermochim. Acta* **287,** 311–318 (1996).
155. Dash, A. K. & Suryanarayanan, R. Solid-state properties of tobramycin. *Pharm. Res.* **8,** 1159–1165 (1991).
156. Bulitta, J. B., Ly, N. S., Landersdorfer, C. B., Wanigaratne, N. A., Velkov, T., Yadav, R., Oliver, A., Martin, L., Shin, B. S., Forrest, A. & Tsuji, B. T. Two mechanisms of killing of Pseudomonas aeruginosa by tobramycin assessed at multiple inocula via mechanism-based modeling. *Antimicrob. Agents Chemother.* **59,** 2315–2327 (2015).
157. Davis, B. D. Mechanism of bactericidal action of aminoglycosides. *Microbiol. Rev.* **51,** 341–350 (1987).
158. Yang, G., Trylska, J., Tor, Y. & McCammon, J. A. Binding of aminoglycosidic antibiotics to the oligonucleotide A-site model and 30S ribosomal subunit: Poisson-Boltzmann model, thermal denaturation, and fluorescence studies. *J. Med. Chem.* **49,** 5478–5490 (2006).
159. Marian, E., Tiţa, B., Jurca, T., Fuliaş, A., Vicaş, L. & Tiţa, D. Thermal behaviour of erythromycin-active substance and tablets. *J. Therm. Anal. Calorim.* **111,** 1025–1031 (2013).
160. Siibak, T., Peil, L., Xiong, L., Mankin, A., Remme, J. & Tenson, T. Erythromycin- and chloramphenicol-induced ribosomal assembly defects are secondary effects of protein synthesis inhibition. *Antimicrob. Agents Chemother.* **53,** 563–571 (2009).
161. Wilson, D. N. Ribosome-targeting antibiotics and mechanisms of bacterial resistance. *Nat. Rev. Microbiol.* **12,** 35–48 (2014).
162. Shishkina, A. V, Makarova, T. M., Tereshchenkov, A. G., Makarov, G. I., Korshunova, G. A. & Bogdanov, A. A. Modeling interactions of erythromycin derivatives with ribosomes. *Biochem.* **80,** 1500–1507 (2015).
163. Harrison, J. J., Stremick, C. A., Turner, R. J., Allan, N. D., Olson, M. E. & Ceri, H. Microtiter susceptibility testing of microbes growing on peg lids: a miniaturized biofilm model for high-throughput screening. *Nat. Protoc.* **5,** 1236–1254 (2010).

164. Kumon, H., Tomochika, K., Matunaga, T., Ogawa, M. & Ohmori, H. A sandwich cup method agents for the penetration assay of antimicrobial agents through Pseudomonas exopolysaccharides. *Microbiol. Immunol.* **38,** 615–619 (1994).
165. Wilke, C. R. & Chang, P. Correlation of diffusion coefficients in dilute solutions. *AIChE J.* **1,** 264–270 (1955).
166. Stewart, P. S., Franklin, M. J., Williamson, K. S., Folsom, J. P., Boegli, L. & James, G. A. Contribution of stress responses to antibiotic tolerance in Pseudomonas aeruginosa biofilms. *Antimicrob. Agents Chemother.* **59,** 3838–3847 (2015).
167. Kadurugamuwa, J. L., Lam, J. S. & Beveridge, T. J. Interaction of gentamicin with the A band and B band lipopolysaccharides of Pseudomonas aeruginosa and its possible lethal effect. *Antimicrob. Agents Chemother.* **37,** 715–721 (1993).
168. Kadurugamuwa, J. L., Clarke, A. J. & Beveridge, T. J. Surface action of gentamicin on Pseudomonas aeruginosa. *J. Bacteriol.* **175,** 5798–5805 (1993).
169. Rogers, S. S., van der Walle, C. & Waigh, T. A. Microrheology of bacterial biofilms in vitro: Staphylococcus aureus and Pseudomonas aeruginosa. *Langmuir* **24,** 13549–13555 (2008).
170. Moree, W. J., Phelan, V. V, Wu, C.-H., Bandeira, N., Cornett, D. S., Duggan, B. M. & Dorrestein, P. C. Interkingdom metabolic transformations captured by microbial imaging mass spectrometry. *PNAS* **109,** 13811–13816 (2012).
171. Phelan, V. V, Moree, W. J., Aguilar, J., Cornett, D. S., Koumoutsi, A., Noble, S. M., Pogliano, K., Guerrero, C. A. & Dorrestein, P. C. Impact of a transposon insertion in phzF2 on the specialized metabolite production and interkingdom interactions of Pseudomonas aeruginosa. *J. Bacteriol.* **196,** 1683–1693 (2014).
172. Phelan, V. V, Fang, J. & Dorrestein, P. C. Mass spectrometry analysis of Pseudomonas aeruginosa treated with azithromycin. *J. Am. Soc. Mass Spectrom.* **26,** 873–877 (2015).
173. Nguyen, D. D., Wu, C.-H., Moree, W. J., Lamsa, A., Medema, M. H., Zhao, X., Gavilan, R. G., Aparicio, M., Atencio, L., Jackson, C., Ballesteros, J., Sanchez, J., Watrous, J. D., Phelan, V. V, van de Wiel, C., Roland, K. D., Mehnaz, S., de Mot, R., Shank, E. A., *et al.* MS/MS networking guided analysis of molecule and gene cluster families. *PNAS* E2611–E2620 (2013).